

Search for Gravitational Waves Associated with Fast Radio Bursts Detected by CHIME/FRB During the
LIGO–Virgo Observing Run O3a

R. ABBOTT,¹ T. D. ABBOTT,² F. ACERNESE,^{3,4} K. ACKLEY,⁵ C. ADAMS,⁶ N. ADHIKARI,⁷ R. X. ADHIKARI,¹ V. B. ADYA,⁸
 C. AFFELDT,^{9,10} D. AGARWAL,¹¹ M. AGATHOS,^{12,13} K. AGATSUMA,¹⁴ N. AGGARWAL,¹⁵ O. D. AGUIAR,¹⁶ L. AIELLO,¹⁷
 A. AIN,¹⁸ P. AJITH,¹⁹ T. AKUTSU,^{20,21} S. ALBANESI,²² A. ALLOCCA,^{23,4} P. A. ALTIN,⁸ A. AMATO,²⁴ C. ANAND,⁵
 S. ANAND,¹ A. ANANYEVA,¹ S. B. ANDERSON,¹ W. G. ANDERSON,⁷ M. ANDO,^{25,26} T. ANDRADE,²⁷ N. ANDRES,²⁸
 T. ANDRIĆ,²⁹ S. V. ANGELOVA,³⁰ S. ANSOLDI,^{31,32} J. M. ANTELIS,³³ S. ANTIER,³⁴ S. APPERT,¹ KOJI ARAI,¹ KOYA ARAI,³⁵
 Y. ARAI,³⁵ S. ARAKI,³⁶ A. ARAYA,³⁷ M. C. ARAYA,¹ J. S. AREEDA,³⁸ M. ARÈNE,³⁴ N. ARITOMI,²⁵ N. ARNAUD,^{39,40}
 S. M. ARONSON,² K. G. ARUN,⁴¹ H. ASADA,⁴² Y. ASALI,⁴³ G. ASHTON,⁵ Y. ASO,^{44,45} M. ASSIDUO,^{46,47} S. M. ASTON,⁶
 P. ASTONE,⁴⁸ F. AUBIN,²⁸ C. AUSTIN,² S. BABAK,³⁴ F. BADARACCO,⁴⁹ M. K. M. BADER,⁵⁰ C. BADGER,⁵¹ S. BAE,⁵²
 Y. BAE,⁵³ A. M. BAER,⁵⁴ S. BAGNASCO,²² Y. BAI,¹ L. BAIOTTI,⁵⁵ J. BAIRD,³⁴ R. BAJPAI,⁵⁶ M. BALL,⁵⁷ G. BALLARDIN,⁴⁰
 S. W. BALLMER,⁵⁸ A. BALSAMO,⁵⁴ G. BALTUS,⁵⁹ S. BANAGIRI,⁶⁰ D. BANKAR,¹¹ J. C. BARAYOGA,¹ C. BARBIERI,^{61,62,63}
 B. C. BARISH,¹ D. BARKER,⁶⁴ P. BARNEO,²⁷ F. BARONE,^{65,4} B. BARR,⁶⁶ L. BARSOTTI,⁶⁷ M. BARSUGLIA,³⁴ D. BARTA,⁶⁸
 J. BARTLETT,⁶⁴ M. A. BARTON,^{66,20} I. BARTOS,⁶⁹ R. BASSIRI,⁷⁰ A. BASTI,^{71,18} M. BAWAJ,^{72,73} J. C. BAYLEY,⁶⁶
 A. C. BAYLOR,⁷ M. BAZZAN,^{74,75} B. BÉCSY,⁷⁶ V. M. BEDAKIHALE,⁷⁷ M. BEJGER,⁷⁸ I. BELAHCENE,³⁹ V. BENEDETTO,⁷⁹
 D. BENIWAL,⁸⁰ T. F. BENNETT,⁸¹ J. D. BENTLEY,¹⁴ M. BENYAALA,³⁰ F. BERGAMIN,^{9,10} B. K. BERGER,⁷⁰ S. BERNUZZI,¹³
 C. P. L. BERRY,^{15,66} D. BERSANETTI,⁸² A. BERTOLINI,⁵⁰ J. BETZWIESER,⁶ D. BEVERIDGE,⁸³ R. BHANDARE,⁸⁴
 U. BHARDWAJ,^{85,50} D. BHATTACHARJEE,⁸⁶ S. BHAUMIK,⁶⁹ I. A. BILENKO,⁸⁷ G. BILLINGSLEY,¹ S. BINI,^{88,89} R. BIRNEY,⁹⁰
 O. BIRNHOLTZ,⁹¹ S. BISCANS,^{1,67} M. BISCHI,^{46,47} S. BISCOVEANU,⁶⁷ A. BISHT,^{9,10} B. BISWAS,¹¹ M. BITOSI,^{40,18}
 M.-A. BIZOUARD,⁹² J. K. BLACKBURN,¹ C. D. BLAIR,^{83,6} D. G. BLAIR,⁸³ R. M. BLAIR,⁶⁴ F. BOBBA,^{93,94} N. BODE,^{9,10}
 M. BOER,⁹² G. BOGAERT,⁹² M. BOLDRINI,^{95,48} L. D. BONAVENTA,⁷⁴ F. BONDU,⁹⁶ E. BONILLA,⁷⁰ R. BONNAND,²⁸
 P. BOOKER,^{9,10} B. A. BOOM,⁵⁰ R. BORK,¹ V. BOSCHI,¹⁸ N. BOSE,⁹⁷ S. BOSE,¹¹ V. BOSSILKOV,⁸³ V. BOUDART,⁵⁹
 Y. BOUFFANAIS,^{74,75} A. BOUMERDASSI,¹⁷ A. BOZZI,⁴⁰ C. BRADASCHIA,¹⁸ P. R. BRADY,⁷ A. BRAMLEY,⁶ A. BRANCH,⁶
 M. BRANCHESI,^{29,98} J. E. BRAU,⁵⁷ M. BRESCHI,¹³ T. BRIANT,⁹⁹ J. H. BRIGGS,⁶⁶ A. BRILLET,⁹² M. BRINKMANN,^{9,10}
 P. BROCKILL,⁷ A. F. BROOKS,¹ J. BROOKS,⁴⁰ D. D. BROWN,⁸⁰ S. BRUNETT,¹ G. BRUNO,⁴⁹ R. BRUNTZ,⁵⁴ J. BRYANT,¹⁴
 J. BUCHANAN,⁵⁴ T. BULIK,¹⁰⁰ H. J. BULTEN,^{101,102} A. BUONANNO,^{101,102} R. BUSCICCHIO,¹⁴ D. BUSKULIC,²⁸ C. BUY,¹⁰³
 R. L. BYER,⁷⁰ L. CADONATI,¹⁰⁴ G. CAGNOLI,²⁴ C. CAHILLANE,⁶⁴ J. CALDERÓN BUSTILLO,^{105,106} J. D. CALLAGHAN,⁶⁶
 T. A. CALLISTER,^{107,108} E. CALLONI,^{23,4} J. CAMERON,⁸³ J. B. CAMP,¹⁰⁹ M. CANEPA,^{110,82} S. CANEVAROLO,¹¹¹
 M. CANNAVACCIUOLO,⁹³ K. C. CANNON,²⁶ H. CAO,⁸⁰ Z. CAO,¹¹² E. CAPOCASA,²⁰ E. CAPOTE,⁵⁸ G. CARAPELLA,^{93,94}
 F. CARBOGNANI,⁴⁰ J. B. CARLIN,¹¹³ M. F. CARNEY,¹⁵ M. CARPINELLI,^{114,115,40} G. CARRILLO,⁵⁷ G. CARULLO,^{71,18}
 T. L. CARVER,¹⁷ J. CASANUEVA DIAZ,⁴⁰ C. CASENTINI,^{116,117} G. CASTALDI,¹¹⁸ S. CAUDILL,^{50,111} M. CAVAGLIÀ,⁸⁶
 F. CAVALIER,³⁹ R. CAVALIERI,⁴⁰ M. CEASAR,¹¹⁹ G. CELLA,¹⁸ P. CERDÁ-DURÁN,¹²⁰ E. CESARINI,¹¹⁷ W. CHAIBI,⁹²
 K. CHAKRAVARTI,¹¹ S. CHALATHADKA SUBRAHMANYA,¹²¹ E. CHAMPION,¹²² C.-H. CHAN,¹²³ C. CHAN,²⁶ C. L. CHAN,¹⁰⁶
 K. CHAN,¹⁰⁶ M. CHAN,¹²⁴ K. CHANDRA,⁹⁷ P. CHANIAL,⁴⁰ S. CHAO,¹²³ P. CHARLTON,¹²⁵ E. A. CHASE,¹⁵
 E. CHASSANDE-MOTTIN,³⁴ C. CHATTERJEE,⁸³ DEBARATI CHATTERJEE,¹¹ DEEP CHATTERJEE,⁷ M. CHATURVEDI,⁸⁴
 S. CHATY,³⁴ C. CHEN,^{126,127} H. Y. CHEN,⁶⁷ J. CHEN,¹²³ K. CHEN,¹²⁸ X. CHEN,⁸³ Y.-B. CHEN,¹²⁹ Y.-R. CHEN,¹³⁰
 Z. CHEN,¹⁷ H. CHENG,⁶⁹ C. K. CHEONG,¹⁰⁶ H. Y. CHEUNG,¹⁰⁶ H. Y. CHIA,⁶⁹ F. CHIADINI,^{131,94} C.-Y. CHIANG,¹³²
 G. CHIARINI,⁷⁵ R. CHIERICI,¹³³ A. CHINCARINI,⁸² M. L. CHIOFALO,^{71,18} A. CHUMMO,⁴⁰ G. CHO,¹³⁴ H. S. CHO,¹³⁵
 R. K. CHOUDHARY,⁸³ S. CHOUDHARY,¹¹ N. CHRISTENSEN,⁹² H. CHU,¹²⁸ Q. CHU,⁸³ Y.-K. CHU,¹³² S. CHUA,⁸
 K. W. CHUNG,⁵¹ G. CIANI,^{74,75} P. CIECIELAG,⁷⁸ M. CIEŚLAR,⁷⁸ M. CIFALDI,^{116,117} A. A. CIOBANU,⁸⁰ R. CIOLFI,^{136,75}
 F. CIPRIANO,⁹² A. CIRONE,^{110,82} F. CLARA,⁶⁴ E. N. CLARK,¹³⁷ J. A. CLARK,^{1,104} L. CLARKE,¹³⁸ P. CLEARWATER,¹³⁹
 S. CLESSE,¹⁴⁰ F. CLEVA,⁹² E. COCCIA,^{29,98} E. CODAZZO,²⁹ P.-F. COHADON,⁹⁹ D. E. COHEN,³⁹ L. COHEN,² M. COLLEONI,¹⁴¹
 C. G. COLLETTE,¹⁴² A. COLOMBO,⁶¹ M. COLPI,^{61,62} C. M. COMPTON,⁶⁴ M. CONSTANCIO JR.,¹⁶ L. CONTI,⁷⁵
 S. J. COOPER,¹⁴ P. CORBAN,⁶ T. R. CORBITT,² I. CORDERO-CARRIÓN,¹⁴³ S. COREZZI,^{73,72} K. R. CORLEY,⁴³ N. CORNISH,⁷⁶
 D. CORRE,³⁹ A. CORSI,¹⁴⁴ S. CORTESE,⁴⁰ C. A. COSTA,¹⁶ R. COTESTA,¹⁰² M. W. COUGHLIN,⁶⁰ J.-P. COULON,⁹²
 S. T. COUNTRYMAN,⁴³ B. COUSINS,¹⁴⁵ P. COUVARES,¹ D. M. COWARD,⁸³ M. J. COWART,⁶ D. C. COYNE,¹ R. COYNE,¹⁴⁶
 J. D. E. CREIGHTON,⁷ T. D. CREIGHTON,¹⁴⁷ A. W. CRISWELL,⁶⁰ M. CROQUETTE,⁹⁹ S. G. CROWDER,¹⁴⁸ J. R. CUDELL,⁵⁹
 T. J. CULLEN,² A. CUMMING,⁶⁶ R. CUMMINGS,⁶⁶ L. CUNNINGHAM,⁶⁶ E. CUOCO,^{40,149,18} M. CURYLO,¹⁰⁰ P. DABADIE,²⁴
 T. DAL CANTON,³⁹ S. DALL'OSSO,²⁹ G. DÁLYA,¹⁵⁰ A. DANA,⁷⁰ L. M. DANESHGARANBAJASTANI,⁸¹ B. D'ANGELO,^{110,82}
 S. DANILISHIN,^{151,50} S. D'ANTONIO,¹¹⁷ K. DANZMANN,^{9,10} C. DARSOW-FROMM,¹²¹ A. DASGUPTA,⁷⁷ L. E. H. DATRIER,⁶⁶
 S. DATTA,¹¹ V. DATTILO,⁴⁰ I. DAVE,⁸⁴ M. DAVIER,³⁹ G. S. DAVIES,¹⁵² D. DAVIS,¹ M. C. DAVIS,¹¹⁹ E. J. DAW,¹⁵³
 R. DEAN,¹¹⁹ D. DEBRA,⁷⁰ M. DEENADAYALAN,¹¹ J. DEGALLAIX,¹⁵⁴ M. DE LAURENTIS,^{23,4} S. DELÉGLISE,⁹⁹
 V. DEL FAVERO,¹²² F. DE LILLO,⁴⁹ N. DE LILLO,⁶⁶ W. DEL POZZO,^{71,18} L. M. DEMARCHI,¹⁵ F. DE MATTEIS,^{116,117}

- 57 V. D'EMILIO,¹⁷ N. DEMOS,⁶⁷ T. DENT,¹⁰⁵ A. DEPASSE,⁴⁹ R. DE PIETRI,^{155,156} R. DE ROSA,^{23,4} C. DE ROSSI,⁴⁰
 58 R. DESALVO,¹¹⁸ R. DE SIMONE,¹³¹ S. DHURANDHAR,¹¹ M. C. DÍAZ,¹⁴⁷ M. DIAZ-ORTIZ JR.,⁶⁹ N. A. DIDIO,⁵⁸
 59 T. DIETRICH,^{102,50} L. DI FIORE,⁴ C. DI FRONZO,¹⁴ C. DI GIORGIO,^{93,94} F. DI GIOVANNI,¹²⁰ M. DI GIOVANNI,²⁹
 60 T. DI GIROLAMO,^{23,4} A. DI LIETO,^{71,18} B. DING,¹⁴² S. DI PACE,^{95,48} I. DI PALMA,^{95,48} F. DI RENZO,^{71,18}
 61 A. K. DIVAKARLA,⁶⁹ A. DMITRIEV,¹⁴ Z. DOCTOR,⁵⁷ L. D'ONOFRIO,^{23,4} F. DONOVAN,⁶⁷ K. L. DOOLEY,¹⁷ S. DORAVARI,¹¹
 62 I. DORRINGTON,¹⁷ M. DRAGO,^{95,48} J. C. DRIGGERS,⁶⁴ Y. DRORI,¹ J.-G. DUCOIN,³⁹ P. DUPEJ,⁶⁶ O. DURANTE,^{93,94}
 63 D. D'URSO,^{114,115} P.-A. DUVERNE,³⁹ S. E. DWYER,⁶⁴ C. EASSA,⁶⁴ P. J. EASTER,⁵ M. EBERSOLD,¹⁵⁷ T. ECKHARDT,¹²¹
 64 G. EDDOLLS,⁶⁶ B. EDELMAN,⁵⁷ T. B. EDO,¹ O. EDY,¹⁵² A. EFFLER,⁶ S. EGUCHI,¹²⁴ J. EICHHOLZ,⁸ S. S. EIKENBERRY,⁶⁹
 65 M. EISENMANN,²⁸ R. A. EISENSTEIN,⁶⁷ A. EJLLI,¹⁷ E. ENGELBY,³⁸ Y. ENOMOTO,²⁵ L. ERRICO,^{23,4} R. C. ESSICK,¹⁵⁸
 66 H. ESTELLÉS,¹⁴¹ D. ESTEVEZ,¹⁵⁹ Z. ETIENNE,¹⁶⁰ T. ETZEL,¹ M. EVANS,⁶⁷ T. M. EVANS,⁶ B. E. EWING,¹⁴⁵
 67 V. FAFONE,^{116,117,29} H. FAIR,⁵⁸ S. FAIRHURST,¹⁷ A. M. FARAH,¹⁵⁸ S. FARINON,⁸² B. FARR,⁵⁷ W. M. FARR,^{107,108}
 68 N. W. FARROW,⁵ E. J. FAUCHON-JONES,¹⁷ G. FAVARO,⁷⁴ M. FAVATA,¹⁶¹ M. FAYS,⁵⁹ M. FAZIO,¹⁶² J. FEICHT,¹
 69 M. M. FEJER,⁷⁰ E. FENYVESI,^{68,163} D. L. FERGUSON,¹⁶⁴ A. FERNANDEZ-GALIANA,⁶⁷ I. FERRANTE,^{71,18} T. A. FERREIRA,¹⁶
 70 F. FIDECARO,^{71,18} P. FIGURA,¹⁰⁰ I. FIORI,⁴⁰ M. FISHBACH,¹⁵ R. P. FISHER,⁵⁴ R. FITTIPALDI,^{165,94} V. FIUMARA,^{166,94}
 71 R. FLAMINIO,^{28,20} E. FLODEN,⁶⁰ H. FONG,²⁶ J. A. FONT,^{120,167} B. FORMAL,¹⁶⁸ P. W. F. FORSYTH,⁸ A. FRANKE,¹²¹
 72 S. FRASCA,^{95,48} F. FRASCONI,¹⁸ C. FREDERICK,¹⁶⁹ J. P. FREED,³³ Z. FREI,¹⁵⁰ A. FREISE,¹⁷⁰ R. FREY,⁵⁷ P. FRITSCHER,⁶⁷
 73 V. V. FROLOV,⁶ G. G. FRONZÉ,²² Y. FUJII,¹⁷¹ Y. FUJIKAWA,¹⁷² M. FUKUNAGA,³⁵ M. FUKUSHIMA,²¹ P. FULDA,⁶⁹
 74 M. FYFFE,⁶ H. A. GABBARD,⁶⁶ B. U. GADRE,¹⁰² J. R. GAIR,¹⁰² J. GAIS,¹⁰⁶ S. GALAUDAGE,⁵ R. GAMBA,¹³
 75 D. GANAPATHY,⁶⁷ A. GANGULY,¹⁹ D. GAO,¹⁷³ S. G. GAONKAR,¹¹ B. GARAVENTA,^{82,110} C. GARCÍA-NÚÑEZ,⁹⁰
 76 C. GARCÍA-QUIRÓS,¹⁴¹ F. GARUFI,^{23,4} B. GATELEY,⁶⁴ S. GAUDIO,³³ V. GAYATHRI,⁶⁹ G.-G. GE,¹⁷³ G. GEMME,⁸²
 77 A. GENNAI,¹⁸ J. GEORGE,⁸⁴ O. GERBERDING,¹²¹ L. GERGELY,¹⁷⁴ P. GEWECKE,¹²¹ S. GHONGE,¹⁰⁴ ABHIRUP GHOSH,¹⁰²
 78 ARCHISMAN GHOSH,¹⁷⁵ SHAON GHOSH,^{7,161} SHROBANA GHOSH,¹⁷ B. GIACOMAZZO,^{61,62,63} L. GIACOPPO,^{95,48}
 79 J. A. GIAIME,^{2,6} K. D. GIARDINA,⁶ D. R. GIBSON,⁹⁰ C. GIER,³⁰ M. GIESLER,¹⁷⁶ P. GIRI,^{18,71} F. GISSI,⁷⁹ J. GLANZER,²
 80 A. E. GLECKL,³⁸ P. GODWIN,¹⁴⁵ E. GOETZ,¹⁷⁷ R. GOETZ,⁶⁹ N. GOHLKE,^{9,10} B. GONCHAROV,^{5,29} G. GONZÁLEZ,²
 81 A. GOPAKUMAR,¹⁷⁸ M. GOSSELIN,⁴⁰ R. GOUATY,²⁸ D. W. GOULD,⁸ B. GRACE,⁸ A. GRADO,^{179,4} M. GRANATA,¹⁵⁴
 82 V. GRANATA,⁹³ A. GRANT,⁶⁶ S. GRAS,⁶⁷ P. GRASSIA,¹ C. GRAY,⁶⁴ R. GRAY,⁶⁶ G. GRECO,⁷² A. C. GREEN,⁶⁹ R. GREEN,¹⁷
 83 A. M. GRETARSSON,³³ E. M. GRETARSSON,³³ D. GRIFFITH,¹ W. GRIFFITHS,¹⁷ H. L. GRIGGS,¹⁰⁴ G. GRIGNANI,^{73,72}
 84 A. GRIMALDI,^{88,89} S. J. GRIMM,^{29,98} H. GROTE,¹⁷ S. GRUNEWALD,¹⁰² P. GRUNING,³⁹ D. GUERRA,¹²⁰ G. M. GUIDI,^{46,47}
 85 A. R. GUIMARAES,² G. GUIXÉ,²⁷ H. K. GULATI,⁷⁷ H.-K. GUO,¹⁶⁸ Y. GUO,⁵⁰ ANCHAL GUPTA,¹ ANURADHA GUPTA,¹⁸⁰
 86 P. GUPTA,^{50,111} E. K. GUSTAFSON,¹ R. GUSTAFSON,¹⁸¹ F. GUZMAN,¹⁸² S. HA,¹⁸³ L. HAEGEL,³⁴ A. HAGIWARA,^{35,184}
 87 S. HAINO,¹³² O. HALIM,^{32,185} E. D. HALL,⁶⁷ E. Z. HAMILTON,¹⁵⁷ G. HAMMOND,⁶⁶ W.-B. HAN,¹⁸⁶ M. HANEY,¹⁵⁷
 88 J. HANKS,⁶⁴ C. HANNA,¹⁴⁵ M. D. HANNAM,¹⁷ O. HANNUKSELA,^{111,50} H. HANSEN,⁶⁴ T. J. HANSEN,³³ J. HANSON,⁶
 89 T. HARDER,⁹² T. HARDWICK,² K. HARIS,^{50,111} J. HARKUS,^{29,98} G. M. HARRY,¹⁸⁷ I. W. HARRY,¹⁵² D. HARTWIG,¹²¹
 90 K. HASEGAWA,³⁵ B. HASKELL,⁷⁸ R. K. HASSKEW,⁶ C.-J. HASTER,⁶⁷ K. HATTORI,¹⁸⁸ K. HAUGHIAN,⁶⁶ H. HAYAKAWA,¹⁸⁹
 91 K. HAYAMA,¹²⁴ F. J. HAYES,⁶⁶ J. HEALY,¹²² A. HEIDMANN,⁹⁹ A. HEIDT,^{9,10} M. C. HEINTZE,⁶ J. HEINZE,^{9,10} J. HEINZEL,¹⁹⁰
 92 H. HEITMANN,⁹² F. HELLMAN,¹⁹¹ P. HELLO,³⁹ A. F. HELMLING-CORNELL,⁵⁷ G. HEMMING,⁴⁰ M. HENDRY,⁶⁶ I. S. HENG,⁶⁶
 93 E. HENNES,⁵⁰ J. HENNIG,¹⁹² M. H. HENNIG,¹⁹² A. G. HERNANDEZ,⁸¹ F. HERNANDEZ VIVANCO,⁵ M. HEURS,^{9,10}
 94 S. HILD,^{151,50} P. HILL,³⁰ Y. HIMEMOTO,¹⁹³ A. S. HINES,¹⁸² Y. HIRANUMA,¹⁹⁴ N. HIRATA,²⁰ E. HIROSE,³⁵ S. HOCHHEIM,^{9,10}
 95 D. HOFMAN,¹⁵⁴ J. N. HOHMANN,¹²¹ D. G. HOLCOMB,¹¹⁹ N. A. HOLLAND,⁸ I. J. HOLLOWES,¹⁵³ Z. J. HOLMES,⁸⁰ K. HOLT,⁶
 96 D. E. HOLZ,¹⁵⁸ Z. HONG,¹⁹⁵ P. HOPKINS,¹⁷ J. HOUGH,⁶⁶ S. HOURIHANE,¹²⁹ E. J. HOWELL,⁸³ C. G. HOY,¹⁷ D. HOYLAND,¹⁴
 97 A. HREIBI,^{9,10} B.-H. HSIEH,³⁵ Y. HSU,¹²³ G.-Z. HUANG,¹⁹⁵ H.-Y. HUANG,¹³² P. HUANG,¹⁷³ Y.-C. HUANG,¹³⁰ Y.-J. HUANG,¹³²
 98 Y. HUANG,⁶⁷ M. T. HÜBNER,⁵ A. D. HUDDART,¹³⁸ B. HUGHEY,³³ D. C. Y. HUI,¹⁹⁶ V. HUI,²⁸ S. HUSA,¹⁴¹
 99 S. H. HUTTNER,⁶⁶ R. HUXFORD,¹⁴⁵ T. HUYNH-DINH,⁶ S. IDE,¹⁹⁷ B. IDZKOWSKI,¹⁰⁰ A. IESS,^{116,117} B. IKENOUE,²¹ S. IMAM,¹⁹⁵
 100 K. INAYOSHI,¹⁹⁸ C. INGRAM,⁸⁰ Y. INOUE,¹²⁸ K. IOKA,¹⁹⁹ M. ISI,⁶⁷ K. ISLEIF,¹²¹ K. ITO,²⁰⁰ Y. ITOH,^{201,202} B. R. IYER,¹⁹
 101 K. IZUMI,²⁰³ V. JABERIANHAMEDAN,⁸³ T. JACQMIN,⁹⁹ S. J. JADHAV,²⁰⁴ S. P. JADHAV,¹¹ A. L. JAMES,¹⁷ A. Z. JAN,¹²²
 102 K. JANI,²⁰⁵ J. JANQUART,^{111,50} K. JANSSENS,^{206,92} N. N. JANTHALUR,²⁰⁴ P. JARANOWSKI,²⁰⁷ D. JARIWALA,⁶⁹ R. JAUME,¹⁴¹
 103 A. C. JENKINS,⁵¹ K. JENNER,⁸⁰ C. JEON,²⁰⁸ M. JEUNON,⁶⁰ W. JIA,⁶⁷ H.-B. JIN,^{209,210} G. R. JOHNS,⁵⁴ A. W. JONES,⁸³
 104 D. I. JONES,²¹¹ J. D. JONES,⁶⁴ P. JONES,¹⁴ R. JONES,⁶⁶ R. J. G. JONKER,⁵⁰ L. JU,⁸³ P. JUNG,⁵³ K. JUNG,¹⁸³
 105 J. JUNKER,^{9,10} V. JUSTE,¹⁵⁹ K. KAIHOTSU,²⁰⁰ T. KAJITA,²¹² M. KAKIZAKI,¹⁸⁸ C. V. KALAGHATGI,^{17,111} V. KALOGERA,¹⁵
 106 B. KAMAI,¹ M. KAMIZUMI,¹⁸⁹ N. KANDA,^{201,202} S. KANDHASAMY,¹¹ G. KANG,²¹³ J. B. KANNER,¹ Y. KAO,¹²³
 107 S. J. KAPADIA,¹⁹ D. P. KAPASI,⁸ S. KARAT,¹ C. KARATHANASIS,²¹⁴ S. KARKI,⁸⁶ R. KASHYAP,¹⁴⁵ M. KASPRZACK,¹
 108 W. KASTAUN,^{9,10} S. KATSANEVAS,⁴⁰ E. KATSAVOUNIDIS,⁶⁷ W. KATZMAN,⁶ T. KAUR,⁸³ K. KAWABE,⁶⁴ K. KAWAGUCHI,³⁵
 109 N. KAWAI,²¹⁵ T. KAWASAKI,²⁵ F. KÉFÉLIAN,⁹² D. KEITEL,¹⁴¹ J. S. KEY,²¹⁶ S. KHADKA,⁷⁰ F. Y. KHALILI,⁸⁷ S. KHAN,¹⁷
 110 E. A. KHAZANOV,²¹⁷ N. KHETAN,^{29,98} M. KHURSHED,⁸⁴ N. KIJBUNCHOO,⁸ C. KIM,²¹⁸ J. C. KIM,²¹⁹ J. KIM,²²⁰ K. KIM,²²¹
 111 W. S. KIM,²²² Y.-M. KIM,²²³ C. KIMBALL,¹⁵ N. KIMURA,¹⁸⁴ M. KINLEY-HANLON,⁶⁶ R. KIRCHHOFF,^{9,10} J. S. KISSEL,⁶⁴
 112 N. KITA,²⁵ H. KITAZAWA,²⁰⁰ L. KLEYBOLTE,¹²¹ S. KLIMENKO,⁶⁹ A. M. KNEE,¹⁷⁷ T. D. KNOWLES,¹⁶⁰ E. KNYAZEV,⁶⁷
 113 P. KOCH,^{9,10} G. KOEKOEK,^{50,151} Y. KOJIMA,²²⁴ K. KOKEYAMA,²²⁵ S. KOLEY,²⁹ P. KOLITSIDOU,¹⁷ M. KOLSTEIN,²¹⁴
 114 K. KOMORI,^{67,25} V. KONDRASHOV,¹ A. K. H. KONG,²²⁶ A. KONTOS,²²⁷ N. KOPER,^{9,10} M. KOROBKO,¹²¹ K. KOTAKE,¹²⁴
 115 M. KOVALAM,⁸³ D. B. KOZAK,¹ C. KOZAKAI,⁴⁴ R. KOZU,¹⁸⁹ V. KRINGEL,^{9,10} N. V. KRISHNENDU,^{9,10} A. KRÓLAK,^{228,229}
 116 G. KUEHN,^{9,10} F. KUEI,¹²³ P. KUIJER,⁵⁰ A. KUMAR,²⁰⁴ P. KUMAR,¹⁷⁶ RAHUL KUMAR,⁶⁴ RAKESH KUMAR,⁷⁷ J. KUME,²⁶
 117 K. KUNS,⁶⁷ C. KUO,¹²⁸ H.-S. KUO,¹⁹⁵ Y. KUROMIYA,²⁰⁰ S. KUROYANAGI,^{230,231} K. KUSAYANAGI,²¹⁵ S. KUWAHARA,²⁶
 118 K. KWAK,¹⁸³ P. LAGABBE,²⁸ D. LAGHI,^{71,18} E. LALANDE,²³² T. L. LAM,¹⁰⁶ A. LAMBERTS,^{92,233} M. LANDRY,⁶⁴

- 119 B. B. LANE,⁶⁷ R. N. LANG,⁶⁷ J. LANGE,¹⁶⁴ B. LANTZ,⁷⁰ I. LA ROSA,²⁸ A. LARTAUD-VOLLARD,³⁹ P. D. LASKY,⁵
120 M. LAXEN,⁶ A. LAZZARINI,¹ C. LAZZARO,^{74,75} P. LEACI,^{95,48} S. LEAVEY,^{9,10} Y. K. LECOEUICHE,¹⁷⁷ H. K. LEE,²³⁴
121 H. M. LEE,¹³⁴ H. W. LEE,²¹⁹ J. LEE,¹³⁴ K. LEE,²³⁵ R. LEE,¹³⁰ J. LEHMANN,^{9,10} A. LEMAÎTRE,²³⁶ M. LEONARDI,²⁰
122 N. LEROY,³⁹ N. LETENDRE,²⁸ C. LEVESQUE,²³² Y. LEVIN,⁵ J. N. LEVITON,¹⁸¹ K. LEYDE,³⁴ A. K. Y. LI,¹ B. LI,¹²³ J. LI,¹⁵
123 K. L. LI,²³⁷ T. G. F. LI,¹⁰⁶ X. LI,¹²⁹ C-Y. LIN,²³⁸ F-K. LIN,¹³² F-L. LIN,¹⁹⁵ H. L. LIN,¹²⁸ L. C.-C. LIN,¹⁸³ F. LINDE,^{239,50}
124 S. D. LINKER,⁸¹ J. N. LINLEY,⁶⁶ T. B. LITTENBERG,²⁴⁰ G. C. LIU,¹²⁶ J. LIU,^{9,10} K. LIU,¹²³ X. LIU,⁷ F. LLAMAS,¹⁴⁷
125 M. LORENS-MONTEAGUDO,¹²⁰ R. K. L. LO,¹ A. LOCKWOOD,²⁴⁴ L. T. LONDON,⁶⁷ A. LONGO,^{242,243} D. LOPEZ,¹⁵⁷
126 M. LOPEZ PORTILLA,¹¹¹ M. LORENZINI,^{116,117} V. LORLETTE,²⁴⁴ M. LORMAND,⁶ G. LOSURDO,¹⁸ T. P. LOTT,¹⁰⁴
127 J. D. LOUGH,^{9,10} C. O. LOUSTO,¹²² G. LOVELACE,³⁸ J. F. LUCACCIONI,¹⁶⁹ H. LÜCK,^{9,10} D. LUMACA,^{116,117}
128 A. P. LUNDGREN,¹⁵² L.-W. LUO,¹³² J. E. LYNAM,⁵⁴ R. MACAS,¹⁵² M. MACINNIS,⁶⁷ D. M. MACLEOD,¹⁷
129 I. A. O. MACMILLAN,¹ A. MACQUET,⁹² I. MAGAÑA HERNANDEZ,⁷ C. MAGAZZÙ,¹⁸ R. M. MAGEE,¹ R. MAGGIORE,¹⁴
130 M. MAGNOZZI,^{82,110} S. MAHESH,¹⁶⁰ E. MAJORANA,^{95,48} C. MAKAREM,¹ I. MAKSIMOVIC,²⁴⁴ S. MALIAKAL,¹ A. MALIK,⁸⁴
131 N. MAN,⁹² V. MANDIC,⁶⁰ V. MANGANO,^{95,48} J. L. MANGO,²⁴⁵ G. L. MANSELL,^{64,67} M. MANSKE,⁷ M. MANTOVANI,⁴⁰
132 M. MAPELLI,^{74,75} F. MARCHESONI,^{246,72,247} M. MARCHIO,²⁰ F. MARION,²⁸ Z. MARK,¹²⁹ S. MÁRKA,⁴³ Z. MÁRKA,⁴³
133 C. MARKAKIS,¹² A. S. MARKOSYAN,⁷⁰ A. MARKOWITZ,¹ E. MAROS,¹ A. MARQUINA,¹⁴³ S. MARSAT,³⁴ F. MARTELLI,^{46,47}
134 I. W. MARTIN,⁶⁶ R. M. MARTIN,¹⁶¹ M. MARTINEZ,²¹⁴ V. A. MARTINEZ,⁶⁹ V. MARTINEZ,²⁴ K. MARTINOVIC,⁵¹
135 D. V. MARTYNOV,¹⁴ E. J. MARX,⁶⁷ H. MASALEHDAN,¹²¹ K. MASON,⁶⁷ E. MASSERA,¹⁵³ A. MASSEROT,²⁸
136 T. J. MASSINGER,⁶⁷ M. MASSO-REID,⁶⁶ S. MASTROGIOVANNI,³⁴ A. MATAS,¹⁰² M. MATEU-LUCENA,¹⁴¹ F. MATICHARD,^{1,67}
137 M. MATIUSHECHKINA,^{9,10} N. MAVALVALA,⁶⁷ J. J. McCANN,⁸³ R. MCCARTHY,⁶⁴ D. E. MCCLELLAND,⁸ P. K. MCCLINCY,¹⁴⁵
138 S. MCCORMICK,⁶ L. MCCULLER,⁶⁷ G. I. MCGHEE,⁶⁶ S. C. MCGUIRE,²⁴⁸ C. MCISAAC,¹⁵² J. MCIVER,¹⁷⁷ T. McRAE,⁸
139 S. T. McWILLIAMS,¹⁶⁰ D. MEACHER,⁷ M. MEHMET,^{9,10} A. K. MEHTA,¹⁰² Q. MEIJER,¹¹¹ A. MELATOS,¹¹³
140 D. A. MELCHOR,³⁸ G. MENDELL,⁶⁴ A. MENENDEZ-VAZQUEZ,²¹⁴ C. S. MENONI,¹⁶² R. A. MERCER,⁷ L. MERENI,¹⁵⁴
141 K. MERFELD,⁵⁷ E. L. MERILH,⁶ J. D. MERRITT,⁵⁷ M. MERZOUGUI,⁹² S. MESHKOV,^{1,*} C. MESSENGER,⁶⁶ C. MESSICK,¹⁶⁴
142 P. M. MEYERS,¹¹³ F. MEYLAHN,^{9,10} A. MHASKE,¹¹ A. MIANI,^{88,89} H. MIAO,¹⁴ I. MICHALOLIAKOS,⁶⁹ C. MICHEL,¹⁵⁴
143 Y. MICHIMURA,²⁵ H. MIDDLETON,¹¹³ L. MILANO,²³ A. L. MILLER,⁴⁹ A. MILLER,⁸¹ B. MILLER,^{85,50} M. MILLHOUSE,¹¹³
144 J. C. MILLS,¹⁷ E. MILOTTI,^{185,32} O. MINAZZOLI,^{92,249} Y. MINENKOV,¹¹⁷ N. MIO,²⁵⁰ LL. M. MIR,²¹⁴ M. MIRAVET-TENÉS,¹²⁰
145 C. MISHRA,²⁵¹ T. MISHRA,⁶⁹ T. MISTRY,¹⁵³ S. MITRA,¹¹ V. P. MITROFANOV,⁸⁷ G. MITSELMAKHER,⁶⁹ R. MITTLEMAN,⁶⁷
146 O. MIYAKAWA,¹⁸⁹ A. MIYAMOTO,²⁰¹ Y. MIYAZAKI,²⁵ K. MIYO,¹⁸⁹ S. MIYOKI,¹⁸⁹ GEOFFREY MO,⁶⁷ E. MOGUEL,¹⁶⁹
147 K. MOGUSHI,⁸⁶ S. R. P. MOHAPATRA,⁶⁷ S. R. MOHITE,⁷ I. MOLINA,³⁸ M. MOLINA-RUIZ,¹⁹¹ M. MONDIN,⁸¹
148 M. MONTANI,^{46,47} C. J. MOORE,¹⁴ D. MORARU,⁶⁴ F. MORAWSKI,⁷⁸ A. MORE,¹¹ C. MORENO,³³ G. MORENO,⁶⁴ Y. MORI,²⁰⁰
149 S. MORISAKI,⁷ Y. MORIWAKI,¹⁸⁸ B. MOURS,¹⁵⁹ C. M. MOW-LOWRY,^{14,170} S. MOZZON,¹⁵² F. MUCIACCIA,^{95,48}
150 ARUNAVA MUKHERJEE,²⁵² D. MUKHERJEE,¹⁴⁵ SOMA MUKHERJEE,¹⁴⁷ SUBROTO MUKHERJEE,⁷⁷ SUVODIP MUKHERJEE,⁸⁵
151 N. MUKUND,^{9,10} A. MULLAVEY,⁶ J. MUNCH,⁸⁰ E. A. MUÑOZ,⁵⁸ P. G. MURRAY,⁶⁶ R. MUSENICH,^{82,110} S. MUUSSE,⁸⁰
152 S. L. NADJI,^{9,10} K. NAGANO,²⁰³ S. NAGANO,²⁵³ A. NAGAR,^{22,254} K. NAKAMURA,²⁰ H. NAKANO,²⁵⁵ M. NAKANO,³⁵
153 R. NAKASHIMA,²¹⁵ Y. NAKAYAMA,²⁰⁰ V. NAPOLANO,⁴⁰ I. NARDECCHIA,^{116,117} T. NARIKAWA,³⁵ L. NATICCHIONI,⁴⁸
154 B. NAYAK,⁸¹ R. K. NAYAK,²⁵⁶ R. NEGISHI,¹⁹⁴ B. F. NEIL,⁸³ J. NELSON,^{79,94} G. NELEMANS,²⁵⁷ T. J. N. NELSON,⁶
155 M. NERY,^{9,10} P. NEUBAUER,¹⁶⁹ A. NEUNZERT,²¹⁶ K. Y. NG,⁶⁷ S. W. S. NG,⁸⁰ C. NGUYEN,³⁴ P. NGUYEN,⁵⁷ T. NGUYEN,⁶⁷
156 L. NGUYEN QUYNH,²⁵⁸ W.-T. NI,^{209,173,130} S. A. NICHOLS,² A. NISHIZAWA,²⁶ S. NISSANKE,²⁶ E. NITOGLIA,¹³³
157 F. NOCERA,⁴⁰ M. NORMAN,¹⁷ C. NORTH,¹⁷ S. NOZAKI,¹⁸⁸ L. K. NUTTALL,¹⁵² J. OBERLING,⁶⁴ B. D. O'BRIEN,⁶⁹
158 Y. OBUCHI,²¹ J. O'DELL,¹³⁸ E. OELKER,⁶⁶ W. OGAKI,³⁵ G. OGANESYAN,^{29,98} J. J. OH,²²² K. OH,¹⁹⁶ S. H. OH,²²²
159 M. OHASHI,¹⁸⁹ N. OHISHI,⁴⁴ M. OHKAWA,¹⁷² F. OHME,^{9,10} H. OHTA,²⁶ M. A. OKADA,¹⁶ Y. OKUTANI,¹⁹⁷ K. OKUTOMI,¹⁸⁹
160 C. OLIVETTO,⁴⁰ K. OOHARA,¹⁹⁴ C. OOI,²⁵ R. ORAM,⁶ B. O'REILLY,⁶ R. G. ORMISTON,⁶⁰ N. D. ORMSBY,⁵⁴
161 L. F. ORTEGA,⁶⁹ R. O'SHAUGHNESSY,¹²² E. O'SHEA,¹⁷⁶ S. OSHINO,¹⁸⁹ S. OSSOKINE,¹⁰² C. OSTHELDER,¹ S. OTABE,²¹⁵
162 D. J. OTTAWAY,⁸⁰ H. OVERMIER,⁶ A. E. PACE,¹⁴⁵ G. PAGANO,^{71,18} M. A. PAGE,⁸³ G. PAGLIAROLI,^{29,98} A. PAI,⁹⁷
163 S. A. PAI,⁸⁴ J. R. PALAMOS,⁵⁷ O. PALASHOV,²¹⁷ C. PALOMBA,⁴⁸ H. PAN,¹²³ K. PAN,^{130,226} P. K. PANDA,²⁰⁴ H. PANG,¹²⁸
164 P. T. H. PANG,^{50,111} C. PANKOW,¹⁵ F. PANNARALE,^{95,48} B. C. PANT,⁸⁴ F. H. PANTHER,⁸³ F. PAOLETTI,¹⁸ A. PAOLI,⁴⁰
165 A. PAOLONE,^{48,259} A. PARISI,¹²⁶ H. PARK,⁷ J. PARK,²⁶⁰ W. PARKER,^{6,248} D. PASCUCCI,⁵⁰ A. PASQUALETTI,⁴⁰
166 R. PASSAQUIETI,^{71,18} D. PASSUELLO,¹⁸ M. PATEL,⁵⁴ M. PATHAK,⁸⁰ B. PATRICELLI,^{40,18} A. S. PATRON,² S. PATRONE,^{95,48}
167 S. PAUL,⁵⁷ E. PAYNE,⁵ M. PEDRAZA,¹ M. PEGORARO,⁷⁵ A. PELE,⁶ F. E. PEÑA ARELLANO,¹⁸⁹ S. PENN,²⁶¹ A. PEREGO,^{88,89}
168 A. PEREIRA,²⁴ T. PEREIRA,²⁶² C. J. PEREZ,⁶⁴ C. PÉRIGOIS,²⁸ C. C. PERKINS,⁶⁹ A. PERRECA,^{88,89} S. PERRIÈS,¹³³
169 J. PETERMANN,¹²¹ D. PETTERSON,¹ H. P. PFEIFFER,¹⁰² K. A. PHAM,⁶⁰ K. S. PHUKON,^{50,239} O. J. PICCINNI,⁴⁸
170 M. PICHOT,⁹² M. PIENDIBENE,^{71,18} F. PIERGIOVANNI,^{46,47} L. PIERINI,^{95,48} V. PIERRO,^{79,94} G. PILLANT,⁴⁰ M. PILLAS,³⁹
171 F. PILO,¹⁸ L. PINARD,¹⁵⁴ I. M. PINTO,^{79,94,263} M. PINTO,⁴⁰ B. J. PIOTRZKOWSKI,⁷ K. PIOTRZKOWSKI,⁴⁹ M. PIRELLO,⁶⁴
172 M. D. PITKIN,²⁶⁴ E. PLACIDI,^{95,48} L. PLANAS,¹⁴¹ W. PLASTINO,^{242,243} C. PLUCHAR,¹³⁷ R. POGGIANI,^{71,18} E. POLINI,²⁸
173 D. Y. T. PONG,¹⁰⁶ S. PONRATHNAM,¹¹ P. POPOLIZIO,⁴⁰ E. K. PORTER,³⁴ R. POULTON,⁴⁰ J. POWELL,¹³⁹ M. PRACCHIA,²⁸
174 T. PRADIER,¹⁵⁹ A. K. PRAJAPATI,⁷⁷ K. PRASAI,⁷⁰ R. PRASANNA,²⁰⁴ G. PRATTEN,¹⁴ M. PRINCIPE,^{79,263,94}
175 G. A. PRODI,^{265,89} L. PROKHOROV,¹⁴ P. PROSPITO,^{116,117} L. PRUDENZI,¹⁰² A. PUECHER,^{50,111} M. PUNTURO,⁷²
176 F. PUOSI,^{18,71} P. PUPPO,⁴⁸ M. PÜRNER,¹⁰² H. QI,¹⁷ V. QUETSCHKE,¹⁴⁷ R. QUITZOW-JAMES,⁸⁶ F. J. RAAB,⁶⁴
177 G. RAALJMAKERS,^{85,50} H. RADKINS,⁶⁴ N. RADULESCO,⁹² P. RAFFAI,¹⁵⁰ S. X. RAIL,²³² S. RAJA,⁸⁴ C. RAJAN,⁸⁴
178 K. E. RAMIREZ,⁶ T. D. RAMIREZ,³⁸ A. RAMOS-BUADES,¹⁰² J. RANA,¹⁴⁵ P. RAPAGNANI,^{95,48} U. D. RAPOL,²⁶⁶ A. RAY,⁷
179 V. RAYMOND,¹⁷ N. RAZA,¹⁷⁷ M. RAZZANO,^{71,18} J. READ,³⁸ L. A. REES,¹⁸⁷ T. REGIMBAU,²⁸ L. REI,⁸² S. REID,³⁰
180 S. W. REID,⁵⁴ D. H. REITZE,^{1,69} P. RELTON,¹⁷ A. RENZINI,¹ P. RETTEGNO,^{267,22} M. REZAC,³⁸ F. RICCI,^{95,48}

- 181 D. RICHARDS,¹³⁸ J. W. RICHARDSON,¹ L. RICHARDSON,¹⁸² G. RIEMENSCHNEIDER,^{267,22} K. RILES,¹⁸¹ S. RINALDI,^{18,71}
 182 K. RINK,¹⁷⁷ M. RIZZO,¹⁵ N. A. ROBERTSON,^{1,66} R. ROBBIE,¹ F. ROBINET,³⁹ A. ROCCHI,¹¹⁷ S. RODRIGUEZ,³⁸ L. ROLLAND,²⁸
 183 J. G. ROLLINS,¹ M. ROMANELLI,⁹⁶ R. ROMANO,^{3,4} C. L. ROMEL,⁶⁴ A. ROMERO-RODRÍGUEZ,²¹⁴ I. M. ROMERO-SHAW,⁵
 184 J. H. ROMIE,⁶ S. RONCHINI,^{29,98} L. ROSA,^{4,23} C. A. ROSE,⁷ D. ROSIŃSKA,¹⁰⁰ M. P. ROSS,²⁴¹ S. ROWAN,⁶⁶
 185 S. J. ROWLINSON,¹⁴ S. ROY,¹¹¹ SANTOSH ROY,¹¹ SOUMEN ROY,²⁶⁸ D. ROZZA,^{114,115} P. RUGGI,⁴⁰ K. RYAN,⁶⁴ S. SACHDEV,¹⁴⁵
 186 T. SADECKI,⁶⁴ J. SADIQ,¹⁰⁵ N. SAGO,²⁶⁹ S. SAITO,²¹ Y. SAITO,¹⁸⁹ K. SAKAI,²⁷⁰ Y. SAKAI,¹⁹⁴ M. SAKELLARIADOU,⁵¹
 187 Y. SAKUNO,¹²⁴ O. S. SALAFIA,^{63,62,61} L. SALCONI,⁴⁰ M. SALEEM,⁶⁰ F. SALEMI,^{88,89} A. SAMAJDAR,^{50,111} E. J. SANCHEZ,¹
 188 J. H. SANCHEZ,³⁸ L. E. SANCHEZ,¹ N. SANCHIS-GUAL,²⁷¹ J. R. SANDERS,²⁷² A. SANUY,²⁷ T. R. SARAVANAN,¹¹ N. SARIN,⁵
 189 B. SASSOLAS,¹⁵⁴ H. SATARI,⁸³ S. SATO,²⁷³ T. SATO,¹⁷² O. SAUTER,⁶⁹ R. L. SAVAGE,⁶⁴ T. SAWADA,²⁰¹ D. SAWANT,⁹⁷
 190 H. L. SAWANT,¹¹ S. SAYAH,¹⁵⁴ D. SCHAETZL,¹ M. SCHEEL,¹²⁹ J. SCHEUER,¹⁵ M. SCHIWORSKI,⁸⁰ P. SCHMIDT,¹⁴
 191 S. SCHMIDT,¹¹¹ R. SCHNABEL,¹²¹ M. SCHNEEWIND,^{9,10} R. M. S. SCHOFIELD,⁵⁷ A. SCHÖNBECK,¹²¹ B. W. SCHULTE,^{9,10}
 192 B. F. SCHUTZ,^{17,9,10} E. SCHWARTZ,¹⁷ J. SCOTT,⁶⁶ S. M. SCOTT,⁸ M. SEGLAR-ARROYO,²⁸ T. SEKIGUCHI,²⁶ Y. SEKIGUCHI,²⁷⁴
 193 D. SELLERS,⁶ A. S. SENGUPTA,²⁶⁸ D. SENTENAC,⁴⁰ E. G. SEO,¹⁰⁶ V. SEQUINO,^{23,4} A. SERGEEV,²¹⁷ Y. SETYAWATI,¹¹¹
 194 T. SHAFFER,⁶⁴ M. S. SHAHRIAR,¹⁵ B. SHAMS,¹⁶⁸ L. SHAO,¹⁹⁸ A. SHARMA,^{29,98} P. SHARMA,⁸⁴ P. SHAWHAN,¹⁰¹
 195 N. S. SHCHEBLANOV,²³⁶ S. SHIBAGAKI,¹²⁴ M. SHIKAUCHI,²⁶ R. SHIMIZU,²¹ T. SHIMODA,²⁵ K. SHIMODE,¹⁸⁹ H. SHINKAI,²⁷⁵
 196 T. SHISHIDO,⁴⁵ A. SHODA,²⁰ D. H. SHOEMAKER,⁶⁷ D. M. SHOEMAKER,¹⁶⁴ S. SHYAMSUNDAR,⁸⁴ M. SIENIAWSKA,¹⁰⁰
 197 D. SIGG,⁶⁴ L. P. SINGER,¹⁰⁹ D. SINGH,¹⁴⁵ N. SINGH,¹⁰⁰ A. SINGHA,^{151,50} A. M. SINTES,¹⁴¹ V. SIPALA,^{114,115} V. SKLIRIS,¹⁷
 198 B. J. J. SLAGMOLEN,⁸ T. J. SLAVEN-BLAIR,⁸³ J. SMETANA,¹⁴ J. R. SMITH,³⁸ R. J. E. SMITH,⁵ J. SOLDATESCHI,^{276,277,47}
 199 S. N. SOMALA,²⁷⁸ K. SOMIYA,²¹⁵ E. J. SON,²²² K. SONI,¹¹ S. SONI,² V. SORDINI,¹³³ F. SORRENTINO,⁸² N. SORRENTINO,^{71,18}
 200 H. SOTANI,²⁷⁹ R. SOULARD,⁹² T. SOURADEEP,^{266,11} E. SOWELL,¹⁴⁴ V. SPAGNUOLO,^{151,50} A. P. SPENCER,⁶⁶ M. SPERA,^{74,75}
 201 R. SRINIVASAN,⁹² A. K. SRIVASTAVA,⁷⁷ V. SRIVASTAVA,⁵⁸ K. STAATS,¹⁵ C. STACHIE,⁹² D. A. STEER,³⁴
 202 J. STEINLECHNER,^{151,50} S. STEINLECHNER,^{151,50} D. J. STOPS,¹⁴ M. STOVER,¹⁶⁹ K. A. STRAIN,⁶⁶ L. C. STRANG,¹¹³
 203 G. STRATTA,^{280,47} A. STRUNK,⁶⁴ R. STURANI,²⁶² A. L. STUVER,¹¹⁹ S. SUDHAGAR,¹¹ V. SUDHIR,⁶⁷ R. SUGIMOTO,^{281,203}
 204 H. G. SUH,⁷ T. Z. SUMMERSCALES,²⁸² H. SUN,⁸³ L. SUN,⁸ S. SUNIL,⁷⁷ A. SUR,⁷⁸ J. SURESH,^{26,35} P. J. SUTTON,¹⁷
 205 TAKAMASA SUZUKI,¹⁷² TOSHIKAZU SUZUKI,³⁵ B. L. SWINKELS,⁵⁰ M. J. SZCZEPAŃCZYK,⁶⁹ P. SZEWCZYK,¹⁰⁰ M. TACCA,⁵⁰
 206 H. TAGOSHI,³⁵ S. C. TAIT,⁶⁶ H. TAKAHASHI,²⁸³ R. TAKAHASHI,²⁰ A. TAKAMORI,³⁷ S. TAKANO,²⁵ H. TAKEDA,²⁵
 207 M. TAKEDA,²⁰¹ C. J. TALBOT,³⁰ C. TALBOT,¹ H. TANAKA,²⁸⁴ KAZUYUKI TANAKA,²⁰¹ KENTA TANAKA,²⁸⁴ TAIKI TANAKA,³⁵
 208 TAKAHIRO TANAKA,²⁶⁹ A. J. TANASIJCZUK,⁴⁹ S. TANIOKA,^{20,45} D. B. TANNER,⁶⁹ D. TAO,¹ L. TAO,⁶⁹
 209 E. N. TAPIA SAN MARTIN,²⁰ E. N. TAPIA SAN MARTÍN,⁵⁰ C. TARANTO,¹¹⁶ J. D. TASSON,¹⁹⁰ S. TELADA,²⁸⁵ R. TENORIO,¹⁴¹
 210 J. E. TERHUNE,¹¹⁹ L. TERKOWSKI,¹²¹ M. P. THIRUGNANASAMBANDAM,¹¹ M. THOMAS,⁶ P. THOMAS,⁶⁴ J. E. THOMPSON,¹⁷
 211 S. R. THONDAPU,⁸⁴ K. A. THORNE,⁶ E. THRANE,⁵ SHUBHANSHU TIWARI,¹⁵⁷ SRISHTI TIWARI,¹¹ V. TIWARI,¹⁷
 212 A. M. TOIVONEN,⁶⁰ K. TOLAND,⁶⁶ A. E. TOLLEY,¹⁵² T. TOMARU,²⁰ Y. TOMIGAMI,²⁰¹ T. TOMURA,¹⁸⁹ M. TONELLI,^{71,18}
 213 A. TORRES-FORNÉ,¹²⁰ C. I. TORRIE,¹ I. TOSTA E MELO,^{114,115} D. TÖYRÄ,⁸ A. TRAPANANTI,^{246,72} F. TRAVASSO,^{72,246}
 214 G. TRAYLOR,⁶ M. TREVOR,¹⁰¹ M. C. TRINGALI,⁴⁰ A. TRIPATHEE,¹⁸¹ L. TROIANO,^{286,94} A. TROVATO,³⁴ L. TROZZO,^{4,189}
 215 R. J. TRUDEAU,¹ D. S. TSAI,¹²³ D. TSAI,¹²³ K. W. TSANG,^{50,287,111} T. TSANG,²⁸⁸ J-S. TSAO,¹⁹⁵ M. TSE,⁶⁷ R. TSO,¹²⁹
 216 K. TSUBONO,²⁵ S. TSUCHIDA,²⁰¹ L. TSUKADA,²⁶ D. TSUNA,²⁶ T. TSUTSUI,²⁶ T. TSUZUKI,²¹ K. TURBANG,^{289,206}
 217 M. TURCONI,⁹² D. TUYENBAYEV,²⁰¹ A. S. UBHI,¹⁴ N. UCHIKATA,³⁵ T. UCHIYAMA,¹⁸⁹ R. P. UDALL,¹ A. UEDA,¹⁸⁴
 218 T. UEHARA,^{290,291} K. UENO,²⁶ G. UESHIMA,²⁹² C. S. UNNIKRISHNAN,¹⁷⁸ F. URAGUCHI,²¹ A. L. URBAN,² T. USHIBA,¹⁸⁹
 219 A. UTINA,^{151,50} H. VAHLBRUCH,^{9,10} G. VAJENTE,¹ A. VAJPEYI,⁵ G. VALDES,¹⁸² M. VALENTINI,^{88,89} V. VALSAN,⁷
 220 N. VAN BAKEL,⁵⁰ M. VAN BEUZEKOM,⁵⁰ J. F. J. VAN DEN BRAND,^{151,293,50} C. VAN DEN BROECK,^{111,50}
 221 D. C. VANDER-HYDE,⁵⁸ L. VAN DER SCHAAF,⁵⁰ J. V. VAN HEIJNINGEN,⁴⁹ J. VANOSKY,¹ M. H. P. M. VAN PUTTEN,²⁹⁴
 222 N. VAN REMORTEL,²⁰⁶ M. VARDARO,^{239,50} A. F. VARGAS,¹¹³ V. VARMA,¹⁷⁶ M. VASÚTH,⁶⁸ A. VECCHIO,¹⁴ G. VEDOVATO,⁷⁵
 223 J. VEITCH,⁶⁶ P. J. VEITCH,⁸⁰ J. VENNEBERG,^{9,10} G. VENUGOPALAN,¹ D. VERKINDT,²⁸ P. VERMA,²²⁹ Y. VERMA,⁸⁴
 224 D. VESKE,⁴³ F. VETRANO,⁴⁶ A. VICERÉ,^{46,47} S. VIDYANT,⁵⁸ A. D. VIETS,²⁴⁵ A. VIJAYKUMAR,¹⁹ V. VILLA-ORTEGA,¹⁰⁵
 225 J.-Y. VINET,⁹² A. VIRTUOSO,^{185,32} S. VITALE,⁶⁷ T. VO,⁵⁸ H. VOCCA,^{73,72} E. R. G. VON REIS,⁶⁴ J. S. A. VON WRANGEL,^{9,10}
 226 C. VORVICK,⁶⁴ S. P. VYATCHANIN,⁸⁷ L. E. WADE,¹⁶⁹ M. WADE,¹⁶⁹ K. J. WAGNER,¹²² R. C. WALET,⁵⁰ M. WALKER,⁵⁴
 227 G. S. WALLACE,³⁰ L. WALLACE,¹ S. WALSH,⁷ J. WANG,¹⁷³ J. Z. WANG,¹⁸¹ W. H. WANG,¹⁴⁷ R. L. WARD,⁸ J. WARNER,⁶⁴
 228 M. WAS,²⁸ T. WASHIMI,²⁰ N. Y. WASHINGTON,¹ K. WATADA,⁵⁴ J. WATCHI,¹⁴² B. WEAVER,⁶⁴ S. A. WEBSTER,⁶⁶
 229 M. WEINERT,^{9,10} A. J. WEINSTEIN,¹ R. WEISS,⁶⁷ C. M. WELLER,²⁴¹ F. WELLMANN,^{9,10} L. WEN,⁸³ P. WESSELS,^{9,10}
 230 K. WETTE,⁸ J. T. WHELAN,¹²² D. D. WHITE,³⁸ B. F. WHITING,⁶⁹ C. WHITTLE,⁶⁷ D. WILKEN,^{9,10} D. WILLIAMS,⁶⁶
 231 M. J. WILLIAMS,⁶⁶ A. R. WILLIAMSON,¹⁵² J. L. WILLIS,¹ B. WILKE,^{9,10} D. J. WILSON,¹³⁷ W. WINKLER,^{9,10} C. C. WIPF,¹
 232 T. WŁODARCZYK,¹⁰² G. WOAN,⁶⁶ J. WOEHLER,^{9,10} J. K. WOFFORD,¹²² I. C. F. WONG,¹⁰⁶ C. WU,¹³⁰ D. S. WU,^{9,10}
 233 H. WU,¹³⁰ S. WU,¹³⁰ D. M. WYSOCKI,⁷ L. XIAO,¹ W-R. XU,¹⁹⁵ T. YAMADA,²⁸⁴ H. YAMAMOTO,¹ KAZUHIRO YAMAMOTO,¹⁸⁸
 234 KOHEI YAMAMOTO,²⁸⁴ T. YAMAMOTO,¹⁸⁹ K. YAMASHITA,²⁰⁰ R. YAMAZAKI,¹⁹⁷ F. W. YANG,¹⁶⁸ L. YANG,¹⁶² Y. YANG,²⁹⁵
 235 YANG YANG,⁶⁹ Z. YANG,⁶⁰ M. J. YAP,⁸ D. W. YEELES,¹⁷ A. B. YELIKAR,¹²² M. YING,¹²³ K. YOKOGAWA,²⁰⁰
 236 J. YOKOYAMA,^{26,25} T. YOKOZAWA,¹⁸⁹ J. YOO,¹⁷⁶ T. YOSHIOKA,²⁰⁰ HANG YU,¹²⁹ HAOCUN YU,⁶⁷ H. YUZURIHARA,³⁵
 237 A. ZADROŻNY,²²⁹ M. ZANOLIN,³³ S. ZEIDLER,²⁹⁶ T. ZELENKOVA,⁴⁰ J.-P. ZENDRI,⁷⁵ M. ZEVIN,¹⁵⁸ M. ZHAN,¹⁷³ H. ZHANG,¹⁹⁵
 238 J. ZHANG,⁸³ L. ZHANG,¹ T. ZHANG,¹⁴ Y. ZHANG,¹⁸² C. ZHAO,⁸³ G. ZHAO,¹⁴² Y. ZHAO,²⁰ YUE ZHAO,¹⁶⁸ R. ZHOU,¹⁹¹
 239 Z. ZHOU,¹⁵ X. J. ZHU,⁵ Z.-H. ZHU,¹¹² A. B. ZIMMERMAN,¹⁶⁴ M. E. ZUCKER,^{1,67} J. ZWEIG,¹ M. BHARDWAJ,^{297,298}
 240 P. J. BOYLE,^{297,298} T. CASSANELLI,^{299,300} F. DONG,³⁰¹ E. FONSECA,^{302,303} V. KASPI,^{297,298} C. LEUNG,^{304,305}
 241 K. W. MASUI,^{304,305} B. W. MEYERS,³⁰¹ D. MICHILLI,^{304,305} C. NG,³⁰⁰ A. B. PEARLMAN,^{297,298,306,307,308}

E. PETROFF,^{297,298,309} Z. PLEUNIS,³⁰⁰ M. RAFIEI-RAVANDI,^{297,310,311} M. RAHMAN,³¹² S. RANSOM,³¹³ P. SCHOLZ,³⁰⁰
 K. SHIN,^{304,305} K. SMITH,³¹⁰ I. STAIRS,³⁰¹ S. P. TENDULKAR,^{314,315} AND A. V. ZWANIGA^{297,298}

THE LIGO SCIENTIFIC COLLABORATION

THE VIRGO COLLABORATION

THE KAGRA COLLABORATION

THE CHIME/FRB COLLABORATION

¹*LIGO Laboratory, California Institute of Technology, Pasadena, CA 91125, USA*

²*Louisiana State University, Baton Rouge, LA 70803, USA*

³*Dipartimento di Farmacia, Università di Salerno, I-84084 Fisciano, Salerno, Italy*

⁴*INFN, Sezione di Napoli, Complesso Universitario di Monte S. Angelo, I-80126 Napoli, Italy*

⁵*OzGrav, School of Physics & Astronomy, Monash University, Clayton 3800, Victoria, Australia*

⁶*LIGO Livingston Observatory, Livingston, LA 70754, USA*

⁷*University of Wisconsin-Milwaukee, Milwaukee, WI 53201, USA*

⁸*OzGrav, Australian National University, Canberra, Australian Capital Territory 0200, Australia*

⁹*Max Planck Institute for Gravitational Physics (Albert Einstein Institute), D-30167 Hannover, Germany*

¹⁰*Leibniz Universität Hannover, D-30167 Hannover, Germany*

¹¹*Inter-University Centre for Astronomy and Astrophysics, Pune 411007, India*

¹²*University of Cambridge, Cambridge CB2 1TN, United Kingdom*

¹³*Theoretisch-Physikalisches Institut, Friedrich-Schiller-Universität Jena, D-07743 Jena, Germany*

¹⁴*University of Birmingham, Birmingham B15 2TT, United Kingdom*

¹⁵*Center for Interdisciplinary Exploration & Research in Astrophysics (CIERA), Northwestern University, Evanston, IL 60208, USA*

¹⁶*Instituto Nacional de Pesquisas Espaciais, 12227-010 São José dos Campos, São Paulo, Brazil*

¹⁷*Gravity Exploration Institute, Cardiff University, Cardiff CF24 3AA, United Kingdom*

¹⁸*INFN, Sezione di Pisa, I-56127 Pisa, Italy*

¹⁹*International Centre for Theoretical Sciences, Tata Institute of Fundamental Research, Bengaluru 560089, India*

²⁰*Gravitational Wave Science Project, National Astronomical Observatory of Japan (NAOJ), Mitaka City, Tokyo 181-8588, Japan*

²¹*Advanced Technology Center, National Astronomical Observatory of Japan (NAOJ), Mitaka City, Tokyo 181-8588, Japan*

²²*INFN Sezione di Torino, I-10125 Torino, Italy*

²³*Università di Napoli “Federico II”, Complesso Universitario di Monte S. Angelo, I-80126 Napoli, Italy*

²⁴*Université de Lyon, Université Claude Bernard Lyon 1, CNRS, Institut Lumière Matière, F-69622 Villeurbanne, France*

²⁵*Department of Physics, The University of Tokyo, Bunkyo-ku, Tokyo 113-0033, Japan*

²⁶*Research Center for the Early Universe (RESCEU), The University of Tokyo, Bunkyo-ku, Tokyo 113-0033, Japan*

²⁷*Institut de Ciències del Cosmos (ICCUB), Universitat de Barcelona, C/ Martí i Franquès 1, Barcelona, 08028, Spain*

²⁸*Laboratoire d’Annecy de Physique des Particules (LAPP), Univ. Grenoble Alpes, Université Savoie Mont Blanc, CNRS/IN2P3, F-74941 Annecy, France*

²⁹*Gran Sasso Science Institute (GSSI), I-67100 L’Aquila, Italy*

³⁰*SUPA, University of Strathclyde, Glasgow G1 1XQ, United Kingdom*

³¹*Dipartimento di Scienze Matematiche, Informatiche e Fisiche, Università di Udine, I-33100 Udine, Italy*

³²*INFN, Sezione di Trieste, I-34127 Trieste, Italy*

³³*Embry-Riddle Aeronautical University, Prescott, AZ 86301, USA*

³⁴*Université de Paris, CNRS, Astroparticule et Cosmologie, F-75006 Paris, France*

³⁵*Institute for Cosmic Ray Research (ICRR), KAGRA Observatory, The University of Tokyo, Kashiwa City, Chiba 277-8582, Japan*

³⁶*Accelerator Laboratory, High Energy Accelerator Research Organization (KEK), Tsukuba City, Ibaraki 305-0801, Japan*

³⁷*Earthquake Research Institute, The University of Tokyo, Bunkyo-ku, Tokyo 113-0032, Japan*

³⁸*California State University Fullerton, Fullerton, CA 92831, USA*

³⁹*Université Paris-Saclay, CNRS/IN2P3, IJCLab, 91405 Orsay, France*

⁴⁰*European Gravitational Observatory (EGO), I-56021 Cascina, Pisa, Italy*

⁴¹*Chennai Mathematical Institute, Chennai 603103, India*

⁴²*Department of Mathematics and Physics, Gravitational Wave Science Project, Hirosaki University, Hirosaki City, Aomori 036-8561, Japan*

⁴³*Columbia University, New York, NY 10027, USA*

⁴⁴*Kamioka Branch, National Astronomical Observatory of Japan (NAOJ), Kamioka-cho, Hida City, Gifu 506-1205, Japan*

⁴⁵*The Graduate University for Advanced Studies (SOKENDAI), Mitaka City, Tokyo 181-8588, Japan*

⁴⁶*Università degli Studi di Urbino “Carlo Bo”, I-61029 Urbino, Italy*

⁴⁷*INFN, Sezione di Firenze, I-50019 Sesto Fiorentino, Firenze, Italy*

⁴⁸*INFN, Sezione di Roma, I-00185 Roma, Italy*

- 299 ⁴⁹ *Université catholique de Louvain, B-1348 Louvain-la-Neuve, Belgium*
300 ⁵⁰ *Nikhef, Science Park 105, 1098 XG Amsterdam, Netherlands*
301 ⁵¹ *King's College London, University of London, London WC2R 2LS, United Kingdom*
302 ⁵² *Korea Institute of Science and Technology Information (KISTI), Yuseong-gu, Daejeon 34141, Korea*
303 ⁵³ *National Institute for Mathematical Sciences, Yuseong-gu, Daejeon 34047, Korea*
304 ⁵⁴ *Christopher Newport University, Newport News, VA 23606, USA*
305 ⁵⁵ *International College, Osaka University, Toyonaka City, Osaka 560-0043, Japan*
306 ⁵⁶ *School of High Energy Accelerator Science, The Graduate University for Advanced Studies (SOKENDAI), Tsukuba City, Ibaraki*
307 *305-0801, Japan*
308 ⁵⁷ *University of Oregon, Eugene, OR 97403, USA*
309 ⁵⁸ *Syracuse University, Syracuse, NY 13244, USA*
310 ⁵⁹ *Université de Liège, B-4000 Liège, Belgium*
311 ⁶⁰ *University of Minnesota, Minneapolis, MN 55455, USA*
312 ⁶¹ *Università degli Studi di Milano-Bicocca, I-20126 Milano, Italy*
313 ⁶² *INFN, Sezione di Milano-Bicocca, I-20126 Milano, Italy*
314 ⁶³ *INAF, Osservatorio Astronomico di Brera sede di Merate, I-23807 Merate, Lecco, Italy*
315 ⁶⁴ *LIGO Hanford Observatory, Richland, WA 99352, USA*
316 ⁶⁵ *Dipartimento di Medicina, Chirurgia e Odontoiatria "Scuola Medica Salernitana", Università di Salerno, I-84081 Baronissi, Salerno,*
317 *Italy*
318 ⁶⁶ *SUPA, University of Glasgow, Glasgow G12 8QQ, United Kingdom*
319 ⁶⁷ *LIGO Laboratory, Massachusetts Institute of Technology, Cambridge, MA 02139, USA*
320 ⁶⁸ *Wigner RCP, RMKI, H-1121 Budapest, Konkoly Thege Miklós út 29-33, Hungary*
321 ⁶⁹ *University of Florida, Gainesville, FL 32611, USA*
322 ⁷⁰ *Stanford University, Stanford, CA 94305, USA*
323 ⁷¹ *Università di Pisa, I-56127 Pisa, Italy*
324 ⁷² *INFN, Sezione di Perugia, I-06123 Perugia, Italy*
325 ⁷³ *Università di Perugia, I-06123 Perugia, Italy*
326 ⁷⁴ *Università di Padova, Dipartimento di Fisica e Astronomia, I-35131 Padova, Italy*
327 ⁷⁵ *INFN, Sezione di Padova, I-35131 Padova, Italy*
328 ⁷⁶ *Montana State University, Bozeman, MT 59717, USA*
329 ⁷⁷ *Institute for Plasma Research, Bhat, Gandhinagar 382428, India*
330 ⁷⁸ *Nicolaus Copernicus Astronomical Center, Polish Academy of Sciences, 00-716, Warsaw, Poland*
331 ⁷⁹ *Dipartimento di Ingegneria, Università del Sannio, I-82100 Benevento, Italy*
332 ⁸⁰ *OzGrav, University of Adelaide, Adelaide, South Australia 5005, Australia*
333 ⁸¹ *California State University, Los Angeles, 5151 State University Dr, Los Angeles, CA 90032, USA*
334 ⁸² *INFN, Sezione di Genova, I-16146 Genova, Italy*
335 ⁸³ *OzGrav, University of Western Australia, Crawley, Western Australia 6009, Australia*
336 ⁸⁴ *RRCAT, Indore, Madhya Pradesh 452013, India*
337 ⁸⁵ *GRAPPA, Anton Pannekoek Institute for Astronomy and Institute for High-Energy Physics, University of Amsterdam, Science Park*
338 *904, 1098 XH Amsterdam, Netherlands*
339 ⁸⁶ *Missouri University of Science and Technology, Rolla, MO 65409, USA*
340 ⁸⁷ *Faculty of Physics, Lomonosov Moscow State University, Moscow 119991, Russia*
341 ⁸⁸ *Università di Trento, Dipartimento di Fisica, I-38123 Povo, Trento, Italy*
342 ⁸⁹ *INFN, Trento Institute for Fundamental Physics and Applications, I-38123 Povo, Trento, Italy*
343 ⁹⁰ *SUPA, University of the West of Scotland, Paisley PA1 2BE, United Kingdom*
344 ⁹¹ *Bar-Ilan University, Ramat Gan, 5290002, Israel*
345 ⁹² *Artemis, Université Côte d'Azur, Observatoire de la Côte d'Azur, CNRS, F-06304 Nice, France*
346 ⁹³ *Dipartimento di Fisica "E.R. Caianiello", Università di Salerno, I-84084 Fisciano, Salerno, Italy*
347 ⁹⁴ *INFN, Sezione di Napoli, Gruppo Collegato di Salerno, Complesso Universitario di Monte S. Angelo, I-80126 Napoli, Italy*
348 ⁹⁵ *Università di Roma "La Sapienza", I-00185 Roma, Italy*
349 ⁹⁶ *Univ Rennes, CNRS, Institut FOTON - UMR6082, F-3500 Rennes, France*
350 ⁹⁷ *Indian Institute of Technology Bombay, Powai, Mumbai 400 076, India*
351 ⁹⁸ *INFN, Laboratori Nazionali del Gran Sasso, I-67100 Assergi, Italy*
352 ⁹⁹ *Laboratoire Kastler Brossel, Sorbonne Université, CNRS, ENS-Université PSL, Collège de France, F-75005 Paris, France*
353 ¹⁰⁰ *Astronomical Observatory Warsaw University, 00-478 Warsaw, Poland*
354 ¹⁰¹ *University of Maryland, College Park, MD 20742, USA*
355 ¹⁰² *Max Planck Institute for Gravitational Physics (Albert Einstein Institute), D-14476 Potsdam, Germany*

- 356 ¹⁰³*L2IT, Laboratoire des 2 Infinis - Toulouse, Université de Toulouse, CNRS/IN2P3, UPS, F-31062 Toulouse Cedex 9, France*
357 ¹⁰⁴*School of Physics, Georgia Institute of Technology, Atlanta, GA 30332, USA*
358 ¹⁰⁵*IGFAE, Campus Sur, Universidad de Santiago de Compostela, 15782 Spain*
359 ¹⁰⁶*The Chinese University of Hong Kong, Shatin, NT, Hong Kong*
360 ¹⁰⁷*Stony Brook University, Stony Brook, NY 11794, USA*
361 ¹⁰⁸*Center for Computational Astrophysics, Flatiron Institute, New York, NY 10010, USA*
362 ¹⁰⁹*NASA Goddard Space Flight Center, Greenbelt, MD 20771, USA*
363 ¹¹⁰*Dipartimento di Fisica, Università degli Studi di Genova, I-16146 Genova, Italy*
364 ¹¹¹*Institute for Gravitational and Subatomic Physics (GRASP), Utrecht University, Princetonplein 1, 3584 CC Utrecht, Netherlands*
365 ¹¹²*Department of Astronomy, Beijing Normal University, Beijing 100875, China*
366 ¹¹³*OzGrav, University of Melbourne, Parkville, Victoria 3010, Australia*
367 ¹¹⁴*Università degli Studi di Sassari, I-07100 Sassari, Italy*
368 ¹¹⁵*INFN, Laboratori Nazionali del Sud, I-95125 Catania, Italy*
369 ¹¹⁶*Università di Roma Tor Vergata, I-00133 Roma, Italy*
370 ¹¹⁷*INFN, Sezione di Roma Tor Vergata, I-00133 Roma, Italy*
371 ¹¹⁸*University of Sannio at Benevento, I-82100 Benevento, Italy and INFN, Sezione di Napoli, I-80100 Napoli, Italy*
372 ¹¹⁹*Villanova University, 800 Lancaster Ave, Villanova, PA 19085, USA*
373 ¹²⁰*Departamento de Astronomía y Astrofísica, Universitat de València, E-46100 Burjassot, València, Spain*
374 ¹²¹*Universität Hamburg, D-22761 Hamburg, Germany*
375 ¹²²*Rochester Institute of Technology, Rochester, NY 14623, USA*
376 ¹²³*National Tsing Hua University, Hsinchu City, 30013 Taiwan, Republic of China*
377 ¹²⁴*Department of Applied Physics, Fukuoka University, Jonan, Fukuoka City, Fukuoka 814-0180, Japan*
378 ¹²⁵*OzGrav, Charles Sturt University, Wagga Wagga, New South Wales 2678, Australia*
379 ¹²⁶*Department of Physics, Tamkang University, Danshui Dist., New Taipei City 25137, Taiwan*
380 ¹²⁷*Department of Physics and Institute of Astronomy, National Tsing Hua University, Hsinchu 30013, Taiwan*
381 ¹²⁸*Department of Physics, Center for High Energy and High Field Physics, National Central University, Zhongli District, Taoyuan City*
382 *32001, Taiwan*
383 ¹²⁹*CaRT, California Institute of Technology, Pasadena, CA 91125, USA*
384 ¹³⁰*Department of Physics, National Tsing Hua University, Hsinchu 30013, Taiwan*
385 ¹³¹*Dipartimento di Ingegneria Industriale (DIIN), Università di Salerno, I-84084 Fisciano, Salerno, Italy*
386 ¹³²*Institute of Physics, Academia Sinica, Nankang, Taipei 11529, Taiwan*
387 ¹³³*Université Lyon, Université Claude Bernard Lyon 1, CNRS, IP2I Lyon / IN2P3, UMR 5822, F-69622 Villeurbanne, France*
388 ¹³⁴*Seoul National University, Seoul 08826, South Korea*
389 ¹³⁵*Pusan National University, Busan 46241, South Korea*
390 ¹³⁶*INAF, Osservatorio Astronomico di Padova, I-35122 Padova, Italy*
391 ¹³⁷*University of Arizona, Tucson, AZ 85721, USA*
392 ¹³⁸*Rutherford Appleton Laboratory, Didcot OX11 0DE, United Kingdom*
393 ¹³⁹*OzGrav, Swinburne University of Technology, Hawthorn VIC 3122, Australia*
394 ¹⁴⁰*Université libre de Bruxelles, Avenue Franklin Roosevelt 50 - 1050 Bruxelles, Belgium*
395 ¹⁴¹*Universitat de les Illes Balears, IAC3—IEEC, E-07122 Palma de Mallorca, Spain*
396 ¹⁴²*Université Libre de Bruxelles, Brussels 1050, Belgium*
397 ¹⁴³*Departamento de Matemáticas, Universitat de València, E-46100 Burjassot, València, Spain*
398 ¹⁴⁴*Texas Tech University, Lubbock, TX 79409, USA*
399 ¹⁴⁵*The Pennsylvania State University, University Park, PA 16802, USA*
400 ¹⁴⁶*University of Rhode Island, Kingston, RI 02881, USA*
401 ¹⁴⁷*The University of Texas Rio Grande Valley, Brownsville, TX 78520, USA*
402 ¹⁴⁸*Bellevue College, Bellevue, WA 98007, USA*
403 ¹⁴⁹*Scuola Normale Superiore, Piazza dei Cavalieri, 7 - 56126 Pisa, Italy*
404 ¹⁵⁰*MTA-ELTE Astrophysics Research Group, Institute of Physics, Eötvös University, Budapest 1117, Hungary*
405 ¹⁵¹*Maastricht University, P.O. Box 616, 6200 MD Maastricht, Netherlands*
406 ¹⁵²*University of Portsmouth, Portsmouth, PO1 3FX, United Kingdom*
407 ¹⁵³*The University of Sheffield, Sheffield S10 2TN, United Kingdom*
408 ¹⁵⁴*Université Lyon, Université Claude Bernard Lyon 1, CNRS, Laboratoire des Matériaux Avancés (LMA), IP2I Lyon / IN2P3, UMR*
409 *5822, F-69622 Villeurbanne, France*
410 ¹⁵⁵*Dipartimento di Scienze Matematiche, Fisiche e Informatiche, Università di Parma, I-43124 Parma, Italy*
411 ¹⁵⁶*INFN, Sezione di Milano Bicocca, Gruppo Collegato di Parma, I-43124 Parma, Italy*
412 ¹⁵⁷*Physik-Institut, University of Zurich, Winterthurerstrasse 190, 8057 Zurich, Switzerland*

- 413 ¹⁵⁸ *University of Chicago, Chicago, IL 60637, USA*
- 414 ¹⁵⁹ *Université de Strasbourg, CNRS, IPHC UMR 7178, F-67000 Strasbourg, France*
- 415 ¹⁶⁰ *West Virginia University, Morgantown, WV 26506, USA*
- 416 ¹⁶¹ *Montclair State University, Montclair, NJ 07043, USA*
- 417 ¹⁶² *Colorado State University, Fort Collins, CO 80523, USA*
- 418 ¹⁶³ *Institute for Nuclear Research, Hungarian Academy of Sciences, Bem tér 18/c, H-4026 Debrecen, Hungary*
- 419 ¹⁶⁴ *Department of Physics, University of Texas, Austin, TX 78712, USA*
- 420 ¹⁶⁵ *CNR-SPIN, c/o Università di Salerno, I-84084 Fisciano, Salerno, Italy*
- 421 ¹⁶⁶ *Scuola di Ingegneria, Università della Basilicata, I-85100 Potenza, Italy*
- 422 ¹⁶⁷ *Observatori Astronòmic, Universitat de València, E-46980 Paterna, València, Spain*
- 423 ¹⁶⁸ *The University of Utah, Salt Lake City, UT 84112, USA*
- 424 ¹⁶⁹ *Kenyon College, Gambier, OH 43022, USA*
- 425 ¹⁷⁰ *Vrije Universiteit Amsterdam, 1081 HV, Amsterdam, Netherlands*
- 426 ¹⁷¹ *Department of Astronomy, The University of Tokyo, Mitaka City, Tokyo 181-8588, Japan*
- 427 ¹⁷² *Faculty of Engineering, Niigata University, Nishi-ku, Niigata City, Niigata 950-2181, Japan*
- 428 ¹⁷³ *State Key Laboratory of Magnetic Resonance and Atomic and Molecular Physics, Innovation Academy for Precision Measurement*
- 429 *Science and Technology (APM), Chinese Academy of Sciences, Xiao Hong Shan, Wuhan 430071, China*
- 430 ¹⁷⁴ *University of Szeged, Dóm tér 9, Szeged 6720, Hungary*
- 431 ¹⁷⁵ *Universiteit Gent, B-9000 Gent, Belgium*
- 432 ¹⁷⁶ *Cornell University, Ithaca, NY 14850, USA*
- 433 ¹⁷⁷ *University of British Columbia, Vancouver, BC V6T 1Z4, Canada*
- 434 ¹⁷⁸ *Tata Institute of Fundamental Research, Mumbai 400005, India*
- 435 ¹⁷⁹ *INAF, Osservatorio Astronomico di Capodimonte, I-80131 Napoli, Italy*
- 436 ¹⁸⁰ *The University of Mississippi, University, MS 38677, USA*
- 437 ¹⁸¹ *University of Michigan, Ann Arbor, MI 48109, USA*
- 438 ¹⁸² *Texas A&M University, College Station, TX 77843, USA*
- 439 ¹⁸³ *Department of Physics, Ulsan National Institute of Science and Technology (UNIST), Ulsu-gun, Ulsan 44919, Korea*
- 440 ¹⁸⁴ *Applied Research Laboratory, High Energy Accelerator Research Organization (KEK), Tsukuba City, Ibaraki 305-0801, Japan*
- 441 ¹⁸⁵ *Dipartimento di Fisica, Università di Trieste, I-34127 Trieste, Italy*
- 442 ¹⁸⁶ *Shanghai Astronomical Observatory, Chinese Academy of Sciences, Shanghai 200030, China*
- 443 ¹⁸⁷ *American University, Washington, D.C. 20016, USA*
- 444 ¹⁸⁸ *Faculty of Science, University of Toyama, Toyama City, Toyama 930-8555, Japan*
- 445 ¹⁸⁹ *Institute for Cosmic Ray Research (ICRR), KAGRA Observatory, The University of Tokyo, Kamioka-cho, Gifu City, Gifu 506-1205,*
- 446 *Japan*
- 447 ¹⁹⁰ *Carleton College, Northfield, MN 55057, USA*
- 448 ¹⁹¹ *University of California, Berkeley, CA 94720, USA*
- 449 ¹⁹² *Maastricht University, 6200 MD, Maastricht, Netherlands*
- 450 ¹⁹³ *College of Industrial Technology, Nihon University, Narashino City, Chiba 275-8575, Japan*
- 451 ¹⁹⁴ *Graduate School of Science and Technology, Niigata University, Nishi-ku, Niigata City, Niigata 950-2181, Japan*
- 452 ¹⁹⁵ *Department of Physics, National Taiwan Normal University, sec. 4, Taipei 116, Taiwan*
- 453 ¹⁹⁶ *Astronomy & Space Science, Chungnam National University, Yuseong-gu, Daejeon 34134, Korea, Korea*
- 454 ¹⁹⁷ *Department of Physics and Mathematics, Aoyama Gakuin University, Sagami-hara City, Kanagawa 252-5258, Japan*
- 455 ¹⁹⁸ *Kavli Institute for Astronomy and Astrophysics, Peking University, Haidian District, Beijing 100871, China*
- 456 ¹⁹⁹ *Yukawa Institute for Theoretical Physics (YITP), Kyoto University, Sakyo-ku, Kyoto City, Kyoto 606-8502, Japan*
- 457 ²⁰⁰ *Graduate School of Science and Engineering, University of Toyama, Toyama City, Toyama 930-8555, Japan*
- 458 ²⁰¹ *Department of Physics, Graduate School of Science, Osaka City University, Sumiyoshi-ku, Osaka City, Osaka 558-8585, Japan*
- 459 ²⁰² *Nambu Yoichiro Institute of Theoretical and Experimental Physics (NITEP), Osaka City University, Sumiyoshi-ku, Osaka City, Osaka*
- 460 *558-8585, Japan*
- 461 ²⁰³ *Institute of Space and Astronautical Science (JAXA), Chuo-ku, Sagami-hara City, Kanagawa 252-0222, Japan*
- 462 ²⁰⁴ *Directorate of Construction, Services & Estate Management, Mumbai 400094, India*
- 463 ²⁰⁵ *Vanderbilt University, Nashville, TN 37235, USA*
- 464 ²⁰⁶ *Universiteit Antwerpen, Prinsstraat 13, 2000 Antwerpen, Belgium*
- 465 ²⁰⁷ *University of Białystok, 15-424 Białystok, Poland*
- 466 ²⁰⁸ *Department of Physics, Ewha Womans University, Seodaemun-gu, Seoul 03760, Korea*
- 467 ²⁰⁹ *National Astronomical Observatories, Chinese Academic of Sciences, Chaoyang District, Beijing, China*
- 468 ²¹⁰ *School of Astronomy and Space Science, University of Chinese Academy of Sciences, Chaoyang District, Beijing, China*
- 469 ²¹¹ *University of Southampton, Southampton SO17 1BJ, United Kingdom*

- 470 ²¹²*Institute for Cosmic Ray Research (ICRR), The University of Tokyo, Kashiwa City, Chiba 277-8582, Japan*
471 ²¹³*Chung-Ang University, Seoul 06974, South Korea*
- 472 ²¹⁴*Institut de Física d'Altes Energies (IFAE), Barcelona Institute of Science and Technology, and ICREA, E-08193 Barcelona, Spain*
473 ²¹⁵*Graduate School of Science, Tokyo Institute of Technology, Meguro-ku, Tokyo 152-8551, Japan*
474 ²¹⁶*University of Washington Bothell, Bothell, WA 98011, USA*
475 ²¹⁷*Institute of Applied Physics, Nizhny Novgorod, 603950, Russia*
476 ²¹⁸*Ewha Womans University, Seoul 03760, South Korea*
477 ²¹⁹*Inje University Gimhae, South Gyeongsang 50834, South Korea*
478 ²²⁰*Department of Physics, Myongji University, Yongin 17058, Korea*
479 ²²¹*Korea Astronomy and Space Science Institute, Daejeon 34055, South Korea*
480 ²²²*National Institute for Mathematical Sciences, Daejeon 34047, South Korea*
481 ²²³*Ulsan National Institute of Science and Technology, Ulsan 44919, South Korea*
482 ²²⁴*Department of Physical Science, Hiroshima University, Higashihiroshima City, Hiroshima 903-0213, Japan*
483 ²²⁵*School of Physics and Astronomy, Cardiff University, Cardiff, CF24 3AA, UK*
484 ²²⁶*Institute of Astronomy, National Tsing Hua University, Hsinchu 30013, Taiwan*
485 ²²⁷*Bard College, 30 Campus Rd, Annandale-On-Hudson, NY 12504, USA*
486 ²²⁸*Institute of Mathematics, Polish Academy of Sciences, 00656 Warsaw, Poland*
487 ²²⁹*National Center for Nuclear Research, 05-400 Świerk-Otwock, Poland*
488 ²³⁰*Instituto de Física Teórica, 28049 Madrid, Spain*
489 ²³¹*Department of Physics, Nagoya University, Chikusa-ku, Nagoya, Aichi 464-8602, Japan*
490 ²³²*Université de Montréal/Polytechnique, Montreal, Quebec H3T 1J4, Canada*
491 ²³³*Laboratoire Lagrange, Université Côte d'Azur, Observatoire Côte d'Azur, CNRS, F-06304 Nice, France*
492 ²³⁴*Department of Physics, Hanyang University, Seoul 04763, Korea*
493 ²³⁵*Sungkyunkwan University, Seoul 03063, South Korea*
494 ²³⁶*NAVIER, École des Ponts, Univ Gustave Eiffel, CNRS, Marne-la-Vallée, France*
495 ²³⁷*Department of Physics, National Cheng Kung University, Tainan City 701, Taiwan*
- 496 ²³⁸*National Center for High-performance computing, National Applied Research Laboratories, Hsinchu Science Park, Hsinchu City*
497 *30076, Taiwan*
- 498 ²³⁹*Institute for High-Energy Physics, University of Amsterdam, Science Park 904, 1098 XH Amsterdam, Netherlands*
499 ²⁴⁰*NASA Marshall Space Flight Center, Huntsville, AL 35811, USA*
500 ²⁴¹*University of Washington, Seattle, WA 98195, USA*
- 501 ²⁴²*Dipartimento di Matematica e Fisica, Università degli Studi Roma Tre, I-00146 Roma, Italy*
502 ²⁴³*INFN, Sezione di Roma Tre, I-00146 Roma, Italy*
503 ²⁴⁴*ESPCI, CNRS, F-75005 Paris, France*
504 ²⁴⁵*Concordia University Wisconsin, Mequon, WI 53097, USA*
505 ²⁴⁶*Università di Camerino, Dipartimento di Fisica, I-62032 Camerino, Italy*
506 ²⁴⁷*School of Physics Science and Engineering, Tongji University, Shanghai 200092, China*
507 ²⁴⁸*Southern University and A&M College, Baton Rouge, LA 70813, USA*
508 ²⁴⁹*Centre Scientifique de Monaco, 8 quai Antoine 1er, MC-98000, Monaco*
- 509 ²⁵⁰*Institute for Photon Science and Technology, The University of Tokyo, Bunkyo-ku, Tokyo 113-8656, Japan*
510 ²⁵¹*Indian Institute of Technology Madras, Chennai 600036, India*
511 ²⁵²*Saha Institute of Nuclear Physics, Bidhannagar, West Bengal 700064, India*
- 512 ²⁵³*The Applied Electromagnetic Research Institute, National Institute of Information and Communications Technology (NICT), Koganei*
513 *City, Tokyo 184-8795, Japan*
- 514 ²⁵⁴*Institut des Hautes Etudes Scientifiques, F-91440 Bures-sur-Yvette, France*
515 ²⁵⁵*Faculty of Law, Ryukoku University, Fushimi-ku, Kyoto City, Kyoto 612-8577, Japan*
516 ²⁵⁶*Indian Institute of Science Education and Research, Kolkata, Mohanpur, West Bengal 741252, India*
- 517 ²⁵⁷*Department of Astrophysics/IMAPP, Radboud University Nijmegen, P.O. Box 9010, 6500 GL Nijmegen, Netherlands*
518 ²⁵⁸*Department of Physics, University of Notre Dame, Notre Dame, IN 46556, USA*
519 ²⁵⁹*Consiglio Nazionale delle Ricerche - Istituto dei Sistemi Complessi, Piazzale Aldo Moro 5, I-00185 Roma, Italy*
520 ²⁶⁰*Korea Astronomy and Space Science Institute (KASI), Yuseong-gu, Daejeon 34055, Korea*
521 ²⁶¹*Hobart and William Smith Colleges, Geneva, NY 14456, USA*
- 522 ²⁶²*International Institute of Physics, Universidade Federal do Rio Grande do Norte, Natal RN 59078-970, Brazil*
523 ²⁶³*Museo Storico della Fisica e Centro Studi e Ricerche "Enrico Fermi", I-00184 Roma, Italy*
524 ²⁶⁴*Lancaster University, Lancaster LA1 4YW, United Kingdom*
525 ²⁶⁵*Università di Trento, Dipartimento di Matematica, I-38123 Povo, Trento, Italy*
526 ²⁶⁶*Indian Institute of Science Education and Research, Pune, Maharashtra 411008, India*

- 527 ²⁶⁷ *Dipartimento di Fisica, Università degli Studi di Torino, I-10125 Torino, Italy*
- 528 ²⁶⁸ *Indian Institute of Technology, Palaj, Gandhinagar, Gujarat 382355, India*
- 529 ²⁶⁹ *Department of Physics, Kyoto University, Sakyou-ku, Kyoto City, Kyoto 606-8502, Japan*
- 530 ²⁷⁰ *Department of Electronic Control Engineering, National Institute of Technology, Nagaoka College, Nagaoka City, Niigata 940-8532,*
- 531 *Japan*
- 532 ²⁷¹ *Departamento de Matemática da Universidade de Aveiro and Centre for Research and Development in Mathematics and Applications,*
- 533 *Campus de Santiago, 3810-183 Aveiro, Portugal*
- 534 ²⁷² *Marquette University, 11420 W. Clybourn St., Milwaukee, WI 53233, USA*
- 535 ²⁷³ *Graduate School of Science and Engineering, Hosei University, Koganei City, Tokyo 184-8584, Japan*
- 536 ²⁷⁴ *Faculty of Science, Toho University, Funabashi City, Chiba 274-8510, Japan*
- 537 ²⁷⁵ *Faculty of Information Science and Technology, Osaka Institute of Technology, Hirakata City, Osaka 573-0196, Japan*
- 538 ²⁷⁶ *Università di Firenze, Sesto Fiorentino I-50019, Italy*
- 539 ²⁷⁷ *INAF, Osservatorio Astrofisico di Arcetri, Largo E. Fermi 5, I-50125 Firenze, Italy*
- 540 ²⁷⁸ *Indian Institute of Technology Hyderabad, Sangareddy, Khandi, Telangana 502285, India*
- 541 ²⁷⁹ *iTHEMS (Interdisciplinary Theoretical and Mathematical Sciences Program), The Institute of Physical and Chemical Research*
- 542 *(RIKEN), Wako, Saitama 351-0198, Japan*
- 543 ²⁸⁰ *INAF, Osservatorio di Astrofisica e Scienza dello Spazio, I-40129 Bologna, Italy*
- 544 ²⁸¹ *Department of Space and Astronautical Science, The Graduate University for Advanced Studies (SOKENDAI), Sagami-hara City,*
- 545 *Kanagawa 252-5210, Japan*
- 546 ²⁸² *Andrews University, Berrien Springs, MI 49104, USA*
- 547 ²⁸³ *Research Center for Space Science, Advanced Research Laboratories, Tokyo City University, Setagaya, Tokyo 158-0082, Japan*
- 548 ²⁸⁴ *Institute for Cosmic Ray Research (ICRR), Research Center for Cosmic Neutrinos (RCCN), The University of Tokyo, Kashiwa City,*
- 549 *Chiba 277-8582, Japan*
- 550 ²⁸⁵ *National Metrology Institute of Japan, National Institute of Advanced Industrial Science and Technology, Tsukuba City, Ibaraki*
- 551 *305-8568, Japan*
- 552 ²⁸⁶ *Dipartimento di Scienze Aziendali - Management and Innovation Systems (DISA-MIS), Università di Salerno, I-84084 Fisciano,*
- 553 *Salerno, Italy*
- 554 ²⁸⁷ *Van Swinderen Institute for Particle Physics and Gravity, University of Groningen, Nijenborgh 4, 9747 AG Groningen, Netherlands*
- 555 ²⁸⁸ *Faculty of Science, Department of Physics, The Chinese University of Hong Kong, Shatin, N.T., Hong Kong*
- 556 ²⁸⁹ *Vrije Universiteit Brussel, Boulevard de la Plaine 2, 1050 Ixelles, Belgium*
- 557 ²⁹⁰ *Department of Communications Engineering, National Defense Academy of Japan, Yokosuka City, Kanagawa 239-8686, Japan*
- 558 ²⁹¹ *Department of Physics, University of Florida, Gainesville, FL 32611, USA*
- 559 ²⁹² *Department of Information and Management Systems Engineering, Nagaoka University of Technology, Nagaoka City, Niigata*
- 560 *940-2188, Japan*
- 561 ²⁹³ *Vrije Universiteit Amsterdam, 1081 HV Amsterdam, Netherlands*
- 562 ²⁹⁴ *Department of Physics and Astronomy, Sejong University, Gwangjin-gu, Seoul 143-747, Korea*
- 563 ²⁹⁵ *Department of Electrophysics, National Chiao Tung University, Hsinchu, Taiwan*
- 564 ²⁹⁶ *Department of Physics, Rikkyo University, Toshima-ku, Tokyo 171-8501, Japan*
- 565 ²⁹⁷ *Department of Physics, McGill University, 3600 rue University, Montréal, QC H3A 2T8, Canada*
- 566 ²⁹⁸ *McGill Space Institute, McGill University, 3550 rue University, Montréal, QC H3A 2A7, Canada*
- 567 ²⁹⁹ *David A. Dunlap Department of Astronomy & Astrophysics, University of Toronto, 50 St. George Street, Toronto, ON M5S 3H4,*
- 568 *Canada*
- 569 ³⁰⁰ *Dunlap Institute for Astronomy & Astrophysics, University of Toronto, 50 St. George Street, Toronto, ON M5S 3H4, Canada*
- 570 ³⁰¹ *Department of Physics and Astronomy, University of British Columbia, 6224 Agricultural Road, Vancouver, BC V6T 1Z1 Canada*
- 571 ³⁰² *Department of Physics and Astronomy, West Virginia University, PO Box 6315, Morgantown, WV 26506, USA*
- 572 ³⁰³ *Center for Gravitational Waves and Cosmology, West Virginia University, Chestnut Ridge Research Building, Morgantown, WV*
- 573 *26505, USA*
- 574 ³⁰⁴ *MIT Kavli Institute for Astrophysics and Space Research, Massachusetts Institute of Technology, 77 Massachusetts Ave, Cambridge,*
- 575 *MA 02139, USA*
- 576 ³⁰⁵ *Department of Physics, Massachusetts Institute of Technology, 77 Massachusetts Ave, Cambridge, MA 02139, USA*
- 577 ³⁰⁶ *Division of Physics, Mathematics, and Astronomy, California Institute of Technology, Pasadena, CA 91125, USA*
- 578 ³⁰⁷ *McGill Space Institute Fellow*
- 579 ³⁰⁸ *FRQNT Postdoctoral Fellow*
- 580 ³⁰⁹ *Anton Pannekoek Institute for Astronomy, University of Amsterdam, Science Park 904, 1098 XH Amsterdam, The Netherlands*
- 581 ³¹⁰ *Perimeter Institute for Theoretical Physics, 31 Caroline Street N, Waterloo, ON N2S 2YL, Canada*
- 582 ³¹¹ *Department of Physics and Astronomy, University of Waterloo, Waterloo, ON N2L 3G1, Canada*
- 583 ³¹² *Sidrat Research, PO Box 73527 RPO Wychwood, Toronto, ON M6C 4A7, Canada*
- 584 ³¹³ *National Radio Astronomy Observatory, 520 Edgemont Rd, Charlottesville, VA 22903, USA*

³¹⁴*Department of Astronomy and Astrophysics, Tata Institute of Fundamental Research, Mumbai, 400005, India*

³¹⁵*National Centre for Radio Astrophysics, Post Bag 3, Ganeshkhind, Pune, 411007, India*

(Dated: October 30, 2022)

ABSTRACT

We search for gravitational-wave (GW) transients associated with fast radio bursts (FRBs) detected by the Canadian Hydrogen Intensity Mapping Experiment Fast Radio Burst Project (CHIME/FRB), during the first part of the third observing run of Advanced LIGO and Advanced Virgo (1 April 2019 15:00 UTC–1 Oct 2019 15:00 UTC). Triggers from 22 FRBs were analyzed with a search that targets compact binary coalescences with at least one neutron star component. A targeted search for generic GW transients was conducted on 40 FRBs. We find no significant evidence for a GW association in either search. Given the large uncertainties in the distances of the FRBs inferred from the dispersion measures in our sample, however, this does not conclusively exclude any progenitor models that include emission of a GW of the types searched for from any of these FRB events. We report 90% confidence lower bounds on the distance to each FRB for a range of GW progenitor models. By combining the inferred maximum distance information for each FRB with the sensitivity of the GW searches, we set upper limits on the energy emitted through GWs for a range of emission scenarios. We find values of order 10^{51} – 10^{57} erg for emission models with central GW frequencies in the range 70–3560 Hz, **which are above predicted GW emissions for the models considered**. We also find no significant coincident detection of GWs with the repeater, FRB 20200120E, which is the closest known extragalactic FRB.

1. INTRODUCTION

Fast radio bursts (FRBs) are bright millisecond duration radio pulses that have been observed out to cosmological distances, several with inferred redshifts greater than unity (Lorimer et al. 2007; Petroff et al. 2019; Cordes & Chatterjee 2019). Although intensely studied for more than a decade, the emission mechanisms and progenitor populations of FRBs are still one of the outstanding questions in astronomy.

Some FRBs have been shown to repeat (Amiri et al. 2019a; CHIME/FRB Collaboration et al. 2019; Kumar et al. 2019), and the recent association of a FRB with the Galactic magnetar SGR 1935+2154 proves that magnetars can produce FRBs (CHIME/FRB Collaboration et al. 2020; Bochenek et al. 2020). Alternative progenitors and mechanisms to produce non-repeating FRBs are still credible and have so far not been ruled out (Zhang 2020a). Data currently suggests that both repeating and non-repeating classes of FRBs have Dispersion Measures (DMs), a quantity equal to the integral of the free electron density along the line of sight, and sky locations consistent with being drawn from the same population. However, the two classes have been shown

to differ in their intrinsic temporal widths and spectral bandwidths (CHIME/FRB Collaboration et al. 2021). Whether genuine non-repeating sources have a different origin to their repeating cousins is an unresolved question.

The first discovery of an FRB was made over a decade ago by Parkes 64m radio telescope (Lorimer et al. 2007). This burst, FRB 010724 or FRB 20010724A, known as the *Lorimer burst*, first indicated an extragalactic origin for FRBs through its observed DM. This burst had a DM of 375 pc cm^{-3} , far in excess of the likely Galactic DM contribution along the line of sight (of order 45 pc cm^{-3} for this event), supporting an extragalactic origin. The precise localizations of FRB host galaxies have since unambiguously confirmed an extragalactic hypothesis (Chatterjee et al. 2017; Bannister et al. 2019; Li & Zhang 2020; Heintz et al. 2020) and constraints on the progenitor population are starting to be understood (e.g. Bhandari et al. 2020). The inferred cosmological distances for many FRBs have shown that these transients have extreme luminosities by radio standards, of the order $10^{38} - 10^{46} \text{ erg s}^{-1}$ (Zhang 2018).

Recent studies suggest a volumetric rate of order $3.5^{+5.7}_{-2.4} \times 10^4 \text{ Gpc}^{-3} \text{ yr}^{-1}$ above $10^{42} \text{ erg s}^{-1}$ (Luo et al. 2020). Up to mid-2018, around 70 FRBs had been publicly announced (Petroff et al. 2016). The majority of

* Deceased, August 2020.

the detections during this period had been made by Parkes (27 FRBs at ~ 1.5 GHz; [Champion et al. 2016](#); [Thornton et al. 2013](#)) and ASKAP (28 FRBs at central frequencies of ~ 1.3 GHz; [Bannister et al. 2017](#); [Shannon et al. 2018](#)). Other detections were contributed by telescopes including UTMOST ([Caleb et al. 2017](#)) and the Green Bank Telescope ([Masui et al. 2015](#)), each operating around 800 MHz, and Arecibo ([Spitler et al. 2014](#)), operating around ~ 1.5 GHz.

The FRB detection rate has greatly increased since the Canadian Hydrogen Intensity Mapping Experiment (CHIME) instrument ([Newburgh et al. 2014](#); [Bandura et al. 2014](#); [CHIME/FRB Collaboration 2020](#), see <https://chime-experiment.ca/>) began its commissioning phase in late 2018, and its first FRB observation run shortly after. The CHIME radio telescope observes in the frequency range 400 – 800 MHz and consists of four 20 m \times 100 m cylindrical parabolical reflectors. Its large collecting area and wide field-of-view (≈ 200 deg²) make it a valuable survey instrument for radio transients. FRB detection for this instrument has been led by the CHIME/FRB project ([CHIME/FRB Collaboration et al. 2018](#)) which published its first sample of 13 FRBs during its early commissioning phase, despite operating at a lower sensitivity and field-of-view than design specifications ([Amiri et al. 2019b](#)).

The CHIME/FRB project recently published a catalog of 535 FRBs detected during their first year of operation; this includes 62 bursts from 18 previously identified repeating sources ([CHIME/FRB Collaboration et al. 2021](#)). This is the first large collection, $\mathcal{O}(100\text{s})$, of FRBs from a homogeneous survey and represents a significant milestone in this area of study. The CHIME/FRB data is supportive of different propagation or emission mechanisms between repeaters and non-repeaters, however, it is still not clear whether all FRBs do repeat ([Ravi 2019](#)) and, significantly, the FRB emission mechanism remains unknown. There presently exist many competing FRB emission theories ([Platts et al. 2019](#)), some of which predict the accompaniment of a time-varying mass quadrupole moment, and thus, the emission of gravitational waves (GWs).

A number of studies have looked at the possibility of GW emission associated with FRBs indirectly, using radio observations to search for coherent FRB-like emissions associated with short, hard gamma-ray bursts (GRBs) ([Anderson et al. 2018](#); [Rowlinson & Anderson 2019](#); [Gourdji et al. 2020](#); [Rowlinson et al. 2020](#); [Bouwhuis et al. 2020](#)).

The identification of an FRB within the sensitive reach of GW interferometric detectors could provide conclusive proof of an association or constrain the pa-

rameters of the emission mechanisms for a given FRB. The increased population of detected FRBs from the CHIME/FRB Project therefore offers a unique chance of achieving this endeavor.

A first search for GW counterparts to transient radio sources was conducted by [Abbott et al. \(2016\)](#). This used a minimally modelled coherent search (X-Pipeline) ± 2 min around the detection time of 6 Parkes FRBs using GW data from GEO600 ([Grote 2010](#)) and initial Virgo ([Accadia et al. 2012](#)). No GW coincidences were found, but this study provided a useful framework for future searches using improved GW sensitivities.

In this paper we present the second targeted GW follow-up of FRBs using bursts detected by CHIME/FRB during the first part of the third observing run of Advanced LIGO and Advanced Virgo (O3a) ([Aasi et al. 2015](#); [Acernese et al. 2015](#)), which took place between 1 April 2019 15:00 UTC and 1 October 2019 15:00 UTC. This search uses both a generic GW transient search and a modelled search targeting coalescing binary systems.

The organization of this paper is as follows: in Section 2 we describe the motivation of this study by discussing possible GW counterparts to FRBs. We introduce the CHIME/FRB data sample in Section 3 and in Section 4 discuss the GW search methods employed; this includes an overview of both of the pipelines used in our analysis. Section 5 provides the results of the GW analysis of the FRB sample. In Section 6 we report results of a gravitational wave analysis of the repeater, FRB 20200120E, which is the closest known extragalactic FRB. Finally, in section 7 we summarize the astrophysical implications of our results and discuss future GW searches for FRB counterparts at greater GW sensitivities.

2. PROPOSED GRAVITATIONAL WAVE COUNTERPARTS TO FRBS

This section will review some of the more popular models of non-repeating and repeating FRBs that could provide plausible GW counterparts and could therefore be constrained or confirmed through GW searches. (An online theory catalog tracks new FRB models; see <https://frbtheorycat.org>).

As the millisecond durations of FRBs indicate compact emission regions, many models of non-repeating FRBs have suggested cataclysmic events, including coalescing compact objects. **As will be discussed below, the fraction of the energy budget emitted by proposed FRB emission models is comparatively small compared to $\mathcal{O}(10^{52})$ erg emitted in GWs (e.g. [Abbott et al. 2017a](#)) but high by radio standards.**

A number of studies have investigated the possibility of FRB-like emissions from binary neutron star (BNS) coalescence around the time of merger (see review in [Platts et al. 2019](#)). During this phase the magnetic fields of the NSs are synchronized to binary rotation and a coherent radiation could be generated due to magnetic braking. **The mechanism requires magnetic fields of order 10^{12} – 10^{13} Gauss and could lead to energy-loss rates of order 10^{45} erg s $^{-1}$.** The predicted FRB pulse widths are consistent with the timescale of the orbital period of the BNS just prior to coalescence ([Totani 2013](#)).

[Wang et al. \(2016\)](#) considered that an FRB could be produced during the final stages of a BNS inspiral through magnetic reconnection due to the interaction of a toroidal magnetic field, produced as the NS magnetospheres approach each other. **The predicted energy-loss rates are order 10^{42} erg s $^{-1}$ assuming magnetic fields of the order 10^{12} Gauss. One should note,** dynamic ejecta launched shortly after the final merger would produce significant opacity over a large solid angle, thus screening an FRB-type signal via absorption ([Yamasaki et al. 2018](#)). [Zhang \(2020b\)](#) has also entertained the idea that similar interactions between the two NS magnetospheres could produce repeating FRB-like coherent radio emissions decades or centuries before the final plunge.

Other mechanisms to produce prompt coherent radio emission on ms timescales include excitation of the circumbinary plasma by GWs ([Moortgat & Kuijpers 2005](#)), from dynamically-generated magnetic fields post-merger ([Pshirkov & Postnov 2010](#)) or from the collision of a GRB forward shock with the surrounding medium ([Usov & Katz 2000](#); [Sagiv & Waxman 2002](#)).

Mergers of significant fractions of BNSs are likely to give rise to millisecond magnetars ([Gao et al. 2016](#); [Margalit et al. 2019](#)), although this is highly dependent on the unknown nuclear equation of state (see [Sarin & Lasky 2021](#), for a review). If the remnant NS mass is greater than the maximum non-rotating mass, it can survive for hundreds to thousands of seconds before collapsing to form a BH ([Ravi & Lasky 2014](#)). As the magnetic field lines snap as they cross the black hole (BH) horizon, an outwardly directed magnetic shock would dissipate as a short, intense radio burst ([Falcke & Rezzolla 2014](#); [Zhang 2014](#)). **The energy in the magnetic shock can be estimated as $\mathcal{O}(10^{47})$ erg which is more than sufficient to support an FRB emission.** This model has been motivated by the observation of relatively long lived X-ray plateaus following short gamma-ray bursts (sGRBs) that exhibit an abrupt decay phase, commonly interpreted as the collapse of the nascent NS

to a BH ([Troja et al. 2007](#); [Lyons et al. 2010](#); [Rowlinson et al. 2010, 2013](#)). Such collapses are expected to occur $\lesssim 5 \times 10^4$ s after the merger ([Ravi & Lasky 2014](#)).

The detection of the intense millisecond duration radio associated with the Galactic magnetar SGR 1935+2154 ([CHIME/FRB Collaboration et al. 2020](#)) has provided significant evidence to an FRB-magnetar connection ([Popov & Postnov 2013](#)). It is known that the energy stored in rotational kinetic energy and the magnetic field of a millisecond pulsar is ample to power a repeating FRB ([Metzger et al. 2017](#)). **In terms of the energy** [Margalit et al. \(2020\)](#) used the energy loss rates of repeater FRB 20121102A to estimate an energy budget for repeaters at least 10^{47} – 10^{49} erg. **This lower limit is based on the so far observed pulses and without consideration of beaming, so could increase with further monitoring of this source** ([Petroff et al. 2022](#)).

Resonant oscillation modes in the core and crust of magnetars have been suggested to cause quasi-periodic oscillations observed in the X-ray tails of giant flares. If the process by which FRBs are created also excites non-radial modes in the magnetars, then GWs could simultaneously be produced (e.g. [Levin & van Hoven 2011](#); [Quitow-James et al. 2017](#)).

The stellar oscillation mode that couples strongest to GW emission is the fundamental f-mode. The frequency of this mode depends on the equation of state, however analyses of the tidal deformability of GW170817 are consistent with NS f-mode frequencies typically being around 2 kHz ([Abbott et al. 2017b](#); [Abbott et al. 2017](#); [Wen et al. 2019](#); [Abbott et al. 2018](#)). This is above the most sensitive frequency of the Advanced LIGO/Virgo observatories.

Early theoretical studies suggested $\sim 10^{48}$ – 10^{49} erg in GW energy emitted at around 1 – 2 kHz ([Ioka 2001](#); [Corsi & Owen 2011](#)); large enough for f-mode oscillations from Galactic magnetar flares to be observable by Advanced LIGO/Virgo. Predictions by [Levin & van Hoven \(2011\)](#); [Zink et al. \(2012\)](#) span a much lower range $\sim 10^{28}$ – 10^{38} erg suggesting lower effective energy conversion to GWs.

Other modes such as gravity modes (known as g-modes - here the restoring force is buoyancy) and r-modes (where the restoring force is the Coriolis force) emit at frequencies closer to the most sensitive range for Advanced LIGO/Virgo, however these modes couple more weakly to gravitational modes, and are therefore not likely to be detectable in association with an FRB.

3. THE CHIME/FRB SAMPLE

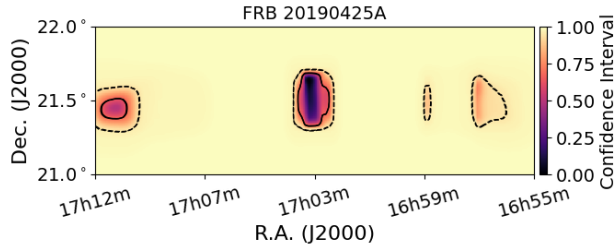


Figure 1. An example of a CHIME localization confidence interval plot for the closest non-repeating burst in our sample, FRB 190425A. The plot shows 4 localization islands and is centered at the beam with the highest SNR.

843 The CHIME/FRB data sample provided for this analysis
 844 consists of 338 bursts observed within O3a **out**
 845 **of 806 total bursts**. Out of this sample, 168 bursts
 846 have been published in the first CHIME/FRB catalog
 847 (CHIME/FRB Collaboration et al. 2021). Within the
 848 sample of 338 bursts, only events overlapping with up-
 849 time of at least one of the three GW observatories were
 850 considered for analysis. Within this sub-sample, the se-
 851 lection of bursts that were analyzed was based on the
 852 inferred distance to each burst. This selection will be
 853 described at the end of this section, after the calcula-
 854 tion of the inferred distance is described.

855 The data for each FRB includes localization informa-
 856 tion, a topocentric arrival time and a measure of the to-
 857 tal DM. For each burst, a Transient Name Server (TNS;
 858 see <https://www.wis-tns.org>) designation was also pro-
 859 vided. The TNS naming convention takes the form
 860 ‘FRB YYYYMMDDLLL’ with YYYY, MM and DD the
 861 year, month and day information in UTC and LLL a
 862 string from ‘A’ to ‘Z’, then from ‘aaa’ to ‘zzz’, indicat-
 863 ing **uploading** order on any given day.

864 The arrival time at the CHIME instrument’s loca-
 865 tion (topocentric) at 400 MHz was converted to a de-
 866 dispersed arrival time using the DM value associated
 867 with each event. This time was used as the central event
 868 time around which each GW search was conducted.

869 The localization information of each FRB is in the
 870 form of up to 5 disjoint error regions of varied morphol-
 871 ogy centered around the region with the highest SNR;
 872 each separate localization “island” has a central value
 873 and a 95% confidence uncertainty region. **An example**
 874 **is shown in Figure 1.**

875 The localization regions are reported in the
 876 sample as a list of 5 right ascension (RA) val-
 877 ues, 5 95% confidence uncertainty region sizes
 878 for the RA values, 5 declination (Dec) values,
 879 and 5 95% confidence uncertainty region sizes
 880 for the Dec values. The different approaches to these

881 localization data adopted by the generic transient and
 882 modelled search pipelines will be described in Section 4.

To determine a measure of the luminosity distance of
 each FRB we employ the Macquart relation (Macquart
 et al. 2020). This relation maps the redshift to the quan-
 tity DM_{IGM} , which is the DM contribution from extra-
 galactic gas along the line of sight; this can be obtained
 after all other contributions are subtracted. Taking into
 account all contributions to the total DM, the quantity
 DM_{T} , a measure of redshift can therefore be determined
 by solving:

$$DM_{\text{T}}(z) = DM_{\text{MW}} + DM_{\text{halo}} + DM_{\text{IGM}}(z) + DM_{\text{host}}(z)/(1+z), \quad (1)$$

883 where DM_{MW} is the Milky Way contribution to the DM
 884 along the line of sight, DM_{halo} is the contribution from
 885 the Milky Way halo and DM_{host} the contribution from
 886 the host galaxy, which is corrected by the cosmic expan-
 887 sion factor. The estimates of z are then converted to a
 888 luminosity distance assuming a ‘flat- Λ ’ cosmology with
 889 the cosmological parameters $\Omega_{\text{m}} = 0.31$, $\Omega_{\Lambda} = 0.69$ and
 890 $H_0 = 67.8 \text{ km s}^{-1} \text{ Mpc}^{-1}$ (Planck Collaboration et al.
 891 2016).

To determine redshift values for each FRB we employ
 the Bayesian Markov-Chain Monte Carlo (MCMC) sam-
 pling framework described in (Bhardwaj et al. 2021a)
 with a posterior distribution defined by:

$$\mathcal{P}(\hat{\theta} | DM_{\text{T},\text{O}}) = \frac{\mathcal{L}(DM_{\text{T},\text{O}} | \hat{\theta}) \pi(\hat{\theta})}{\mathcal{Z}}, \quad (2)$$

where $\mathcal{L}(DM_{\text{T},\text{O}} | \hat{\theta})$ is the likelihood distribution of the
 observed quantity $DM_{\text{T},\text{O}}$ given the parameters $\hat{\theta}$, $\pi(\hat{\theta})$
 are the prior distributions on $\hat{\theta}$ and \mathcal{Z} is the Bayesian
 evidence; this latter factor enters Eq. (2) as a normal-
 ization factor independent of the model parameters and
 can be ignored if one is only interested in the posterior
 distribution rather than model selection. We assume a
 Gaussian likelihood function provided as:

$$\mathcal{L}(DM_{\text{T},\text{O}} | \hat{\theta}) = \frac{1}{\sqrt{2\pi\sigma^2}} \exp \left[-\frac{(DM_{\text{T},\text{O}} - DM_{\text{T}}(\hat{\theta}))^2}{2\sigma^2} \right], \quad (3)$$

892 with σ the uncertainty on $DM_{\text{T},\text{O}}$ for each burst and
 893 DM_{T} given by Eq. (1) (Rafiei-Ravandi et al. 2021).

894 For the Milky Way contribution DM_{MW} , there is no
 895 consensus between the two popular models of Cordes &
 896 Lazio (2002) and Yao et al. (2017). Therefore, we follow
 897 Bhardwaj et al. (2021a) and assume a Gaussian prior
 898 based around the minimum of DM_{MW} from these two
 899 models along the line of sight; a standard deviation of
 900 20% of this value is also used.

The contribution DM_{halo} has been estimated in a number of studies but is quite uncertain. For example, [Yamasaki & Totani \(2020\)](#) found values of $DM_{\text{halo}} \sim 30 - 245 \text{ pc cm}^{-3}$ using a two component model. Studies by [Dolag et al. \(2015\)](#) found values between $DM_{\text{halo}} \sim 30 - 50 \text{ pc cm}^{-3}$ based on cosmological simulation and [Prochaska & Zheng \(2019\)](#) estimated values between $30 - 80 \text{ pc cm}^{-3}$. To take account of the large uncertainty in this quantity we follow [Bhardwaj et al. \(2021a\)](#) and assume a Gaussian prior such that at 3σ , DM_{halo} has a value 0 or 80 pc cm^{-3} .

The prior on DM_{IGM} assumes the parameterization $\Delta = DM_{\text{IGM}} / \langle DM_{\text{IGM}} \rangle$ with the denominator obtained through the Macquart relation. This takes the form provided in [Macquart et al. \(2020\)](#):

$$P(\Delta) = A\Delta^{-\beta} \exp\left[\frac{-(\Delta^{-\alpha} - C^2)}{2\alpha^2\sigma_{\text{DM}}^2}\right], \quad (4)$$

with $\sigma_{\text{DM}} = 0.2z^{-0.5}$ and $[\alpha, \beta] = 3$; the value of C is determined by requiring that $\langle \Delta \rangle = 1$. The form of this model is motivated by the requirement that the DM distribution approaches a Gaussian at small σ_{DM} in accordance with the Gaussianity of large scale structure. It also incorporates a skew at large σ_{DM} to reflect the possibility of over-densities along the line of sight.

Finally, for a prior on DM_{host} , we adopt a lognormal distribution with median $e^\mu = 68.2$ and logarithmic width parameter $\sigma_{\text{host}} = 0.88$ as in [Macquart et al. \(2020\)](#).

The quantities outlined above have a large range of uncertainty and there could be additional contributions e.g., circumburst material. As a result, redshift values calculated from DMs are generally taken as upper limits. We perform MCMC sampling using the `emcee` package ([Foreman-Mackey et al. 2013](#)) based on an affine-invariant sampling algorithm ([Goodman & Weare 2010](#)) using 256 walkers of 20,000 samples. Inferred values of z , and thereby luminosity distance, and their 90% credible intervals are thus determined for each FRB, based on the observed values of DM_{T} , RA and Dec, the estimated DM_{MW} along the line of sight and the priors on other DM contributions described above.

Given the large uncertainties in the distances of FRBs, we based our analysis and results on the 90% credible intervals inferred for the CHIME/FRB sample of bursts. However, for illustration, we show in [Fig. 2](#) the distribution of the median distances of the total sample of 338 FRBs that occurred during O3a. The plot shows that most events seem to occur within 1700 Mpc ($z \sim 0.3$) and 6000 Mpc ($z \sim 0.9$). The closest events in the distribution include a significant number of repeating FRBs. Due to the relatively limited range of

the GW detectors, in selecting which bursts to analyze, we first downselected the sample to all bursts from the closest 10% of CHIME/FRB non-repeating bursts that have GW detector network data available for analysis (if the recent CHIME/FRB catalog of 535 bursts is representative of the FRB population, at least around 11% of FRBs repeat). Within this selection, a coherent analysis using modelled waveforms was then conducted on a smaller subset of the closest 22 non-repeating events for which data was available from at least one interferometric GW detector, and a generic transient coherent analysis was conducted on a subset of FRBs for which data was available from at least two interferometric GW detectors. The further downselection to the final set of analyzes reported was based on two considerations. For some events, the systematic noise in the detector was too significant near the time of the burst for one or both of our two searches, and these events were then excluded. Finally, as each search requires significant personpower and computational resources, we performed searches on the remaining subset of events in order of increasing distance, until we reached a point of diminishing returns caused by the reduced overlap between the effective detection range of the GW detection network and the inferred distance to each FRB event. These considerations yielded a sample of 34 non-repeating FRBs that were analyzed by one or both types of analysis. Using the same considerations for selection, we analyzed a total of 11 repeated bursts from the closest 3 repeating sources: FRB 20180916B (7 repeat events during O3A), FRB 20180814A (2 repeat events) and FRB 20190303A (2 events). The lower and upper 90% limits of the credible intervals on the luminosity distances to each of the non-repeating FRBs analyzed are included in the tables in [Section 5](#).

4. SEARCH METHODS

Here we will provide a description of the two targeted search methods used in this paper. These are the same methods applied to search for GW events coincident with GRBs that occurred during the first ([Abbott et al. 2017](#)), second ([Abbott et al. 2019a](#)) and third ([Abbott et al. 2021](#)) Advanced LIGO and Advanced Virgo observing runs. In [Section 4.1](#) we describe the modelled search method that aims to uncover sub-threshold GW signals emitted by BNS and neutron star-black hole (NSBH) binaries (`PyGRB`; [Harry & Fairhurst 2011](#); [Williamson et al. 2014](#)), highlighting choices in analysis configuration that are unique to the followup of FRB events. In [Section 4.2](#) we discuss the search for generic GW transients (`X-Pipeline`; [Sutton et al. 2010](#); [Was et al. 2012](#)).

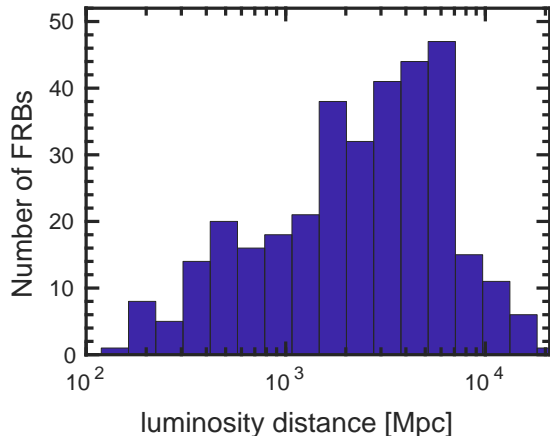


Figure 2. The distribution of inferred median distances for the CHIME/FRB data sample based on the MCMC analysis of Section 3; there is a large uncertainty in these distances, thus this distribution should be taken as only an approximate representation. The distribution peaks between 1700 Mpc ($z \sim 0.3$) and 6000 Mpc ($z \sim 0.9$). The closest non-repeating event analyzed in our sample was FRB 20190425A for which we inferred a median distance of 133 Mpc and a range [13–386] Mpc at 90% confidence; the most distant was FRB 20190601C with a median inferred distance of 914 Mpc within a range [199–1737] Mpc.

4.1. *PyGRB*- Modelled search for binary mergers

The modelled search for GWs associated with FRB events makes use of the *PyGRB* data analysis pipeline (Harry & Fairhurst 2011; Williamson et al. 2014), and the search is configured to be similar to the search for GW signals coincident with GRBs in O3a (Abbott et al. 2021). This is a coherent matched-filtering pipeline that compares the GW detector network data with a bank of pre-generated waveforms, including the inspiral of BNS and NSBH binaries. *PyGRB* uses the *PyCBC* (Nitz et al. 2020) open-source framework for distribution of the analysis of the GW data across large computing clusters, and also relies on several elements of the *LALSuite* software library (LIGO Scientific Collaboration 2018).

The *PyGRB* analysis searches the combined detector data in the range 30–1000 Hz. A set of coherent data streams is formed by combining the data from the detectors, using a sample of sky-positions in the region reported for the FRB event that is being studied. These data streams are then compared using matched filtering to the same predefined bank of waveform templates (Owen & Sathyaprakash 1999) used in the search for GWs associated with GRBs events in O3a (Abbott et al. 2021). The bank is created with a hybrid of geometric and stochastic template placement methods across

target search space (Harry et al. 2008; Brown et al. 2012; Harry et al. 2014; Capano et al. 2016; Dal Canton & Harry 2017), using a phenomenological inspiral-merger-ringdown waveform model for non-precessing point-particle binaries (*IMRPhenomD*; Husa et al. 2016; Khan et al. 2016). This bank of templates is designed to cover binary masses in the range $[1.0, 2.8]M_{\odot}$ for NSs, and $[1.0, 25.0]M_{\odot}$ for BHs. The bank also allows for aligned-spin, zero-eccentricity BNS and NSBH, with dimensionless spins in the range $[0, 0.05]$ for NSs and $[0, 0.998]$ for BHs.

Coherent matched filtering can be susceptible to loud transient noise in the detector data and can produce a high SNR (Nitz et al. 2017). To combat this, the analysis performs additional tests on each point of high SNR data, which we also refer to as triggers. These tests can either remove the trigger or re-weight the SNR using a χ^2 test. This latter test determines how well the data agrees with the template over the whole template duration. Such cuts and re-weighting significantly improve the ability of the search to distinguish a GW from many types of transient noise, thus improving the significance of real GW triggers. The final re-weighted SNR of each candidate event is used as the measure of its relative significance, or ranking statistic, within the search.

The *PyGRB* analysis searches for GW inspiral events that merge within 12 s of the de-dispersed event time of each FRB, with an asymmetric *on-source window* starting 10 s before the FRB event and ending 2 s after the event. The search window is chosen to strike a balance between maximizing the possible progenitor models through a wider window or maximizing the sensitivity of the search by using a narrower window. In this search we seek a GW signal with a merger time close to the time of the FRB, assuming the FRB results from the interaction of the two binary components.

The sensitivity of the search is governed by the comparison between the most significant event in the on-source window and the most significant event in equivalent trial searches of 12 s windows in the surrounding data, known as the *off-source trials*. These off-source trials form the background data for the search, and if a sufficient number of background trials are conducted, this allows the search to determine the significance of any candidate events in the on-source window to the level needed to make a confident detection statement by computing a false-alarm probability.

If multiple detectors are available, then additional effective background data can be produced by combining the data from the detectors with an intentional misalignment in time of at least the light-travel time across the network to ensure any detected events cannot possi-

bly be true coherent GW candidates (Williamson et al. 2014). This can be repeated for multiple possible time shifts, and in this search, these time shifts are set to match the on-source window length of 12 s. This produces fewer time shifts than a 6 s on-source window, as used in previous searches for GW associated with GRB events such as Abbott et al. (2021). This again impacts the effective significance of any detected events, because the amount of background data used by the search is limited by the amount of coherently analyzable data for all detectors in the network that surrounds the target time. Thus, a search is only conducted if a minimum of 30 min of data are available.

In the results section, we report the effective range of each search conducted as a 90% exclusion distance, D_{90} . This is calculated by first creating a set of simulated GW signals to inject into the off-source data, then attempting to find these injected signals with the standard search pipeline. The signals are injected with amplitudes appropriate for a distribution of distances between their simulated origin and the detectors, and the D_{90} distance is defined as the distance within which 90% of the injected simulated signals are recovered with a ranking statistic greater than the loudest on-source event.

Mirroring the approach taken in the O3a search for GW events associated with GRB detections (Abbott et al. 2021), the injected signals include BNS systems with dimensionless spins in the range -0.4 to 0.4 , taken from observed pulsar spins (Hessels et al. 2006), and are distributed uniformly in spin and with random orientations. Injections also include aligned spin NSBH binaries, and NSBH binaries with generically oriented spins up to 0.98 , motivated by X-ray binary observations (e.g., Özel et al. 2010; Kreidberg et al. 2012; Miller & Miller 2014). The simulated signals are intentionally generated using different GW signal models than those used in the matched-filtering template bank, to approximate the target search space difference between the approximate templates used and the true GW signals. In particular, the injected waveforms are identical to those used in the equivalent O3a GRB event follow up analysis (Abbott et al. 2021). Precessing BNS signals are simulated using the TaylorT2 time-domain, post-Newtonian inspiral approximant (SpinTaylorT2; Sathyaprakash & Dhurandhar 1991; Blanchet et al. 1996; Bohé et al. 2013; Arun et al. 2009; Mikoczi et al. 2005; Bohé et al. 2015; Mishra et al. 2016), while NSBH injected waveforms are generated assuming a point-particle effective-one-body model tuned to numerical simulations which can allow for precession effects from misaligned spins (SEOBNRv3; Pan et al. 2014; Taracchini et al. 2014; Babak et al.

2017). Again, identical to the injections used in Abbott et al. (2021), NS masses for the injections are taken between $1 M_{\odot}$ and $3 M_{\odot}$ from a normal distribution centered at $1.4 M_{\odot}$ with a standard deviation of $0.2 M_{\odot}$ (Kiziltan et al. 2013) and $0.4 M_{\odot}$ for BNS and NSBH systems, respectively. BH masses are taken to be between $3 M_{\odot}$ and $25 M_{\odot}$ from a normal distribution centered at $10 M_{\odot}$ with a standard deviation of $6 M_{\odot}$.

Although this PyGRB follow up of FRB events mirrors the search conducted for GWs associated with GRB events in O3a (Abbott et al. 2021) where appropriate, there were several differences in the choices of analysis parameters for the FRB analysis. The first major difference has been noted above, wherein a 12 s on-source window is used, which is double that of the GRB analysis. This does reduce the significance of any detected signals, but has the benefit of allowing for more progenitor models where the EM emission occurs further in time from the peak of the GW emission.

Another significant change was the method of determining the area of sky over which to search for the GW signals. The FRB data sample contains multiple localizations for each event, each with their own RA and Dec uncertainties. This effectively creates multiple patches on the sky where the source could potentially reside. The effective GW network localization capability results in 90% credible regions for detections on the order of $\approx 10 - 10000 \text{ deg}^2$, with an average of order 100 deg^2 . In contrast, the multiple O3a FRB sample localizations spanned only order 1 deg^2 in total (Abbott et al. 2020). The sensitivity of the search also did not vary significantly over the sky localizations, and so the final set of sky positions considered by the analysis was one circular patch on the sky with a size large enough to ensure coverage over all possible provided FRB localizations. **This circular region is centered on the median of the provided RA and DEC values, with a radius scaled to match either the largest position error provided or the largest RA or DEC separation between the 5 localization points, using whichever is greater.** Within this patch, the sky is sampled by creating a circular grid of sky positions such that the time-delay between grid points is kept below 0.5 s (Williamson et al. 2014). This ensures coverage of the possible sky location of the source. For each sky position, the timestream data from each GW detector is combined with the appropriately different time offsets required to form a coherent streams of data for that point on the grid. These multiple coherent time streams are finally each considered in the search.

4.2. *X-Pipeline*- Unmodelled search for generic transients

The search for generic transients is performed with the coherent analysis algorithm *X-Pipeline* (Sutton et al. 2010; Was et al. 2012). This targeted search uses the sky localization and time window for each CHIME/FRB trigger to identify consistent excess power that is coherent across the network of GW detectors. We use different search parameters in our searches for repeating and non-repeating FRB sources.

There are a number of differences between our generic transient search on non-repeated sources and those previously conducted on GRBs (Abbott et al. 2017, 2019a, 2021). As in GRB searches, the on-source time window is chosen to start 600 s before the trigger, but is extended from 60 s seconds post trigger to 120 s to allow for the possibility of GW emissions delayed relative to the FRB emission. This on-source window is also longer than the ± 120 s window employed in the previous FRB search (Abbott et al. 2016). The extended window allows for a greater number of non-Compact Binary Coalescence (CBC) sources than those considered in GRB searches and possible GW emissions from magnetars, given the recent FRB-magnetar association (CHIME/FRB Collaboration et al. 2020).

The broadband search for FRBs with *X-Pipeline* covers the range 32 Hz up to 2 kHz, the upper range being higher than the GRB search (20–500 Hz) in order to include GW emissions from oscillation modes of NSs that are likely to occur above 1 kHz, specifically f-modes (Wen et al. 2019; Ho et al. 2020). We note that above 300 Hz a $\propto f^2$ frequency dependence in energy (see later Eq. (5)) combined with the $\propto f^1$ of the noise power spectral density of the detector increases the GW energy required to enable a confident detection as $\propto f^3$. Although including high frequency data increases the computational cost, including this data allows us to set limits on a wider variety of signal models.

***X-Pipeline* processes the on-source data around each FRB trigger by combining the GW data coherently after the data is whitened by dividing by each detector’s amplitude spectrum (Abbott et al. 2020). The coherent combination is formed by taking into account the antenna response and noise level of each detector to generate a series of time–frequency maps.** The maps show the temporal evolution of the spectral properties of the signal and allow searches for clusters of pixels with excess energy significantly greater than one would expect from background noise. These clusters are referred to as *events*.

Events are given a ranking statistic based on energy and are subjected to coherent consistency tests based on the signal correlations between data in different detectors. This allows *X-Pipeline* to veto events that have properties similar to the noise background.

The surviving event with the largest ranking statistic is taken to be the best candidate for a GW detection. Its significance is quantified as the probability for the background alone to produce such an event. This is done by comparing the SNR of the trigger within the 720 s on-source to the distribution of the SNRs of the loudest triggers in the off-source trials. The off-source data are set to consist of at least 1.5 hours of coincident data from at least two detectors around the trigger time. This window is small enough to select data where the detectors should be in a similar state of operation as during the on-source interval, and large enough so that through artificial time-shifting, probabilities can be estimated at the sub-percent level.

We quantify the sensitivity of the generic transient search by injecting simulated signals into off-source data and recovering them. We account for calibration errors by jittering the amplitude and arrival time of the injections according to a Gaussian distribution representative of the typical calibration uncertainties expected in O3a. We compute the percentage of injections that have a significance higher than the best event candidate and determine the amplitude at which this percentage is above 90%; this value sets the upper limit.

As discussed in Section 3, localization information for each FRB is in the form of up to 5 non-contiguous or overlapping error regions of varied morphology. Occasionally these islands can be dominated by the uncertainty of a single island. The sky position errors can span a few degrees or more in RA. This could result in a temporal shift causing a GW signal to be rejected by a coherent consistency test (Was et al. 2012). For each island we set up a circular grid around the central location of the island, with overlapping grid points discarded. A coherent data stream is formed from the GW detector data with an appropriate time offset for each point on the grid. These data streams are then analyzed. Grid positions are large enough to cover the error radius and dense enough to ensure a maximum timing delay error, set as 1.25×10^{-4} s, is within 25% of the signal period at our frequency upper limit of 2000 Hz. This is 4 times finer than GRB searches that typically analyze data up to a frequency cutoff of 500 Hz. Using this grid approach, the antenna responses change only slightly over sky position; of order a few percent over a few degrees (Aasi et al. 2014). The responses are known to change

1278 rapidly near a null of the response; in such a case they
1279 are already negligible.

1280 A particular difference between this search and other
1281 searches focused on GRBs is the increased number of
1282 simulated waveform types used in this study. Given
1283 the uncertainty in plausible GW emissions, we consider
1284 a larger range of generic burst scenarios, using an ex-
1285 tended set of those used in both GRB and magnetar
1286 searches (Abbott et al. 2021, 2019b). Also, as we have
1287 no knowledge on whether or not FRBs are beamed along
1288 the rotation axis of the progenitor, all of our signal mod-
1289 els correspond to elliptical and random polarization.

1290 The waveforms chosen to cover the search parame-
1291 ter space are from 3 families that have different mor-
1292 phological characteristics: binary signals, generic burst-
1293 like signals and accretion disk instability (ADI) mod-
1294 els. X-Pipeline is equally adept at detecting signals
1295 whose frequency decreases with time (ADI) and sig-
1296 nals whose frequency increases with time (CBC models;
1297 Abadie et al. (2012); Abbott et al. (2017)). This paper
1298 reports the results for CBCs when obtained using the
1299 dedicated modelled search (described in Section 4.1), so
1300 we will limit our discussions here to only the latter two
1301 waveform families.

1302 The generic burst-type waveforms are described in Ta-
1303 ble 1, where we list the most important parameters (see
1304 also Abbott et al. 2019c). In all cases, to determine ex-
1305 clusion distances for this model family, we assume an op-
1306 timistic emission of energy in GWs of $E_{\text{GW}} = 10^{-2} M_{\odot} c^2$
1307 (Abbott et al. 2021). Waveforms in this family aim to
1308 capture the general characteristics of a burst of GW en-
1309 ergy:

1310 **Sine–Gaussian:** These signals have been used previ-
1311 ously to represent the GWs from stellar collapses.
1312 The models are defined in Eq. (1) of Abbott et al.
1313 (2017) with a Q factor of 9 and varying central fre-
1314 quency as shown in Table 1. They can also model
1315 f-modes in the core of a canonical NS. We there-
1316 fore also include them in the search over repeating
1317 sources, and include SG waveforms at additional
1318 frequencies listed in Table 1. In order to better
1319 constrain some models, we also include circularly
1320 polarized SG chirplets at the frequencies nearest
1321 the f-mode range (1600 Hz and 1995 Hz) in the
1322 search over repeated sources.

1323 **Ringdowns (DS2P):** These signals capture the form
1324 of damped sinusoids (DS2P) at a frequency of
1325 1500 Hz and decay constants of 100 ms and 200 ms.

1326 **White Noise Bursts (WNB):** These signals mimic
1327 broad bursts of uncorrelated white noise, time-

Table 1. The main parameters of the waveform injections used for the generic transient search. Models and their parameters have been chosen to cover as large a parameter space as possible. For all models the central frequencies are shown. We note that WNB models are defined by an additional frequency bandwidth, this parameter is shown in parenthesis. For the SG and WNB waveforms the duration parameter scales the width of the Gaussian envelope; for the DS2P models this parameter defines the decay time constant. An asterisk (*) denotes waveforms used in the repeaters search only; ^c denotes waveforms with a circular polarization.

Label	Frequency [Hz]	Duration Parameter [ms]
Sine–Gaussian Chirplets		
SG-A	70	14
SG-B	90	11
SG-C	145	6.9
SG-D	290	3.4
SG-E	650	1.5
SG-F	1100	0.9
SG-G	1600	0.6
SG-H	1995	0.5
SG-I*	2600	0.38
SG-J*	3100	0.32
SG-K*	3560	0.28
SG-L* ^c	1600	0.6
SG-M* ^c	1995	0.5
Ringdowns		
DS2P-A	1500	100
DS2P-B	1500	200
White noise bursts		
WNB-A	150 (100–200)	11
WNB-B	150 (100–200)	100
WNB-C	550 (100–1000)	11
WNB-D	550 (100–1000)	100

1328 shaped by a Gaussian envelope. We use two mod-
1329 els band-limited within frequencies of 100–200 Hz
1330 and 100–1000 Hz, and with time constants of
1331 11 ms and 100 ms.

1332 Following the predictions from oscillation modes for
1333 NS starquakes (Wen et al. 2019; Li et al. 2019), the first
1334 two waveforms in this family (SG and DS2P) have been
1335 used in the search for GWs associated with magnetar
1336 bursts (Abbott et al. 2019b).

1337 We also consider a range of Accretion Disk Instability
1338 (ADI) models. These are long-lasting waveforms which
1339 are modelled to represent the GW emissions from in-

1340 stabilities in a magnetically suspended torus around a
1341 rapidly spinning BH. The model specifics and parame-
1342 ters used to generate the five types of ADI signals, des-
1343 ignating ADI-A to ADI-E, are the same used in the pre-
1344 vious searches (see Table 1 of [Abbott et al. 2017](#)).

1345 The version of `X-Pipeline` used in this analysis has
1346 a new feature named autogating. This feature increases
1347 the sensitivity of the longer-duration ($\gtrsim 10$ s) signals,
1348 previously limited by loud background noise transients
1349 ([Abbott et al. 2021](#)). This technique gates the whitened
1350 data from a single detector if the average energy over
1351 a 1-second window exceeds a user-specified threshold.
1352 To minimize the possibility of a loud GW transient be-
1353 gated, this procedure is canceled if the average energy at
1354 the same time in any other detector exceeds the thresh-
1355 old.

1356 4.2.1. *X-pipeline Search on Repeating FRBs*

1357 A subset of 11 of the FRBs that we analyze have
1358 been identified to repeat. Repeating FRBs are **pos-**
1359 **sibly** caused by a process distinct from those that pro-
1360 duce singular FRBs; most notably they are unlikely to
1361 be associated with CBC events. We therefore only run
1362 the `X-Pipeline` generic transient search on these events,
1363 and we choose the parameters to provide maximal sensi-
1364 tivity to the GW transients that would most probably
1365 be produced by flaring magnetars.

1366 This search is similar to that for GW events associated
1367 with magnetars during the third observing run of Ad-
1368 vanced LIGO and Advanced Virgo (O3) ([Abbott et al. in
1369 preparation](#)). The frequency band of the search ranges
1370 from 50 Hz to 4000 Hz, which encapsulates the NS f-
1371 mode frequency band, but excludes the lowest frequen-
1372 cies where nonstationary noise could potentially ‘pol-
1373 lute’ the search statistics. The search spans 8 s of time
1374 centered within one second of the arrival time of the
1375 FRB to ensure optimal sensitivity at the event time.
1376 Injected waveforms are chosen to reasonably model the
1377 f-modes of a canonical NS as described in [Kokkotas et al.
1378 \(2001\)](#). This includes a series of SG chirplets with a Q
1379 factor of 9 and varying center frequencies as shown in
1380 Table 1. We also neglect to use the autogating algorithm
1381 for noise transients as described above, as its tendency
1382 is also to gate fast injections such as SG. We also inject
1383 white noise bursts to estimate sensitivity at broadband
1384 frequency ranges.

1385 4.3. *RAVEN Coincident Analysis*

1386 To perform a wider sweep of the O3a data, we also
1387 looked for coincidences between these CHIME/FRB
1388 events and existing GW candidates using the tools
1389 of the Rapid, on-source VOEvent Coincidence Mon-
1390 itor (RAVEN; [Urban 2016](#); [Cho 2019](#)) to query the

1391 Gravitational-Wave Candidate Event Database GraceDB
1392 ([Pace et al. 2012](#)). This query to GraceDB tests
1393 whether any GW candidates were found by any of the
1394 modelled or generic transient low-latency GW search
1395 pipelines within a time window around the FRB events.
1396 The queries used the same on-source search windows
1397 as our modelled and generic transient searches, with
1398 $[-10 \text{ s}, +2 \text{ s}]$ and $[-600 \text{ s}, +120 \text{ s}]$ windows around the
1399 FRB triggers, respectively. We then computed the joint
1400 false-alarm rate of any coincident GW candidate within
1401 these windows using the overall rate of FRB events in
1402 the CHIME/FRB sample calculated across the full span
1403 of the O3a observing run and the false-alarm rate of the
1404 GW candidate. **The joint false-alarm-rates were
1405 compared against thresholds of around 6/year
1406 and 1/year for modelled and generic transient
1407 searches respectively. This analysis, although
1408 not as sensitive as a targeted search, is a strat-
1409 egy that allows us to perform a broad search
1410 across O3a data for possible coincidences missed
1411 by our analysis.**

1412 5. RESULTS OF ANALYSIS

1413 5.1. *Analysis Subsample*

1414 We performed two different searches: for non-
1415 repeating FRBs, a `PyGRB` modelled search was com-
1416 pleted on a total of 22 FRB events and an `X-Pipeline`
1417 search for generic transient signals was completed on a
1418 total of 29 non-repeaters and 11 repeating FRBs.

1419 5.2. *The false-alarm probability (p -value) distribution*

1420 The searches conducted for GW counterparts returned
1421 no likely GW signals in association with any of the an-
1422 alyzed repeating or non-repeating FRB events.

1423 The most significant events found by the `PyGRB` search
1424 and the `X-Pipeline` search had p -values of 3.74×10^{-2}
1425 and 1.90×10^{-2} , respectively. For the `X-Pipeline`
1426 analysis of the repeating FRBs, the lowest p -value was
1427 1.3×10^{-1} , corresponding to the repeat FRB 20190702B
1428 of burst FRB 20190303A, for which we analyzed 2 burst
1429 events.

1430 The cumulative p -value distributions from both search
1431 methods are shown in Fig. 3 and Fig. 4. In both fig-
1432 ures, the dashed lines indicate the expected background
1433 distribution under the no-signal hypothesis, and the dot-
1434 ted lines indicate the 90% confidence band around the
1435 no-signal hypothesis.

1436 5.3. *Exclusion Distance Results*

1437 Fig. 5 shows the cumulative 90% exclusion distances
1438 for the 22 FRBs followed up with the modelled search.
1439 The lowest exclusion distances, of order 40 Mpc, were

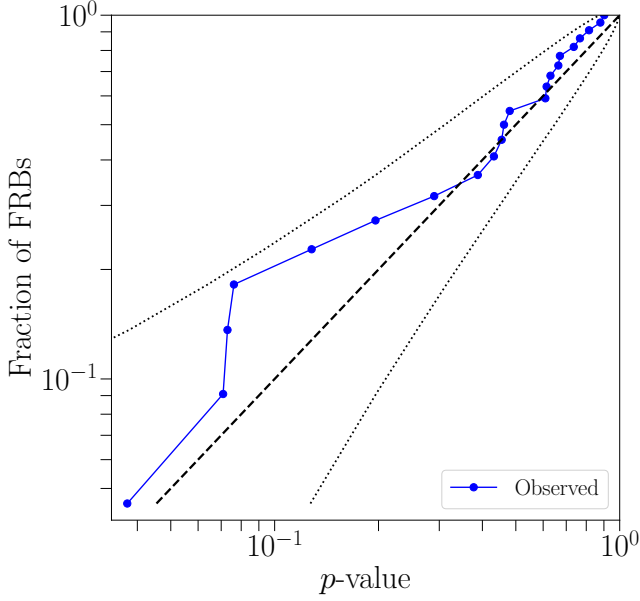


Figure 3. The cumulative distribution of p -values for the loudest on-source events for the modelled search in O3a around CHIME/FRB data. The dashed line indicates an expected uniform distribution of p -values under a no-signal hypothesis, with the corresponding 90% confidence band shown by the dotted lines.

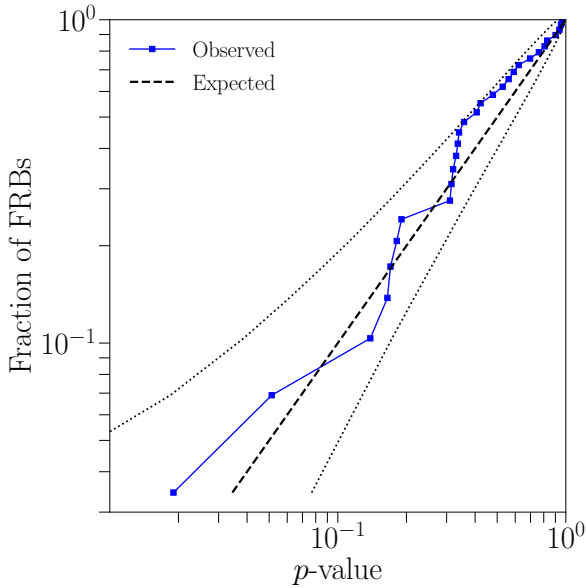


Figure 4. The cumulative distribution of p -values for the loudest events from the generic transient search for transient GWs associated with 29 non-repeating CHIME/FRB bursts. The dashed line represents the expected distribution under the no-signal hypothesis, with the 90% bands shown as dotted lines.

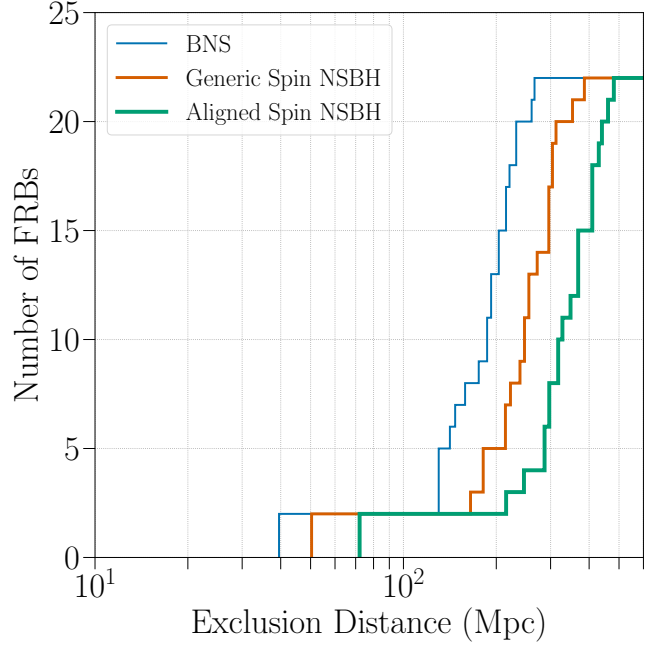


Figure 5. Cumulative histograms of the 90% confidence exclusion distances, D_{90} , for the 22 CHIME/FRB bursts followed up by the modelled search. The blue line shows generically spinning BNS models, the orange line shows generically spinning NSBH models, and the thick green line shows aligned spin NSBH models. We define D_{90} as the distance within which 90% of the simulated GW signals injected into the off-source data were recovered with a significance greater than the most significant on-source trigger.

1440 obtained for FRBs that occurred during times in which
1441 only Virgo data was available.

1442 For each of the three simulated signal classes consid-
1443 ered in the modelled search, we quote the median of
1444 the D_{90} results in the top row of Table 2; we see values
1445 of the order of 190 Mpc for BNS and around 260 Mpc
1446 (350 Mpc) for NSBH with generic (aligned) spins.

1447 Fig. 6 provides the cumulative 90% exclusion dis-
1448 tances for 29 non-repeating FRBs considered in the
1449 generic transient search. This plot shows three represen-
1450 tative burst models; ADI-A, SG-C and a WNB-C; the
1451 latter two have central frequencies of 145 Hz and 550 Hz
1452 respectively. Based on a standard $E_{\text{GW}} \sim 10^{-2} M_{\odot} c^2$ of
1453 emitted GW energy, there is a noticeable offset between
1454 the SG and the other two GW burst models. For the
1455 ADI-A waveform model, this is due to the energy of the
1456 former being distributed over a longer signal duration,
1457 of order ~ 40 s; for the WNB-C model, this effect is
1458 due to a significant portion of its energy content being
1459 at higher frequency where detector performance is more
1460 comparatively limited.

1461 The lower rows of Table 2 show the median of the
1462 D_{90} estimates for all other waveforms considered by the

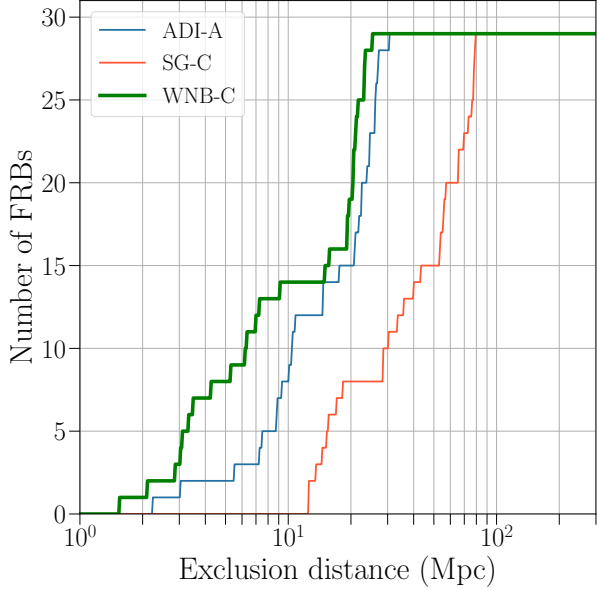


Figure 6. Cumulative histograms of the 90% confidence exclusion distances, D_{90} , for SG model C (orange line), accretion disk instability (ADI) signal model A (blue line) and white noise burst (WNB) model C (green, thick line). The quantity has the same definition as described in Fig. 5.

Table 2. Median values for the 90% confidence level exclusion distances, D_{90} . Modelled search results are shown for three classes of BNS progenitor model, and generic transient search results are shown for models described in Table 1.

Modelled search	NSBH		NSBH			
	BNS	Generic Spins	Aligned Spins			
D_{90} [Mpc]	191.9	256.6	345.1			
Unmodelled search	SG A	SG B	SG C	SG D		
D_{90} [Mpc]	77.9	63.3	43.7	24.9		
Unmodelled search	SG E	SG F	SG G	SG H		
D_{90} [Mpc]	6.8	2.3	1.2	0.5		
Unmodelled search	DS2P A	DS2P B	WNB A	WNB B	WNB C	WNB D
D_{90} [Mpc]	0.7	0.7	66.4	71.7	15.2	9.2
Unmodelled search	ADI A	ADI B	ADI C	ADI D	ADI E	
D_{90} [Mpc]	17.6	64.9	23.1	8.4	25.7	

generic transient search. We see that SG models spanning central frequencies 70 Hz to 2000 Hz have corresponding median values of D_{90} in the range 78 Mpc to 0.5 Mpc; the latter models' performance diminished at higher frequency through detector response. This is also clearly evident for the DS2P ringdown models, which are more likely to encounter a transient burst of noise than SG models due to their longer durations. Similarly, the median D_{90} values for the higher frequency WNB models are lower in comparison with the lower frequency models (WNB-A and WNB-B). These median D_{90} values of the 150 Hz and 550 Hz models differ by around a factor of at least 4. Overall, the median D_{90} varies within a range approaching 2 orders of magnitude, reflecting the wide range of models used in the analysis.

In comparison with D_{90} values obtained in the O3a GRB paper (Abbott et al. 2021) the values in Table 2 are almost systematically a factor of 2 smaller for the SG and ADI models used in that study. We find that this is a result of the sky locations surveyed by CHIME corresponding with a region of weak sensitivity for the Virgo interferometric detector, due to their relative locations on the surface of the Earth. The average antenna responses for the LIGO Hanford (H1) and LIGO Livingston (L1) detectors are of order 0.72 and 0.65 respectively; the same metric for the V1 instrument is 0.28. This has a severe effect when V1 is one of only two detectors in a network, a situation that has occurred 55% of the time for the generic transient analysis of non-repeating FRBs. Looking ahead, this type of sensitivity bias will be a feature of future searches for CHIME/FRB triggers, as well as surveys by other facilities, depending on their location on the Earth.

In Table 3 we present the exclusion distances achieved for each of the FRBs analyzed in our joint analysis. For the modelled search we quote values from each of the 3 classes of compact binary progenitor models considered. For the generic transient search we present values of D_{90} for a representative sample of SG, ADI, DS2P and WNB models. We also provide information relating to the times and positions of these events as well as values of the DM, and the inferred 90% credible intervals on the luminosity distance. Table 3 allows comparison of the inferred luminosity distances of each FRB with the D_{90} value for different searches.

Table 3. Details of the FRB sample and the 90% exclusion distances for each of the events considered in this analysis. The TNS name is provided in the first column. The Network column lists the GW detector network used: H1 = LIGO Hanford, L1 = LIGO Livingston, V1 = Virgo. The total DM for each FRB is listed in the DM column and the 90% credible intervals on the luminosity distance of each burst are provided in columns $D_{L\text{-Low}}$ and $D_{L\text{-High}}$. Where the generic transient search (Section 4.2) and the modelled search (Section 4.1) used a different IFO network, the network used by the generic transient search is shown in parentheses. The last 8 columns show the 90% confidence exclusion distances for each FRB (D_{90}) for the following emission scenarios: BNS, generic and aligned spin NSBH from the modelled search, and from the generic transient search, SG-C, SG-F, ADI-A, DS2P-A and WNB-C; for the latter 5 types of GW bursts we assume a total radiated energy $E_{\text{GW}} = 10^{-2} M_{\odot} c^2$.

FRB Name	UTC Time	R.A.	Dec.	Network	DM [pc cm^{-3}]	$D_{L\text{-Low}}$ [Mpc]	$D_{L\text{-High}}$ [Mpc]	D_{90} [Mpc]													
								BNS	Generic	Aligned	SG	SG	F	A	A	C	A	C			
FRB 20190410A	12:19:41	17 ^h 33 ^m 43 ^s	-2°10'	L1V1	270	60	960	160	190	300	36	1.1	15	0.57	6.4	-	-	-	-	-	-
FRB 20190418A	22:34:17	4 ^h 21 ^m 07 ^s	15°27'	V1	180	27	610	40	50	72	-	-	-	-	-	-	-	-	-	-	-
FRB 20190419B	22:38:24	17 ^h 02 ^m 02 ^s	86°44'	L1V1	170	25	580	130	170	250	34	1.1	10	0.5	6.2	-	-	-	-	-	-
FRB 20190423B	13:51:43	19 ^h 54 ^m 44 ^s	26°19'	H1V1	590	58	1700	190	250	320	13	0.33	5.6	0.16	3.1	-	-	-	-	-	-
FRB 20190425A	10:47:49	17 ^h 02 ^m 47 ^s	21°30'	H1L1V1	130	13	390	240	390	440	66	3.2	27	0.13	21	-	-	-	-	-	-
FRB 20190517B	20:33:37	4 ^h 16 ^m 49 ^s	73°10'	V1	190	20	540	130	230	300	-	-	-	-	-	-	-	-	-	-	-
FRB 20190517C	22:06:34	5 ^h 50 ^m 57 ^s	26°34'	L1V1	340	44	1000	-	-	-	40	1.3	10	0.72	7.4	-	-	-	-	-	-
FRB 20190518D	09:04:35	12 ^h 06 ^m 50 ^s	89°25'	H1L1	200	62	850	140	190	220	54	3.2	21	1	16	-	-	-	-	-	-
FRB 20190531B	08:47:40	17 ^h 31 ^m 26 ^s	49°18'	L1V1	170	37	680	210	310	370	56	3.5	23	2.1	20	-	-	-	-	-	-
FRB 20190601C	21:13:28	5 ^h 55 ^m 06 ^s	28°28'	H1L1V1	420	200	1700	-	-	-	66	3.2	21	1.1	21	-	-	-	-	-	-
FRB 20190604G	23:12:19	8 ^h 03 ^m 13 ^s	59°32'	L1V1	230	97	1100	-	-	-	14	0.47	8.8	0.3	1.6	-	-	-	-	-	-
FRB 20190605C	02:20:41	11 ^h 14 ^m 04 ^s	-5°18'	L1V1	190	68	890	190	260	370	29	0.94	15	0.59	5.4	-	-	-	-	-	-
FRB 20190606B	22:19:30	7 ^h 14 ^m 42 ^s	86°58'	H1L1V1	280	170	1500	-	-	-	44	2.3	18	0.95	15	-	-	-	-	-	-
FRB 20190611A	18:52:42	4 ^h 05 ^m 12 ^s	73°37'	V1	200	19	550	43	57	72	-	-	-	-	-	-	-	-	-	-	-
FRB 20190612B	05:30:37	14 ^h 48 ^m 53 ^s	4°21'	H1L1	190	65	920	220	300	410	70	3.3	26	1.1	21	-	-	-	-	-	-
FRB 20190613B	18:56:15	4 ^h 23 ^m 08 ^s	42°37'	H1L1V1	290	28	780	270	320	470	78	4.3	28	1.5	23	-	-	-	-	-	-
FRB 20190616A	05:56:30	15 ^h 34 ^m 04 ^s	34°21'	H1V1	210	110	1100	-	-	-	17	0.64	9	0.31	4.3	-	-	-	-	-	-
FRB 20190617A	02:12:33	11 ^h 49 ^m 13 ^s	83°50'	H1L1V1	200	62	870	210	310	420	54	2.9	23	1.4	19	-	-	-	-	-	-
FRB 20190618A	11:42:06	21 ^h 24 ^m 28 ^s	25°25'	H1L1	230	78	960	270	360	480	80	4.3	25	1.6	26	-	-	-	-	-	-
FRB 20190621A	02:21:17	12 ^h 06 ^m 36 ^s	74°43'	L1V1	200	78	980	150	220	300	15	0.41	2.2	0.31	2.9	-	-	-	-	-	-
FRB 20190624B	22:11:00	20 ^h 01 ^m 07 ^s	73°34'	H1V1	210	47	820	-	-	-	30	1.3	7.5	0.45	9.2	-	-	-	-	-	-
FRB 20190710A	22:09:19	9 ^h 26 ^m 32 ^s	63°06'	H1L1	200	89	1000	-	-	-	78	4.3	31	1.9	23	-	-	-	-	-	-
FRB 20190713A	02:19:56	1 ^h 35 ^m 49 ^s	72°53'	H1V1	340	140	1400	-	-	-	29	0.9	11	0.39	7	-	-	-	-	-	-
FRB 20190718A	01:11:16	13 ^h 04 ^m 18 ^s	74°14'	H1L1	200	72	970	220	300	410	58	3.5	25	1.6	21	-	-	-	-	-	-
FRB 20190722A	18:30:18	6 ^h 35 ^m 11 ^s	64°17'	L1V1	250	98	1100	-	-	-	18	0.65	11	0.39	2.1	-	-	-	-	-	-

D_{90} [Mpc]

FRB Name	UTC Time	R.A.	Dec.	Network	DM [pc cm ⁻³]	D_L -Low [Mpc]	D_L -High [Mpc]	BNS	Generic NSBH	Aligned BHNS	SG		SG		WNB
											C	F	A	C	
FRB 20190812A	04:35:08	17 ^h 53 ^m 14 ^s	50°48'	HIL1V1	250	190	1400	-	-	-	79	4.1	24	1.5	24
FRB 20190903A	12:25:19	3 ^h 12 ^m 01 ^s	21°25'	L1V1	210	67	930	180	260	360	13	0.33	7.3	0.27	3.1
FRB 20190912A	00:50:21	16 ^h 13 ^m 58 ^s	22°13'	L1V1	210	98	1100	-	-	-	15	0.46	9.4	0.29	3.5
FRB 20190912B	08:51:31	0 ^h 15 ^m 57 ^s	6°12'	H1L1	130	23	490	240	300	440	74	3.6	27	1.1	21
FRB 20190912C	09:46:46	1 ^h 13 ^m 16 ^s	67°08'	H1	340	42	1000	190	240	320	-	-	-	-	-
FRB 20190913A	15:11:12	6 ^h 40 ^m 02 ^s	39°39'	L1	230	32	710	200	250	330	-	-	-	-	-
FRB 20190922A	00:11:04	16 ^h 14 ^m 10 ^s	68°48'	H1V1	200	66	960	140	220	290	16	0.53	3.1	0.19	3.4
FRB 20190928A	21:32:10	14 ^h 00 ^m 25 ^s	80°06'	HIL1V1	140	20	510	220	270	370	57	3	22	1.1	19
FRB 20190929B	13:32:01	6 ^h 02 ^m 53 ^s	11°51'	HIL1V1	380	150	1500	-	-	-	77	3.9	26	1.7	22

Fig. 7 compares the D_{90} values for the BNS and NSBH (with generic spin) emission models with the 90% credible intervals on D_L inferred by the MCMC analysis. The plot shows the FRB sample in order of increasing distance. No event can be fully excluded from any of the models we have considered for this search, because there is still a sufficient region of space from which the FRB events could have originated that is outside the detection range of the searches performed.

5.4. RAVEN Analysis Results

As described in Section 4.3, two RAVEN coincidence searches were completed with differing time windows, $[-600 \text{ s}, +120 \text{ s}]$ for the generic transient search and $[-10 \text{ s}, +2 \text{ s}]$ for the modelled search. The generic transient search found 8 coincidences and the modelled search found 1 coincidence. However, none of these were of sufficient significance, as determined by the computed joint false-alarm rate from the two samples, to be distinguished from random coincidences. All of the FRBs in these coincidences had distances that were well beyond the values of D_{90} obtained, with the exception being FRB 20190518E, a repeat of burst FRB 20190518A, with 9 episodes occurring during O3a. Of these 9 repeating episodes, 7 were also analyzed using our generic transient search method, as described earlier. Again, none of the repeating episodes returned a significant false-alarm probability, with the minimum p -value across the search of repeating FRB events equal to 1.3×10^{-1} .

5.5. Upper Limits on GW Energy

A measure of the inferred distance to a FRB source also allows one to place constraints on the energy carried in a burst of GWs. The GW energy, E_{GW} , emitted by an elliptically polarized GW burst signal can be related to the root-sum-square signal amplitude h_{rSS} and the central frequency of the source, f_0 , through (Sutton 2013):

$$E_{\text{GW}} = \frac{2}{5} \frac{\pi^2 c^3}{G} D_L^2 f_0^2 h_{\text{rSS}}^2, \quad (5)$$

where D_L is the luminosity distance to the source. As the DMs of FRBs provide a measure of the maximum distance, one can use Eq. (5) to place 90% upper limits on the GW energy emitted by each FRB source, $E_{\text{GW}}^{90\%}$. This estimate, calculated using $h_{\text{rSS}}^{90\%}$, the 90% detection upper limit on the root-sum-squared GW amplitude, is highly dependent on the detector sensitivity and antenna factors at the time of the FRB as well as the central frequency of the simulated waveform injections.

Table A1 and Table A2 provide the upper limits on $E_{\text{GW}}^{90\%}$ for SG models and DS2P or WNB GW burst mod-

els respectively. These limits assume that the FRB distances are at the lower limits of their inferred distance ranges. Given a large range of models, and since this quantity scales as $h_{\text{rSS}}^2 f_0^2$, one would expect the lower frequency models to provide the most constraining limits. For SG models, the most constraining estimate was 2.5×10^{50} erg for the 70 Hz SG-A model and for the highest frequency model considered, SG-H at 1995 Hz, the upper limit was 7.9×10^{54} erg. These values were obtained for the closest inferred burst in the sample, FRB 20190425A. The same burst yielded upper limit values in the range $4.8 - 470 \times 10^{50}$ erg for the WNB model. The DS2P model gave the best constraints, $5.8 - 6.4 \times 10^{54}$ erg, for FRB 20190531B.

For completeness, in Table A3 and Table A4, we also provide less constraining limits on $E_{\text{GW}}^{90\%}$ based on the upper credible intervals on the distance of each FRB.

Table 4 lists the repeating bursts that were analyzed in the generic transient search. The most sensitive counterpart to a repeating FRB was for CHIME/FRB event FRB20190825A. The SG injection centered at 1600 Hz (which most closely models an f-mode) was recovered 90% of the time at $h_{\text{rSS}} = 2.62 \times 10^{-22}$. The distance to this event is 148.1 Mpc to 149.9 Mpc. This corresponds to an energy upper limit range of 5.83×10^{55} erg to 5.98×10^{55} erg.

These estimates are well above predictions of the GW emissions through the NS's fundamental f-mode discussed in section 2.

6. THE M81 REPEATER FRB 20200120E

A repeater, FRB 20200120E, which was discovered by CHIME/FRB on 20 Jan 2020, overlaps with the second part of the third observing run of Advanced LIGO and Advanced Virgo (O3b) **which took place between 1 October 2019 15:00 UTC and 27 March 2020 15:00 UTC**. This burst is at 3.6 Mpc, the closest extragalactic FRB so far discovered (Bhardwaj et al. 2021b). This event was shown to be conclusively associated with a globular cluster in the M81 galactic system (Kirsten et al. 2021) which supports the possibility that it was formed from an evolved stellar population such as a compact binary system. Due to the proximity and significance of this burst, we discuss it in this paper, despite it being discovered after O3a.

The burst FRB 20200120E was shown to repeat at least 4 times. Two of the repeats occurred after O3b; another episode, despite being consistent with the localization of the other associated bursts, had no intensity data saved. Therefore, we discuss here only the initial burst FRB 20200120E, for which GW data exists.

Table 4. Details of the 3 repeating FRBs analyzed in the generic transient search and their various repeating episodes. The TNS name is provided in the first column. The Network column lists the GW detector network used: H1 = LIGO Hanford, L1 = LIGO Livingston, V1 = Virgo. The total DM for each FRB is listed in the DM column and the 90% credible intervals on the luminosity distance are provided in columns D_L -low and D_L -High. 11 total events were analyzed for the three different FRB repeaters considered. For FRB 20190518A and its associated repeats, we list only the distance of [Marcote et al. \(2020\)](#) obtained by galaxy localization.

FRB Name	UTC Time [s]	R.A.	Dec.	Network	DM [pc cm ⁻³]	D_L -Low [Mpc]	D_L -high [Mpc]
FRB20190817A	14:39:52	4 ^h 21 ^m 08 ^s	73°47′	H1L1V1	190	19	540
FRB20190929C	11:58:29	4 ^h 22 ^m 25 ^s	73°40′	H1L1V1	190	21	550
FRB20190518A	18:13:33	1 ^h 58 ^m 14 ^s	65°46′	L1V1	350.5	148.1	149.9
FRB20190518E	18:20:57	1 ^h 57 ^m 50 ^s	65°43′	L1V1	350.0	148.1	149.9
FRB20190519A	17:50:16	1 ^h 43 ^m 44 ^s	65°48′	H1V1	350.0	148.1	149.9
FRB20190519C	18:10:41	1 ^h 58 ^m 00 ^s	65°47′	H1V1	348.8	148.1	149.9
FRB20190809A	12:50:40	1 ^h 58 ^m 16 ^s	65°43′	H1L1	356.2	148.1	149.9
FRB20190825A	11:48:18	1 ^h 58 ^m 07 ^s	65°42′	H1L1	349.6	148.1	149.9
FRB20190825B	11:51:54	1 ^h 58 ^m 04 ^s	65°23′	H1L1	349.9	148.1	149.9
FRB20190421A	08:00:04	13 ^h 51 ^m 57 ^s	48°10′	H1L1V1	230	130	1300
FRB20190702B	03:14:36	13 ^h 52 ^m 25 ^s	48°15′	L1V1	220	130	1300

At the time of FRB20200120E, only H1 data was available, thus a generic transient search was not conducted. Likewise, since this is a repeating event, it does not pass our criteria for conducting a modelled search. Due to these restrictions, only a RAVEN coincidence search was conducted within a $[-6000, +6000]$ s time window. No coincidences were found with sufficient significance as determined by the coincident false-alarm rate. Given the relative close proximity of this burst, further repeat emissions will be of interest for GW follow-up during the fourth observing run of Advanced LIGO, Advanced Virgo and Kagra (O4) ([Abbott et al. 2020](#)) **when constraints on the energy emitted in GWs will be of order 10^{50} at around 500Hz.**

7. CONCLUSIONS

We performed a targeted search for GWs associated with FRBs detected by the CHIME/FRB project during O3a. As the sources of non-repeating FRBs are currently not known, we ran both a modelled search for BNS and NSBH signals ([Harry & Fairhurst 2011](#); [Williamson et al. 2014](#)) and a generic transient search for generic GW transient signals ([Sutton et al. 2010](#); [Was et al. 2012](#)).

Our searches found no significant GW event candidates in association with the analyzed FRBs. We set 90% confidence lower bounds on the distances to FRB progenitors for several different emission models. Additionally, we present 90% credible intervals on the luminosity distance, D_L , inferred from the DM measurement of each FRB source.

The D_L information can be used to test models based on the simulated injections used for calculating the D_{90} values of each FRB. However, the significant uncertainties in the relative contributions to the total DM for each FRB produce relatively wide credible intervals for the D_L posteriors. We find no FRB event can be fully excluded from any of the models we have considered due to some posterior support on D_L existing for the FRB outside the detection range of the analyzes performed.

The results however, as illustrated in [Fig. 7](#), indicate that the GW network’s detection range is advancing into cosmological volumes where FRB emissions are expected. This is encouraging as we look forward to future GW searches at higher sensitivity. Furthermore, the redshifts obtained from the ongoing efforts to localize host galaxies (there are currently 18 FRBs with an associated host galaxy (see <http://frbhosts.org/>) could significantly improve the chances of constraining progenitor populations ([Heintz et al. 2020](#); [Bhandari et al. 2021](#)).

The distance estimates for each FRB allowed us to place 90% upper limits on the GW energy emitted by each FRB source, $E_{\text{GW}}^{90\%}$. For each non-repeating FRB analyzed with a generic transient search, we provided limits on $E_{\text{GW}}^{90\%}$ for a range of emission models. Repeating FRBs were also analyzed to determine 90% upper limits on the energy emitted through GWs. For the most sensitive repeating FRB analysis in our sample we find an energy upper limit range of 5.83×10^{54} erg to 5.98×10^{55} erg, well above the predictions for GW emissions from the fundamental f-modes of NSs. Based on

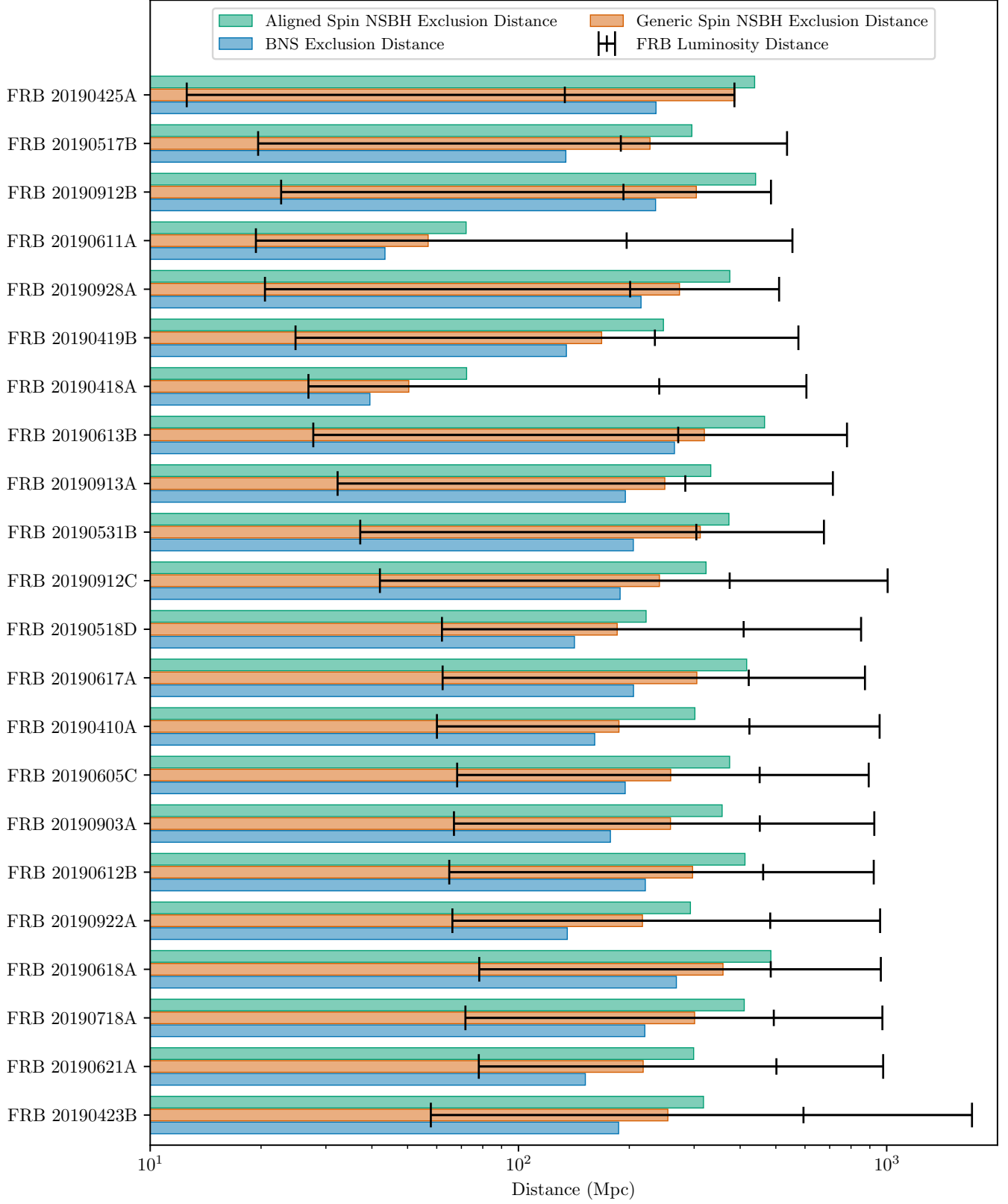


Figure 7. Lower limits on the 90% confidence level exclusion distances for BNS (lower bar), generic spin NSBH (middle bar), and aligned spin NSBH (upper bar) progenitor systems are shown as found by the modelled search. These are compared to the 90% credible intervals (whisker plot) on the D_L posterior determined by the MCMC method for the FRBs considered in this study.

Equation 5, an FRB event such as that associated with SGR 1935+2154 occurring during O3a would have allowed the search to probe the more optimistic of these estimates allowing limits, $E_{\text{GW}} \sim 10^{47}$ erg, assuming a generic burst waveform emitting at roughly 1 kHz at 10 kpc.

We also analyzed the repeater, FRB 20200120E, discovered on 20 Jan 2020 during O3b. A RAVEN (Urban 2016; Cho 2019) coincidence search for any previously detected compact binary coalescence GW events was conducted within a $[-6000, +6000]$ s time window around the first burst of this repeater. No coincidences were found with sufficient significance to be distinguished from random coincidences, as determined by the computed joint false-alarm rate from the two samples.

A comparison of the expected volumetric rates is one avenue to yield insights on possible associations between two transient source populations. Analysis of the most recent Gravitational Wave Transient Catalog 3 (GWTC-3 The LIGO Scientific Collaboration et al. 2021a,b) has inferred merger rates in the ranges 10–1700 $\text{Gpc}^{-3} \text{yr}^{-1}$ for BNS and 7.8–140 for NSBH populations. These estimates are significantly lower than estimates of the FRB rate $3.5_{-2.4}^{+5.7} \times 10^4 \text{Gpc}^{-3} \text{yr}^{-1}$ provided by Luo et al. (2020) for sources above $10^{42} \text{erg s}^{-1}$. Based on these numbers, the percentage of BNS events that could possibly be associated with FRBs is in the range 0.01–17 % and for NSBH sources, 0.008–3 %. As noted by (Luo et al. 2020), if BNS/NSBH sources were only associated with FRBs from the high end of the luminosity function ($> 10^{43} \text{erg s}^{-1}$) such rates could be comparable.

However, there are a number of unknown factors that complicate reconciling the GW and FRB source populations; these include the proportion of FRBs that may repeat or the possible effects of beaming (Ravi 2019; Connor et al. 2020).

Probing the local population of FRBs through targeted searches, the strategy adopted in this study, can constrain associations between GW sources and FRBs. The distance uncertainties in the FRB sample are a particular obstacle and ongoing efforts to identify FRB host galaxies (Chatterjee et al. 2017) could provide a valuable prior information for FRBs discovered within the BNS/NSBH detection range of future searches.

CHIME/FRB is deploying a set of Outrigger telescopes located at sufficient distances to al-

low autonomous very-long-baseline interferometry on CHIME/FRB detected bursts (Mena-Parra et al. 2022; Cassanelli et al. 2022). This development promises sub-arcsecond localisations on hundreds of FRBs/year allowing host galaxy identification and redshift determination through optical follow-ups or through cross matching of positional data with photometric galaxy surveys (Shin et al. 2022). The resulting sample of FRBs at low-redshift will be a significant development for GW detection networks, particularly as the sensitive volume increases with future observation runs and should allow targeted searches to obtain statistical evidence towards supporting or ruling out GW-FRB associations.

This material is based upon work supported by NSF’s LIGO Laboratory which is a major facility fully funded by the National Science Foundation. The authors also gratefully acknowledge the support of the Science and Technology Facilities Council (STFC) of the United Kingdom, the Max-Planck-Society (MPS), and the State of Niedersachsen/Germany for support of the construction of Advanced LIGO and construction and operation of the GEO 600 detector. Additional support for Advanced LIGO was provided by the Australian Research Council. The authors gratefully acknowledge the Italian Istituto Nazionale di Fisica Nucleare (INFN), the French Centre National de la Recherche Scientifique (CNRS) and the Netherlands Organization for Scientific Research (NWO), for the construction and operation of the Virgo detector and the creation and support of the EGO consortium. The authors also gratefully acknowledge research support from these agencies as well as by the Council of Scientific and Industrial Research of India, the Department of Science and Technology, India, the Science & Engineering Research Board (SERB), India, the Ministry of Human Resource Development, India, the Spanish Agencia Estatal de Investigación (AEI), the Spanish Ministerio de Ciencia e Innovación and Ministerio de Universidades, the Conselleria de Fons Europeus, Universitat i Cultura and the Direcció General de Política Universitaria i Recerca del Govern de les Illes Balears, the Conselleria d’Innovació, Universitats, Ciència i Societat Digital de la Generalitat Valenciana and the CERCA Programme Generalitat de Catalunya, Spain, the National Science Centre of Poland and the European Union – European Regional Development Fund; Foundation for Polish Science (FNP), the Swiss National Science Foundation (SNSF), the Russian Foundation for Basic Research, the Rus-

1769 sian Science Foundation, the European Commission,
 1770 the European Social Funds (ESF), the European Re-
 1771 gional Development Funds (ERDF), the Royal Society,
 1772 the Scottish Funding Council, the Scottish Universi-
 1773 ties Physics Alliance, the Hungarian Scientific Research
 1774 Fund (OTKA), the French Lyon Institute of Origins
 1775 (LIO), the Belgian Fonds de la Recherche Scientifique
 1776 (FRS-FNRS), Actions de Recherche Concertées (ARC)
 1777 and Fonds Wetenschappelijk Onderzoek – Vlaanderen
 1778 (FWO), Belgium, the Paris Île-de-France Region, the
 1779 National Research, Development and Innovation Office
 1780 Hungary (NKFIH), the National Research Foundation
 1781 of Korea, the Natural Science and Engineering Research
 1782 Council Canada, Canadian Foundation for Innovation
 1783 (CFI), the Brazilian Ministry of Science, Technology,
 1784 and Innovations, the International Center for Theoret-
 1785 ical Physics South American Institute for Fundamental
 1786 Research (ICTP-SAIFR), the Research Grants Council
 1787 of Hong Kong, the National Natural Science Foundation
 1788 of China (NSFC), the Leverhulme Trust, the Research
 1789 Corporation, the Ministry of Science and Technology
 1790 (MOST), Taiwan, the United States Department of En-
 1791 ergy, and the Kavli Foundation. The authors gratefully
 1792 acknowledge the support of the NSF, STFC, INFN and
 1793 CNRS for provision of computational resources.

1794 This work was supported by MEXT, JSPS Leading-
 1795 edge Research Infrastructure Program, JSPS Grant-in-
 1796 Aid for Specially Promoted Research 26000005, JSPS
 1797 Grant-in-Aid for Scientific Research on Innovative Ar-
 1798 eas 2905: JP17H06358, JP17H06361 and JP17H06364,
 1799 JSPS Core-to-Core Program A. Advanced Research Net-
 1800 works, JSPS Grant-in-Aid for Scientific Research (S)
 1801 17H06133 and 20H05639, JSPS Grant-in-Aid for Trans-
 1802 formative Research Areas (A) 20A203: JP20H05854,
 1803 the joint research program of the Institute for Cosmic
 1804 Ray Research, University of Tokyo, National Research
 1805 Foundation (NRF), Computing Infrastructure Project
 1806 of KISTI-GSDC, Korea Astronomy and Space Science
 1807 Institute (KASI), and Ministry of Science and ICT
 1808 (MSIT) in Korea, Academia Sinica (AS), AS Grid Cen-

1809 ter (ASGC) and the Ministry of Science and Technology
 1810 (MoST) in Taiwan under grants including AS-CDA-105-
 1811 M06, Advanced Technology Center (ATC) of NAOJ,
 1812 and Mechanical Engineering Center of KEK.

1813 We acknowledge that CHIME is located on the
 1814 traditional, ancestral, and unceded territory of the
 1815 Syilx/Okanagan people.

1816 We thank the Dominion Radio Astrophysical Ob-
 1817 servatory, operated by the National Research Council
 1818 Canada, for gracious hospitality and expertise. CHIME
 1819 is funded by a grant from the Canada Foundation for In-
 1820 novation (CFI) 2012 Leading Edge Fund (Project 31170)
 1821 and by contributions from the provinces of British
 1822 Columbia, Québec and Ontario. The CHIME/FRB
 1823 Project is funded by a grant from the CFI 2015 Innova-
 1824 tion Fund (Project 33213) and by contributions from the
 1825 provinces of British Columbia and Québec, and by the
 1826 Dunlap Institute for Astronomy and Astrophysics at the
 1827 University of Toronto. Additional support was provided
 1828 by the Canadian Institute for Advanced Research (CI-
 1829 FAR), McGill University and the McGill Space Institute
 1830 via the Trottier Family Foundation, and the University
 1831 of British Columbia. The Dunlap Institute is funded
 1832 through an endowment established by the David Dun-
 1833 lap family and the University of Toronto. Research at
 1834 Perimeter Institute is supported by the Government of
 1835 Canada through Industry Canada and by the Province
 1836 of Ontario through the Ministry of Research & Inno-
 1837 vation. The National Radio Astronomy Observatory
 1838 is a facility of the National Science Foundation (NSF)
 1839 operated under cooperative agreement by Associated
 1840 Universities, Inc. FRB research at UBC is supported
 1841 by an NSERC Discovery Grant and by the Canadian
 1842 Institute for Advanced Research. The CHIME/FRB
 1843 baseband system is funded in part by a CFI John R.
 1844 Evans Leaders Fund award to IHS.

1845 We would like to thank all of the essential workers who
 1846 put their health at risk during the COVID-19 pandemic,
 1847 without whom we would not have been able to complete
 1848 this work.

1849 APPENDIX

1850 A. TABLES OF UPPER LIMITS ON THE ENERGY EMITTED THROUGH GWS FOR THE GENERIC 1851 TRANSIENT SEARCH

1852 This section provides the supplemental tables containing the upper limits on the energy emitted through GWs for
 1853 the generic transient search for different waveform models and luminosity distance estimates. Table A1 and Table
 1854 A2 provide the upper limits on $E_{\text{GW}}^{90\%}$ for SG models and DS2P or WNB GW burst models respectively. These limits
 1855 assume that the FRB distances are at the lower limits of their inferred distance ranges. Table A3 and Table A4,
 1856 provide less constraining limits on $E_{\text{GW}}^{90\%}$ based on the upper credible intervals on the distance of each FRB.

Table A1. The upper limits on the energy emitted through GWs in erg for the generic transient search using the SG waveforms described in Table 1. The distances represent the lower bounds of 90% credible intervals from the MCMC inference described in Section 3.

FRB	D_L [Mpc]	SG	SG	SG	SG	SG	SG	SG	SG
		A	B	C	D	E	F	G	H
FRB 20190410A	6.0×10^1	1.5×10^{52}	2.8×10^{52}	4.9×10^{52}	4.1×10^{53}	5.5×10^{54}	5.4×10^{55}	3.0×10^{56}	1.1×10^{57}
FRB 20190419B	2.5×10^1	2.6×10^{51}	4.3×10^{51}	9.7×10^{51}	5.9×10^{52}	9.4×10^{53}	8.9×10^{54}	5.0×10^{55}	1.5×10^{58}
FRB 20190423B	5.8×10^1	5.9×10^{52}	8.9×10^{52}	3.7×10^{53}	3.7×10^{54}	4.6×10^{55}	5.6×10^{56}	3.4×10^{57}	1.1×10^{58}
FRB 20190425A	1.3×10^1	2.5×10^{50}	3.5×10^{50}	6.5×10^{50}	3.4×10^{51}	2.6×10^{52}	2.7×10^{53}	1.6×10^{54}	7.9×10^{54}
FRB 20190517C	4.4×10^1	5.8×10^{51}	8.8×10^{51}	2.2×10^{52}	1.3×10^{53}	2.3×10^{54}	2.1×10^{55}	9.8×10^{55}	3.5×10^{56}
FRB 20190518D	6.2×10^1	9.5×10^{51}	1.3×10^{52}	2.3×10^{52}	9.5×10^{52}	1.1×10^{54}	6.8×10^{54}	3.6×10^{55}	2.0×10^{56}
FRB 20190531B	3.7×10^1	3.2×10^{51}	3.4×10^{51}	7.9×10^{51}	3.3×10^{52}	2.5×10^{53}	2.0×10^{54}	8.1×10^{54}	3.1×10^{55}
FRB 20190601C	2.0×10^2	8.6×10^{52}	1.1×10^{53}	1.6×10^{53}	6.3×10^{53}	1.1×10^{55}	6.8×10^{55}	4.8×10^{56}	1.5×10^{57}
FRB 20190604G	9.7×10^1	1.1×10^{53}	3.2×10^{53}	9.0×10^{53}	3.7×10^{54}	8.7×10^{55}	7.5×10^{56}	3.2×10^{57}	1.2×10^{58}
FRB 20190605C	6.8×10^1	3.0×10^{52}	2.8×10^{52}	1.0×10^{53}	5.2×10^{53}	8.7×10^{54}	9.4×10^{55}	5.2×10^{56}	1.6×10^{57}
FRB 20190606B	1.7×10^2	1.7×10^{53}	1.3×10^{53}	2.7×10^{53}	8.2×10^{53}	1.1×10^{55}	9.6×10^{55}	3.6×10^{56}	1.4×10^{57}
FRB 20190612B	6.5×10^1	8.2×10^{51}	8.5×10^{51}	1.5×10^{52}	7.3×10^{52}	8.0×10^{53}	7.0×10^{54}	3.7×10^{55}	3.6×10^{56}
FRB 20190613B	2.8×10^1	1.2×10^{51}	1.0×10^{51}	2.2×10^{51}	1.3×10^{52}	9.3×10^{52}	7.4×10^{53}	4.2×10^{54}	1.8×10^{55}
FRB 20190616A	1.1×10^2	1.9×10^{53}	2.1×10^{53}	6.9×10^{53}	3.1×10^{54}	3.5×10^{55}	5.1×10^{56}	2.8×10^{57}	8.2×10^{57}
FRB 20190617A	6.2×10^1	9.5×10^{51}	1.3×10^{52}	2.4×10^{52}	9.2×10^{52}	9.2×10^{53}	8.3×10^{54}	4.2×10^{55}	8.8×10^{55}
FRB 20190618A	7.8×10^1	6.0×10^{51}	7.7×10^{51}	1.7×10^{52}	7.0×10^{52}	6.8×10^{53}	5.9×10^{54}	3.0×10^{55}	1.4×10^{56}
FRB 20190621A	7.8×10^1	1.1×10^{53}	1.2×10^{53}	4.6×10^{53}	1.5×10^{54}	5.4×10^{55}	6.5×10^{56}	1.7×10^{57}	4.9×10^{57}
FRB 20190624B	4.7×10^1	1.3×10^{52}	1.9×10^{52}	4.2×10^{52}	1.7×10^{53}	2.9×10^{54}	2.3×10^{55}	1.5×10^{56}	8.3×10^{56}
FRB 20190710A	8.9×10^1	1.1×10^{52}	1.6×10^{52}	2.3×10^{52}	1.0×10^{53}	9.4×10^{53}	7.6×10^{54}	3.3×10^{55}	1.4×10^{56}
FRB 20190713A	1.4×10^2	1.2×10^{53}	1.6×10^{53}	4.3×10^{53}	2.3×10^{54}	4.2×10^{55}	4.4×10^{56}	2.2×10^{57}	6.7×10^{57}
FRB 20190718A	7.2×10^1	1.1×10^{52}	1.1×10^{52}	2.8×10^{52}	1.1×10^{53}	1.1×10^{54}	7.7×10^{54}	3.1×10^{55}	1.2×10^{56}
FRB 20190722A	9.8×10^1	7.0×10^{52}	1.3×10^{53}	5.0×10^{53}	3.3×10^{54}	5.4×10^{55}	4.0×10^{56}	1.6×10^{57}	9.6×10^{57}
FRB 20190812A	1.9×10^2	3.7×10^{52}	4.1×10^{52}	9.9×10^{52}	4.3×10^{53}	4.3×10^{54}	3.7×10^{55}	1.6×10^{56}	5.8×10^{56}
FRB 20190903A	6.7×10^1	9.0×10^{52}	9.8×10^{52}	5.0×10^{53}	4.4×10^{54}	5.5×10^{55}	7.4×10^{56}	3.4×10^{57}	9.2×10^{57}
FRB 20190912A	9.8×10^1	1.2×10^{53}	2.0×10^{53}	7.9×10^{53}	4.6×10^{54}	1.0×10^{56}	8.1×10^{56}	3.8×10^{57}	1.7×10^{58}
FRB 20190912B	2.3×10^1	7.1×10^{50}	9.1×10^{50}	1.7×10^{51}	8.1×10^{51}	6.9×10^{52}	7.1×10^{53}	3.9×10^{54}	1.5×10^{55}
FRB 20190922A	6.6×10^1	5.1×10^{52}	7.7×10^{52}	3.1×10^{53}	1.5×10^{54}	2.4×10^{55}	2.8×10^{56}	1.5×10^{57}	4.7×10^{57}
FRB 20190928A	2.0×10^1	9.9×10^{50}	1.1×10^{51}	2.3×10^{51}	9.2×10^{51}	1.1×10^{53}	8.2×10^{53}	3.7×10^{54}	1.4×10^{55}
FRB 20190929B	1.5×10^2	2.9×10^{52}	3.9×10^{52}	6.7×10^{52}	3.4×10^{53}	2.8×10^{54}	2.6×10^{55}	1.2×10^{56}	4.0×10^{56}

Table A2. The upper limits on the energy emitted through GWs in erg for the generic transient search using the DS2P and WNB waveforms described in Table 1. The distances represent the lower bounds of 90% credible intervals from the MCMC inference described in Section 3.

FRB	D_L [Mpc]	DS2P		WNB		WNB	
		A	B	A	B	C	D
FRB 20190410A	6.0×10^1	2.0×10^{56}	1.8×10^{56}	1.2×10^{53}	9.5×10^{52}	3.4×10^{54}	1.0×10^{55}
FRB 20190419B	2.5×10^1	4.4×10^{55}	3.0×10^{55}	1.6×10^{54}	1.8×10^{52}	6.0×10^{53}	1.7×10^{54}
FRB 20190423B	5.8×10^1	2.4×10^{57}	2.6×10^{57}	2.8×10^{53}	3.0×10^{53}	1.4×10^{55}	3.6×10^{55}
FRB 20190425A	1.3×10^1	1.7×10^{56}	4.6×10^{54}	4.8×10^{50}	7.9×10^{50}	1.4×10^{52}	4.7×10^{52}
FRB 20190517C	4.4×10^1	6.7×10^{55}	5.8×10^{55}	2.4×10^{52}	3.1×10^{52}	1.4×10^{54}	7.3×10^{54}
FRB 20190518D	6.2×10^1	6.7×10^{55}	1.1×10^{56}	2.0×10^{52}	2.6×10^{52}	5.8×10^{53}	1.7×10^{54}
FRB 20190531B	3.7×10^1	5.8×10^{54}	6.4×10^{54}	5.7×10^{51}	8.6×10^{51}	1.4×10^{53}	5.6×10^{53}
FRB 20190601C	2.0×10^2	5.5×10^{56}	8.3×10^{56}	1.2×10^{53}	1.6×10^{53}	3.4×10^{54}	8.6×10^{54}
FRB 20190604G	9.7×10^1	1.9×10^{57}	1.6×10^{57}	—	4.9×10^{54}	1.5×10^{56}	3.4×10^{56}
FRB 20190605C	6.8×10^1	2.4×10^{56}	1.7×10^{56}	3.5×10^{53}	1.6×10^{53}	6.2×10^{54}	1.8×10^{55}
FRB 20190606B	1.7×10^2	5.7×10^{56}	9.9×10^{56}	3.6×10^{53}	2.0×10^{53}	4.7×10^{54}	1.3×10^{55}
FRB 20190612B	6.5×10^1	6.2×10^{55}	1.1×10^{58}	1.3×10^{52}	2.1×10^{52}	3.7×10^{53}	1.2×10^{54}
FRB 20190613B	2.8×10^1	6.2×10^{54}	1.1×10^{55}	1.6×10^{51}	2.5×10^{51}	5.4×10^{52}	1.6×10^{53}
FRB 20190616A	1.1×10^2	2.2×10^{57}	2.7×10^{57}	1.1×10^{54}	7.3×10^{53}	2.4×10^{55}	1.4×10^{56}
FRB 20190617A	6.2×10^1	3.6×10^{55}	5.1×10^{55}	3.3×10^{52}	2.7×10^{52}	3.9×10^{53}	1.6×10^{54}
FRB 20190618A	7.8×10^1	4.4×10^{55}	7.0×10^{55}	9.9×10^{51}	1.8×10^{52}	3.6×10^{53}	1.2×10^{54}
FRB 20190621A	7.8×10^1	1.1×10^{57}	4.8×10^{56}	—	9.3×10^{53}	2.8×10^{55}	5.9×10^{55}
FRB 20190624B	4.7×10^1	1.9×10^{56}	3.6×10^{56}	2.8×10^{52}	4.4×10^{52}	1.0×10^{54}	3.7×10^{54}
FRB 20190710A	8.9×10^1	3.9×10^{55}	4.3×10^{55}	1.7×10^{52}	2.6×10^{52}	5.6×10^{53}	1.6×10^{54}
FRB 20190713A	1.4×10^2	2.3×10^{57}	3.7×10^{57}	3.1×10^{53}	5.0×10^{53}	1.5×10^{55}	4.4×10^{55}
FRB 20190718A	7.2×10^1	3.7×10^{55}	6.1×10^{55}	1.7×10^{52}	2.3×10^{52}	4.6×10^{53}	1.4×10^{54}
FRB 20190722A	9.8×10^1	1.1×10^{57}	8.0×10^{56}	9.2×10^{55}	2.7×10^{54}	8.2×10^{55}	1.8×10^{56}
FRB 20190812A	1.9×10^2	2.7×10^{56}	5.3×10^{56}	8.2×10^{52}	1.1×10^{53}	2.4×10^{54}	7.1×10^{54}
FRB 20190903A	6.7×10^1	1.1×10^{57}	7.3×10^{56}	5.0×10^{53}	3.6×10^{53}	1.7×10^{55}	4.5×10^{55}
FRB 20190912A	9.8×10^1	2.0×10^{57}	1.5×10^{57}	7.9×10^{53}	6.6×10^{53}	2.9×10^{55}	8.9×10^{55}
FRB 20190912B	2.3×10^1	7.6×10^{54}	1.4×10^{55}	1.4×10^{51}	1.7×10^{51}	4.3×10^{52}	1.2×10^{53}
FRB 20190922A	6.6×10^1	2.2×10^{57}	3.2×10^{57}	1.5×10^{54}	4.2×10^{53}	1.5×10^{55}	3.9×10^{55}
FRB 20190928A	2.0×10^1	6.2×10^{54}	1.1×10^{55}	1.8×10^{51}	2.6×10^{51}	4.3×10^{52}	1.7×10^{53}
FRB 20190929B	1.5×10^2	1.4×10^{56}	3.0×10^{56}	6.6×10^{52}	7.3×10^{52}	1.8×10^{54}	4.7×10^{54}

Table A3. As for Table A1 but with distances based on the the upper bounds of 90% credible intervals on the luminosity distance.

FRB	D_L [Mpc]	SG	SG	SG	SG	SG	SG	SG	SG
		A	B	C	D	E	F	G	H
FRB 20190410A	9.6×10^2	3.9×10^{54}	7.2×10^{54}	1.2×10^{55}	1.0×10^{56}	1.4×10^{57}	1.4×10^{58}	7.5×10^{58}	2.7×10^{59}
FRB 20190419B	5.8×10^2	1.4×10^{54}	2.3×10^{54}	5.2×10^{54}	3.2×10^{55}	5.1×10^{56}	4.8×10^{57}	2.7×10^{58}	8.0×10^{60}
FRB 20190423B	1.7×10^3	5.1×10^{55}	7.7×10^{55}	3.2×10^{56}	3.2×10^{57}	4.0×10^{58}	4.9×10^{59}	2.9×10^{60}	9.4×10^{60}
FRB 20190425A	3.9×10^2	2.4×10^{53}	3.3×10^{53}	6.1×10^{53}	3.2×10^{54}	2.4×10^{55}	2.5×10^{56}	1.6×10^{57}	7.5×10^{57}
FRB 20190517C	1.0×10^3	3.1×10^{54}	4.7×10^{54}	1.2×10^{55}	6.8×10^{55}	1.2×10^{57}	1.1×10^{58}	5.3×10^{58}	1.9×10^{59}
FRB 20190518D	8.5×10^2	1.8×10^{54}	2.4×10^{54}	4.4×10^{54}	1.8×10^{55}	2.0×10^{56}	1.3×10^{57}	6.9×10^{57}	3.8×10^{58}
FRB 20190531B	6.8×10^2	1.0×10^{54}	1.1×10^{54}	2.6×10^{54}	1.1×10^{55}	8.2×10^{55}	6.7×10^{56}	2.7×10^{57}	1.0×10^{58}
FRB 20190601C	1.7×10^3	6.6×10^{54}	8.3×10^{54}	1.2×10^{55}	4.8×10^{55}	8.2×10^{56}	5.2×10^{57}	3.6×10^{58}	1.1×10^{59}
FRB 20190604G	1.1×10^3	1.5×10^{55}	4.5×10^{55}	1.3×10^{56}	5.1×10^{56}	1.2×10^{58}	1.0×10^{59}	4.5×10^{59}	1.6×10^{60}
FRB 20190605C	8.9×10^2	5.1×10^{54}	4.9×10^{54}	1.7×10^{55}	8.9×10^{55}	1.5×10^{57}	1.6×10^{58}	8.9×10^{58}	2.7×10^{59}
FRB 20190606B	1.5×10^3	1.3×10^{55}	9.6×10^{54}	2.0×10^{55}	6.2×10^{55}	8.3×10^{56}	7.3×10^{57}	2.7×10^{58}	1.0×10^{59}
FRB 20190612B	9.2×10^2	1.7×10^{54}	1.7×10^{54}	3.1×10^{54}	1.5×10^{55}	1.6×10^{56}	1.4×10^{57}	7.4×10^{57}	7.3×10^{58}
FRB 20190613B	7.8×10^2	9.7×10^{53}	8.2×10^{53}	1.8×10^{54}	1.0×10^{55}	7.4×10^{55}	5.8×10^{56}	3.4×10^{57}	1.4×10^{58}
FRB 20190616A	1.1×10^3	2.1×10^{55}	2.4×10^{55}	7.6×10^{55}	3.4×10^{56}	3.9×10^{57}	5.6×10^{58}	3.1×10^{59}	9.0×10^{59}
FRB 20190617A	8.7×10^2	1.9×10^{54}	2.5×10^{54}	4.7×10^{54}	1.8×10^{55}	1.8×10^{56}	1.6×10^{57}	8.2×10^{57}	1.7×10^{58}
FRB 20190618A	9.6×10^2	9.1×10^{53}	1.2×10^{54}	2.6×10^{54}	1.1×10^{55}	1.0×10^{56}	9.0×10^{56}	4.5×10^{57}	2.1×10^{58}
FRB 20190621A	9.8×10^2	1.7×10^{55}	2.0×10^{55}	7.2×10^{55}	2.3×10^{56}	8.4×10^{57}	1.0×10^{59}	2.6×10^{59}	7.7×10^{59}
FRB 20190624B	8.2×10^2	4.0×10^{54}	5.8×10^{54}	1.3×10^{55}	5.1×10^{55}	8.9×10^{56}	7.0×10^{57}	4.6×10^{58}	2.5×10^{59}
FRB 20190710A	1.0×10^3	1.4×10^{54}	2.0×10^{54}	2.9×10^{54}	1.2×10^{55}	1.2×10^{56}	9.5×10^{56}	4.1×10^{57}	1.7×10^{58}
FRB 20190713A	1.4×10^3	1.2×10^{55}	1.6×10^{55}	4.4×10^{55}	2.4×10^{56}	4.4×10^{57}	4.6×10^{58}	2.2×10^{59}	6.9×10^{59}
FRB 20190718A	9.7×10^2	2.0×10^{54}	2.1×10^{54}	5.1×10^{54}	2.0×10^{55}	1.9×10^{56}	1.4×10^{57}	5.8×10^{57}	2.3×10^{58}
FRB 20190722A	1.1×10^3	9.4×10^{54}	1.7×10^{55}	6.7×10^{55}	4.4×10^{56}	7.2×10^{57}	5.3×10^{58}	2.2×10^{59}	1.3×10^{60}
FRB 20190812A	1.4×10^3	2.0×10^{54}	2.2×10^{54}	5.3×10^{54}	2.3×10^{55}	2.3×10^{56}	2.0×10^{57}	8.7×10^{57}	3.1×10^{58}
FRB 20190903A	9.3×10^2	1.7×10^{55}	1.9×10^{55}	9.6×10^{55}	8.4×10^{56}	1.0×10^{58}	1.4×10^{59}	6.5×10^{59}	1.8×10^{60}
FRB 20190912A	1.1×10^3	1.5×10^{55}	2.5×10^{55}	9.9×10^{55}	5.8×10^{56}	1.2×10^{58}	1.0×10^{59}	4.7×10^{59}	2.2×10^{60}
FRB 20190912B	4.9×10^2	3.2×10^{53}	4.1×10^{53}	7.7×10^{53}	3.7×10^{54}	3.1×10^{55}	3.3×10^{56}	1.8×10^{57}	6.7×10^{57}
FRB 20190922A	9.6×10^2	1.1×10^{55}	1.6×10^{55}	6.6×10^{55}	3.2×10^{56}	5.0×10^{57}	5.9×10^{58}	3.2×10^{59}	9.8×10^{59}
FRB 20190928A	5.1×10^2	6.1×10^{53}	6.9×10^{53}	1.5×10^{54}	5.7×10^{54}	6.6×10^{55}	5.1×10^{56}	2.3×10^{57}	8.4×10^{57}
FRB 20190929B	1.5×10^3	3.0×10^{54}	4.1×10^{54}	7.1×10^{54}	3.6×10^{55}	3.0×10^{56}	2.8×10^{57}	1.3×10^{58}	4.2×10^{58}

Table A4. As for Table A2 but with distances based on the the upper bounds of 90% credible intervals on the luminosity distance.

FRB	D_L [Mpc]	DS2P		WNB		WNB	
		A	B	A	B	C	D
FRB 20190410A	9.6×10^2	5.0×10^{58}	4.5×10^{58}	3.2×10^{55}	2.4×10^{55}	8.6×10^{56}	2.5×10^{57}
FRB 20190419B	5.8×10^2	2.3×10^{58}	1.6×10^{58}	8.3×10^{56}	9.5×10^{54}	3.2×10^{56}	9.0×10^{56}
FRB 20190423B	1.7×10^3	2.1×10^{60}	2.2×10^{60}	2.4×10^{56}	2.6×10^{56}	1.2×10^{58}	3.2×10^{58}
FRB 20190425A	3.9×10^2	1.6×10^{59}	4.4×10^{57}	4.5×10^{53}	7.4×10^{53}	1.3×10^{55}	4.4×10^{55}
FRB 20190517C	1.0×10^3	3.6×10^{58}	3.2×10^{58}	1.3×10^{55}	1.7×10^{55}	7.5×10^{56}	4.0×10^{57}
FRB 20190518D	8.5×10^2	1.3×10^{58}	2.1×10^{58}	3.7×10^{54}	4.9×10^{54}	1.1×10^{56}	3.2×10^{56}
FRB 20190531B	6.8×10^2	1.9×10^{57}	2.1×10^{57}	1.9×10^{54}	2.9×10^{54}	4.5×10^{55}	1.8×10^{56}
FRB 20190601C	1.7×10^3	4.2×10^{58}	6.4×10^{58}	9.4×10^{54}	1.2×10^{55}	2.6×10^{56}	6.6×10^{56}
FRB 20190604G	1.1×10^3	2.6×10^{59}	2.2×10^{59}	—	6.8×10^{56}	2.0×10^{58}	4.7×10^{58}
FRB 20190605C	8.9×10^2	4.1×10^{58}	2.9×10^{58}	5.9×10^{55}	2.7×10^{55}	1.1×10^{57}	3.0×10^{57}
FRB 20190606B	1.5×10^3	4.3×10^{58}	7.5×10^{58}	2.7×10^{55}	1.5×10^{55}	3.6×10^{56}	9.7×10^{56}
FRB 20190612B	9.2×10^2	1.3×10^{58}	2.2×10^{60}	2.7×10^{54}	4.2×10^{54}	7.5×10^{55}	2.5×10^{56}
FRB 20190613B	7.8×10^2	4.9×10^{57}	8.9×10^{57}	1.3×10^{54}	2.0×10^{54}	4.3×10^{55}	1.3×10^{56}
FRB 20190616A	1.1×10^3	2.4×10^{59}	3.0×10^{59}	1.2×10^{56}	8.0×10^{55}	2.6×10^{57}	1.6×10^{58}
FRB 20190617A	8.7×10^2	7.1×10^{57}	1.0×10^{58}	6.4×10^{54}	5.3×10^{54}	7.7×10^{55}	3.2×10^{56}
FRB 20190618A	9.6×10^2	6.7×10^{57}	1.1×10^{58}	1.5×10^{54}	2.7×10^{54}	5.4×10^{55}	1.8×10^{56}
FRB 20190621A	9.8×10^2	1.8×10^{59}	7.6×10^{58}	—	1.5×10^{56}	4.4×10^{57}	9.2×10^{57}
FRB 20190624B	8.2×10^2	5.9×10^{58}	1.1×10^{59}	8.5×10^{54}	1.4×10^{55}	3.1×10^{56}	1.1×10^{57}
FRB 20190710A	1.0×10^3	4.8×10^{57}	5.4×10^{57}	2.1×10^{54}	3.2×10^{54}	6.9×10^{55}	2.0×10^{56}
FRB 20190713A	1.4×10^3	2.4×10^{59}	3.8×10^{59}	3.2×10^{55}	5.2×10^{55}	1.6×10^{57}	4.5×10^{57}
FRB 20190718A	9.7×10^2	6.7×10^{57}	1.1×10^{58}	3.2×10^{54}	4.2×10^{54}	8.4×10^{55}	2.6×10^{56}
FRB 20190722A	1.1×10^3	1.5×10^{59}	1.1×10^{59}	1.2×10^{58}	3.6×10^{56}	1.1×10^{58}	2.3×10^{58}
FRB 20190812A	1.4×10^3	1.4×10^{58}	2.8×10^{58}	4.4×10^{54}	6.1×10^{54}	1.3×10^{56}	3.8×10^{56}
FRB 20190903A	9.3×10^2	2.1×10^{59}	1.4×10^{59}	9.6×10^{55}	7.0×10^{55}	3.3×10^{57}	8.7×10^{57}
FRB 20190912A	1.1×10^3	2.5×10^{59}	1.8×10^{59}	9.9×10^{55}	8.2×10^{55}	3.7×10^{57}	1.1×10^{58}
FRB 20190912B	4.9×10^2	3.5×10^{57}	6.4×10^{57}	6.5×10^{53}	7.9×10^{53}	2.0×10^{55}	5.3×10^{55}
FRB 20190922A	9.6×10^2	4.7×10^{59}	6.7×10^{59}	3.2×10^{56}	8.8×10^{55}	3.1×10^{57}	8.3×10^{57}
FRB 20190928A	5.1×10^2	3.8×10^{57}	7.1×10^{57}	1.1×10^{54}	1.6×10^{54}	2.6×10^{55}	1.1×10^{56}
FRB 20190929B	1.5×10^3	1.5×10^{58}	3.1×10^{58}	7.0×10^{54}	7.8×10^{54}	1.9×10^{56}	5.0×10^{56}

REFERENCES

- 1857 Aasi, J., et al. 2014, *PhRvD*, 89, 122004,
1858 doi: [10.1103/PhysRevD.89.122004](https://doi.org/10.1103/PhysRevD.89.122004)
- 1859 Aasi, J., et al. 2015, *Class. Quant. Grav.*, 32, 074001
- 1860 Abadie, J., Abbott, B. P., Abbott, R., et al. 2012, *ApJ*,
1861 760, 12, doi: [10.1088/0004-637X/760/1/12](https://doi.org/10.1088/0004-637X/760/1/12)
- 1862 Abbott, B., et al. 2016, *Phys. Rev. D*, 93, 122008,
1863 doi: [10.1103/PhysRevD.93.122008](https://doi.org/10.1103/PhysRevD.93.122008)
- 1864 Abbott, B. P., J., LIGO Scientific Collaboration, & Virgo
1865 Collaboration. 2017a, *PhRvL*, 119, 161101,
1866 doi: [10.1103/PhysRevLett.119.161101](https://doi.org/10.1103/PhysRevLett.119.161101)
- 1867 Abbott, B. P., Abbott, R., Abbott, T. D., et al. 2017b,
1868 *PhRvL*, 119, 161101,
1869 doi: [10.1103/PhysRevLett.119.161101](https://doi.org/10.1103/PhysRevLett.119.161101)
- 1870 Abbott, B. P., et al. 2017, *Astrophys. J.*, 848, L13,
1871 doi: [10.3847/2041-8213/aa920c](https://doi.org/10.3847/2041-8213/aa920c)
- 1872 Abbott, B. P., Abbott, R., Abbott, T. D., et al. 2017, *ApJ*,
1873 841, 89, doi: [10.3847/1538-4357/aa6c47](https://doi.org/10.3847/1538-4357/aa6c47)
- 1874 Abbott, B. P., et al. 2018, *Phys. Rev. Lett.*, 121, 161101,
1875 doi: [10.1103/PhysRevLett.121.161101](https://doi.org/10.1103/PhysRevLett.121.161101)
- 1876 Abbott, B. P., Abbott, R., Abbott, T. D., et al. 2019a,
1877 *ApJ*, 886, 75, doi: [10.3847/1538-4357/ab4b48](https://doi.org/10.3847/1538-4357/ab4b48)
- 1878 —. 2019b, *ApJ*, 874, 163, doi: [10.3847/1538-4357/ab0e15](https://doi.org/10.3847/1538-4357/ab0e15)
- 1879 —. 2019c, *PhRvD*, 100, 024017,
1880 doi: [10.1103/PhysRevD.100.024017](https://doi.org/10.1103/PhysRevD.100.024017)
- 1881 Abbott, B. P., Abbott, R., Abbott, T. D., et al. 2020,
1882 *Living Reviews in Relativity*, 23, 3,
1883 doi: [10.1007/s41114-020-00026-9](https://doi.org/10.1007/s41114-020-00026-9)
- 1884 Abbott, B. P., et al. 2020, *Classical and Quantum Gravity*,
1885 37, 055002, doi: [10.1088/1361-6382/ab685e](https://doi.org/10.1088/1361-6382/ab685e)
- 1886 Abbott, R., LIGO Scientific Collaboration, et al. in
1887 preparation, Search for gravitational wave transients
1888 associated with magnetar bursts during the third
1889 Advanced LIGO and Advanced Virgo observing run
- 1890 Abbott, R., Abbott, T. D., Abraham, S., et al. 2021, *ApJ*,
1891 915, 86, doi: [10.3847/1538-4357/abee15](https://doi.org/10.3847/1538-4357/abee15)
- 1892 Accadia, T., et al. 2012, *JINST*, 7, P03012,
1893 doi: [10.1088/1748-0221/7/03/P03012](https://doi.org/10.1088/1748-0221/7/03/P03012)
- 1894 Acernese, F., et al. 2015, *Class. Quant. Grav.*, 32, 024001
- 1895 Amiri, M., et al. 2019a, *Nature*, 566, 235,
1896 doi: [10.1038/s41586-018-0864-x](https://doi.org/10.1038/s41586-018-0864-x)
- 1897 —. 2019b, *Nature*, 566, 230, doi: [10.1038/s41586-018-0867-7](https://doi.org/10.1038/s41586-018-0867-7)
- 1898 Anderson, M. M., Hallinan, G., Eastwood, M. W., et al.
1899 2018, *ApJ*, 864, 22, doi: [10.3847/1538-4357/aad2d7](https://doi.org/10.3847/1538-4357/aad2d7)
- 1900 Arun, K. G., Buonanno, A., Faye, G., & Ochsner, E. 2009,
1901 *Phys. Rev.*, D79, 104023, doi: [10.1103/PhysRevD.79.](https://doi.org/10.1103/PhysRevD.79.104023)
1902 [104023,10.1103/PhysRevD.84.049901](https://doi.org/10.1103/PhysRevD.84.049901)
- 1903 Babak, S., Taracchini, A., & Buonanno, A. 2017, *Phys.*
1904 *Rev.*, D95, 024010, doi: [10.1103/PhysRevD.95.024010](https://doi.org/10.1103/PhysRevD.95.024010)
- 1905 Bandura, K., Addison, G. E., Amiri, M., et al. 2014, in
1906 Society of Photo-Optical Instrumentation Engineers
1907 (SPIE) Conference Series, Vol. 9145, Ground-based and
1908 Airborne Telescopes V, ed. L. M. Stepp, R. Gilmozzi, &
1909 H. J. Hall, 914522, doi: [10.1117/12.2054950](https://doi.org/10.1117/12.2054950)
- 1910 Bannister, K. W., Shannon, R. M., Macquart, J.-P., et al.
1911 2017, *ApJL*, 841, L12, doi: [10.3847/2041-8213/aa71ff](https://doi.org/10.3847/2041-8213/aa71ff)
- 1912 Bannister, K. W., Deller, A. T., Phillips, C., et al. 2019,
1913 *Science*, 365, 565, doi: [10.1126/science.aaw5903](https://doi.org/10.1126/science.aaw5903)
- 1914 Bhandari, S., Sadler, E. M., Prochaska, J. X., et al. 2020,
1915 *ApJL*, 895, L37, doi: [10.3847/2041-8213/ab672e](https://doi.org/10.3847/2041-8213/ab672e)
- 1916 Bhandari, S., Heintz, K. E., Aggarwal, K., et al. 2021,
1917 arXiv e-prints, arXiv:2108.01282.
1918 <https://arxiv.org/abs/2108.01282>
- 1919 Bhardwaj, M., Kirichenko, A. Y., Michilli, D., et al. 2021a,
1920 *ApJL*, 919, L24, doi: [10.3847/2041-8213/ac223b](https://doi.org/10.3847/2041-8213/ac223b)
- 1921 Bhardwaj, M., Gaensler, B. M., Kaspi, V. M., et al. 2021b,
1922 *ApJL*, 910, L18, doi: [10.3847/2041-8213/abeaa6](https://doi.org/10.3847/2041-8213/abeaa6)
- 1923 Blanchet, L., Iyer, B. R., Will, C. M., & Wiseman, A. G.
1924 1996, *Class. Quant. Grav.*, 13, 575,
1925 doi: [10.1088/0264-9381/13/4/002](https://doi.org/10.1088/0264-9381/13/4/002)
- 1926 Bochenek, C. D., Ravi, V., Belov, K. V., et al. 2020,
1927 *Nature*, 587, 59, doi: [10.1038/s41586-020-2872-x](https://doi.org/10.1038/s41586-020-2872-x)
- 1928 Bohé, A., Faye, G., Marsat, S., & Porter, E. K. 2015, *Class.*
1929 *Quant. Grav.*, 32, 195010,
1930 doi: [10.1088/0264-9381/32/19/195010](https://doi.org/10.1088/0264-9381/32/19/195010)
- 1931 Bohé, A., Marsat, S., & Blanchet, L. 2013, *Class. Quant.*
1932 *Grav.*, 30, 135009, doi: [10.1088/0264-9381/30/13/135009](https://doi.org/10.1088/0264-9381/30/13/135009)
- 1933 Bouwhuis, M., Bannister, K. W., Macquart, J.-P., et al.
1934 2020, *Monthly Notices of the Royal Astronomical*
1935 *Society*, 497, 125, doi: [10.1093/mnras/staa1889](https://doi.org/10.1093/mnras/staa1889)
- 1936 Brown, D. A., Harry, I., Lundgren, A., & Nitz, A. H. 2012,
1937 *Physical Review D*, 86, doi: [10.1103/physrevd.86.084017](https://doi.org/10.1103/physrevd.86.084017)
- 1938 Caleb, M., Flynn, C., Bailes, M., et al. 2017, *MNRAS*, 468,
1939 3746, doi: [10.1093/mnras/stx638](https://doi.org/10.1093/mnras/stx638)
- 1940 Capano, C., Harry, I., Privitera, S., & Buonanno, A. 2016,
1941 *PhRvD*, 93, 124007, doi: [10.1103/PhysRevD.93.124007](https://doi.org/10.1103/PhysRevD.93.124007)
- 1942 Cassanelli, T., Leung, C., Rahman, M., et al. 2022, *AJ*,
1943 163, 65, doi: [10.3847/1538-3881/ac3d2f](https://doi.org/10.3847/1538-3881/ac3d2f)
- 1944 Champion, D. J., Petroff, E., Kramer, M., et al. 2016,
1945 *MNRAS*, 460, L30, doi: [10.1093/mnrasl/slw069](https://doi.org/10.1093/mnrasl/slw069)
- 1946 Chatterjee, S., Law, C. J., Wharton, R. S., et al. 2017,
1947 *Nature*, 541, 58, doi: [10.1038/nature20797](https://doi.org/10.1038/nature20797)
- 1948 CHIME/FRB Collaboration. 2020, The Canadian
1949 Hydrogen Intensity Mapping Experiment is a
1950 revolutionary new Canadian radio telescope designed to
1951 answer major questions in astrophysics and cosmology.,
1952 <https://chime-experiment.ca/>

- 1953 CHIME/FRB Collaboration, Andersen, B. C., Bandura,
1954 K. M., et al. 2020, *Nature*, 587, 54,
1955 doi: [10.1038/s41586-020-2863-y](https://doi.org/10.1038/s41586-020-2863-y)
- 1956 CHIME/FRB Collaboration, Andersen, B. C., et al. 2019,
1957 CHIME/FRB Detection of Eight New Repeating Fast
1958 Radio Burst Sources. <https://arxiv.org/abs/1908.03507>
- 1959 CHIME/FRB Collaboration, Amiri, M., Bandura, K.,
1960 Berger, P., et al. 2018, *ApJ*, 863, 48,
1961 doi: [10.3847/1538-4357/aad188](https://doi.org/10.3847/1538-4357/aad188)
- 1962 CHIME/FRB Collaboration, Amiri, M., et al. 2021, arXiv
1963 e-prints, arXiv:2106.04352.
1964 <https://arxiv.org/abs/2106.04352>
- 1965 Cho, M.-A. 2019, PhD thesis, University of Maryland
- 1966 Connor, L., Miller, M. C., & Gardenier, D. W. 2020,
1967 *MNRAS*, 497, 3076, doi: [10.1093/mnras/staa2074](https://doi.org/10.1093/mnras/staa2074)
- 1968 Cordes, J. M., & Chatterjee, S. 2019, *ARA&A*, 57, 417,
1969 doi: [10.1146/annurev-astro-091918-104501](https://doi.org/10.1146/annurev-astro-091918-104501)
- 1970 Cordes, J. M., & Lazio, T. J. W. 2002, arXiv e-prints,
1971 astro. <https://arxiv.org/abs/astro-ph/0207156>
- 1972 Corsi, A., & Owen, B. J. 2011, *PhRvD*, 83, 104014,
1973 doi: [10.1103/PhysRevD.83.104014](https://doi.org/10.1103/PhysRevD.83.104014)
- 1974 Dal Canton, T., & Harry, I. W. 2017, arXiv e-prints,
1975 arXiv:1705.01845. <https://arxiv.org/abs/1705.01845>
- 1976 Dolag, K., Gaensler, B. M., Beck, A. M., & Beck, M. C.
1977 2015, *MNRAS*, 451, 4277, doi: [10.1093/mnras/stv1190](https://doi.org/10.1093/mnras/stv1190)
- 1978 Falcke, H., & Rezzolla, L. 2014, *A&A*, 562, A137,
1979 doi: [10.1051/0004-6361/201321996](https://doi.org/10.1051/0004-6361/201321996)
- 1980 Foreman-Mackey, D., Hogg, D. W., Lang, D., & Goodman,
1981 J. 2013, *PASP*, 125, 306, doi: [10.1086/670067](https://doi.org/10.1086/670067)
- 1982 Gao, H., Zhang, B., & Lü, H.-J. 2016, *PhRvD*, 93, 044065,
1983 doi: [10.1103/PhysRevD.93.044065](https://doi.org/10.1103/PhysRevD.93.044065)
- 1984 Goodman, J., & Weare, J. 2010, *Communications in*
1985 *Applied Mathematics and Computational Science*, 5, 65,
1986 doi: [10.2140/camcos.2010.5.65](https://doi.org/10.2140/camcos.2010.5.65)
- 1987 Gourdji, K., Rowlinson, A., Wijers, R. A. M. J., &
1988 Goldstein, A. 2020, *MNRAS*, 497, 3131,
1989 doi: [10.1093/mnras/staa2128](https://doi.org/10.1093/mnras/staa2128)
- 1990 Grote, H. 2010, *Class. Quant. Grav.*, 27, 084003,
1991 doi: [10.1088/0264-9381/27/8/084003](https://doi.org/10.1088/0264-9381/27/8/084003)
- 1992 Harry, I. W., & Fairhurst, S. 2011, *Phys. Rev.*, D83,
1993 084002, doi: [10.1103/PhysRevD.83.084002](https://doi.org/10.1103/PhysRevD.83.084002)
- 1994 Harry, I. W., Fairhurst, S., & Sathyaprakash, B. S. 2008,
1995 *Class. Quant. Grav.*, 25, 184027,
1996 doi: [10.1088/0264-9381/25/18/184027](https://doi.org/10.1088/0264-9381/25/18/184027)
- 1997 Harry, I. W., Nitz, A. H., Brown, D. A., et al. 2014,
1998 *Physical Review D*, 89, doi: [10.1103/physrevd.89.024010](https://doi.org/10.1103/physrevd.89.024010)
- 1999 Heintz, K. E., Prochaska, J. X., Simha, S., et al. 2020, *ApJ*,
2000 903, 152, doi: [10.3847/1538-4357/abb6fb](https://doi.org/10.3847/1538-4357/abb6fb)
- 2001 Hessels, J. W. T., Ransom, S. M., Stairs, I. H., et al. 2006,
2002 *Science*, 311, 1901, doi: [10.1126/science.1123430](https://doi.org/10.1126/science.1123430)
- 2003 Ho, W. C. G., Jones, D. I., Andersson, N., & Espinoza,
2004 C. M. 2020, *PhRvD*, 101, 103009,
2005 doi: [10.1103/PhysRevD.101.103009](https://doi.org/10.1103/PhysRevD.101.103009)
- 2006 Husa, S., Khan, S., Hannam, M., et al. 2016, *Phys. Rev.*,
2007 D93, 044006, doi: [10.1103/PhysRevD.93.044006](https://doi.org/10.1103/PhysRevD.93.044006)
- 2008 Ioka, K. 2001, *MNRAS*, 327, 639,
2009 doi: [10.1046/j.1365-8711.2001.04756.x](https://doi.org/10.1046/j.1365-8711.2001.04756.x)
- 2010 Khan, S., Husa, S., Hannam, M., et al. 2016, *Phys. Rev.*,
2011 D93, 044007, doi: [10.1103/PhysRevD.93.044007](https://doi.org/10.1103/PhysRevD.93.044007)
- 2012 Kirsten, F., Marcote, B., Nimmo, K., et al. 2021, arXiv
2013 e-prints, arXiv:2105.11445.
2014 <https://arxiv.org/abs/2105.11445>
- 2015 Kiziltan, B., Kottas, A., De Yoreo, M., & Thorsett, S. E.
2016 2013, *ApJ*, 778, 66, doi: [10.1088/0004-637X/778/1/66](https://doi.org/10.1088/0004-637X/778/1/66)
- 2017 Kokkotas, K. D., Apostolatos, T. A., & Andersson, N.
2018 2001, *MNRAS*, 320, 307–315,
2019 doi: [10.1046/j.1365-8711.2001.03945.x](https://doi.org/10.1046/j.1365-8711.2001.03945.x)
- 2020 Kreidberg, L., Bailyn, C. D., Farr, W. M., & Kalogera, V.
2021 2012, *Astrophys. J.*, 757, 36,
2022 doi: [10.1088/0004-637X/757/1/36](https://doi.org/10.1088/0004-637X/757/1/36)
- 2023 Kumar, P., Shannon, R. M., Osłowski, S., et al. 2019, *The*
2024 *Astrophysical Journal*, 887, L30,
2025 doi: [10.3847/2041-8213/ab5b08](https://doi.org/10.3847/2041-8213/ab5b08)
- 2026 Levin, Y., & van Hoven, M. 2011, *MNRAS*, 418, 659,
2027 doi: [10.1111/j.1365-2966.2011.19515.x](https://doi.org/10.1111/j.1365-2966.2011.19515.x)
- 2028 Li, B.-A., Krastev, P. G., Wen, D.-H., & Zhang, N.-B. 2019,
2029 *European Physical Journal A*, 55, 117,
2030 doi: [10.1140/epja/i2019-12780-8](https://doi.org/10.1140/epja/i2019-12780-8)
- 2031 Li, Y., & Zhang, B. 2020, *ApJL*, 899, L6,
2032 doi: [10.3847/2041-8213/aba907](https://doi.org/10.3847/2041-8213/aba907)
- 2033 LIGO Scientific Collaboration. 2018, *LIGO Algorithm*
2034 *Library*, doi: [10.7935/GT1W-FZ16](https://doi.org/10.7935/GT1W-FZ16)
- 2035 Lorimer, D. R., Bailes, M., McLaughlin, M. A., Narkevic,
2036 D. J., & Crawford, F. 2007, *Science*, 318, 777–780,
2037 doi: [10.1126/science.1147532](https://doi.org/10.1126/science.1147532)
- 2038 Luo, R., Men, Y., Lee, K., et al. 2020, *MNRAS*, 494, 665,
2039 doi: [10.1093/mnras/staa704](https://doi.org/10.1093/mnras/staa704)
- 2040 Lyons, N., et al. 2010, *MNRAS*, 402, 705
- 2041 Macquart, J. P., Prochaska, J. X., McQuinn, M., et al.
2042 2020, *Nature*, 581, 391, doi: [10.1038/s41586-020-2300-2](https://doi.org/10.1038/s41586-020-2300-2)
- 2043 Marcote, B., Nimmo, K., Hessels, J. W. T., et al. 2020,
2044 *Nature*, 577, 190, doi: [10.1038/s41586-019-1866-z](https://doi.org/10.1038/s41586-019-1866-z)
- 2045 Margalit, B., Berger, E., & Metzger, B. D. 2019, *ApJ*, 886,
2046 110, doi: [10.3847/1538-4357/ab4c31](https://doi.org/10.3847/1538-4357/ab4c31)
- 2047 Margalit, B., Metzger, B. D., & Sironi, L. 2020, *MNRAS*,
2048 494, 4627, doi: [10.1093/mnras/staa1036](https://doi.org/10.1093/mnras/staa1036)
- 2049 Masui, K., Lin, H.-H., Sievers, J., et al. 2015, *Nature*, 528,
2050 523, doi: [10.1038/nature15769](https://doi.org/10.1038/nature15769)
- 2051 Mena-Parra, J., Leung, C., Cary, S., et al. 2022, *AJ*, 163,
2052 48, doi: [10.3847/1538-3881/ac397a](https://doi.org/10.3847/1538-3881/ac397a)

- 2053 Metzger, B. D., Berger, E., & Margalit, B. 2017, *ApJ*, 841,
2054 14, doi: [10.3847/1538-4357/aa633d](https://doi.org/10.3847/1538-4357/aa633d)
- 2055 Mikoczi, B., Vasuth, M., & Gergely, L. A. 2005, *Phys. Rev.*,
2056 D71, 124043, doi: [10.1103/PhysRevD.71.124043](https://doi.org/10.1103/PhysRevD.71.124043)
- 2057 Miller, M. C., & Miller, J. M. 2014, *Phys. Rept.*, 548, 1,
2058 doi: [10.1016/j.physrep.2014.09.003](https://doi.org/10.1016/j.physrep.2014.09.003)
- 2059 Mishra, C. K., Kela, A., Arun, K. G., & Faye, G. 2016,
2060 *Phys. Rev.*, D93, 084054,
2061 doi: [10.1103/PhysRevD.93.084054](https://doi.org/10.1103/PhysRevD.93.084054)
- 2062 Moortgat, J., & Kuijpers, J. 2005, in 22nd Texas
2063 Symposium on Relativistic Astrophysics, ed. P. Chen,
2064 E. Bloom, G. Madejski, & V. Patrosian, 326–331
- 2065 Newburgh, L. B., Addison, G. E., Amiri, M., et al. 2014, in
2066 Society of Photo-Optical Instrumentation Engineers
2067 (SPIE) Conference Series, Vol. 9145, Ground-based and
2068 Airborne Telescopes V, ed. L. M. Stepp, R. Gilmozzi, &
2069 H. J. Hall, 91454V, doi: [10.1117/12.2056962](https://doi.org/10.1117/12.2056962)
- 2070 Nitz, A., Harry, I., Brown, D., et al. 2020, *gwastro/pycbc*:
2071 *PyCBC*, Zenodo, doi: [10.5281/zenodo.3961510](https://doi.org/10.5281/zenodo.3961510)
- 2072 Nitz, A. H., Dent, T., Dal Canton, T., Fairhurst, S., &
2073 Brown, D. A. 2017, *ApJ*, 849, 118,
2074 doi: [10.3847/1538-4357/aa8f50](https://doi.org/10.3847/1538-4357/aa8f50)
- 2075 Owen, B. J., & Sathyaprakash, B. S. 1999, *Phys. Rev. D*,
2076 60, 022002, doi: [10.1103/PhysRevD.60.022002](https://doi.org/10.1103/PhysRevD.60.022002)
- 2077 Özel, F., Psaltis, D., Narayan, R., & McClintock, J. E.
2078 2010, *Astrophys. J.*, 725, 1918,
2079 doi: [10.1088/0004-637X/725/2/1918](https://doi.org/10.1088/0004-637X/725/2/1918)
- 2080 Pace, A., Prestegard, T., Moe, B., & Stephens, B. 2012,
2081 *Gravitational-Wave Candidate Event Database*,
2082 <https://gracedb.ligo.org>
- 2083 Pan, Y., Buonanno, A., Taracchini, A., et al. 2014, *Phys.*
2084 *Rev.*, D89, 084006, doi: [10.1103/PhysRevD.89.084006](https://doi.org/10.1103/PhysRevD.89.084006)
- 2085 Petroff, E., Hessels, J. W. T., & Lorimer, D. R. 2019,
2086 *Astron. Astrophys. Rev.*, 27, 4,
2087 doi: [10.1007/s00159-019-0116-6](https://doi.org/10.1007/s00159-019-0116-6)
- 2088 Petroff, E., Hessels, J. W. T., & Lorimer, D. R. 2022,
2089 *A&A Rv*, 30, 2, doi: [10.1007/s00159-022-00139-w](https://doi.org/10.1007/s00159-022-00139-w)
- 2090 Petroff, E., Barr, E. D., Jameson, A., et al. 2016, *PASA*, 33,
2091 e045, doi: [10.1017/pasa.2016.35](https://doi.org/10.1017/pasa.2016.35)
- 2092 Planck Collaboration, Ade, P. A. R., Aghanim, N., et al.
2093 2016, *A&A*, 594, A13, doi: [10.1051/0004-6361/201525830](https://doi.org/10.1051/0004-6361/201525830)
- 2094 Platts, E., Weltman, A., Walters, A., et al. 2019, *Physics*
2095 *Reports*, 821, 1–27, doi: [10.1016/j.physrep.2019.06.003](https://doi.org/10.1016/j.physrep.2019.06.003)
- 2096 Popov, S. B., & Postnov, K. A. 2013, *arXiv:1307.4924*
2097 [astro-ph]. <http://arxiv.org/abs/1307.4924>
- 2098 Prochaska, J. X., & Zheng, Y. 2019, *MNRAS*, 485, 648,
2099 doi: [10.1093/mnras/stz261](https://doi.org/10.1093/mnras/stz261)
- 2100 Pshirkov, M. S., & Postnov, K. A. 2010, *Ap&SS*, 330, 13,
2101 doi: [10.1007/s10509-010-0395-x](https://doi.org/10.1007/s10509-010-0395-x)
- 2102 Quitzow-James, R., Brau, J., Clark, J. A., et al. 2017,
2103 *Class. Quant. Grav.*, 34, 164002,
2104 doi: [10.1088/1361-6382/aa7d5b](https://doi.org/10.1088/1361-6382/aa7d5b)
- 2105 Rafei-Ravandi, M., et al. 2021.
2106 <https://arxiv.org/abs/2106.04354>
- 2107 Ravi, V. 2019, *Nature Astronomy*, 3, 928,
2108 doi: [10.1038/s41550-019-0831-y](https://doi.org/10.1038/s41550-019-0831-y)
- 2109 Ravi, V., & Lasky, P. D. 2014, *MNRAS*, 441, 2433,
2110 doi: [10.1093/mnras/stu720](https://doi.org/10.1093/mnras/stu720)
- 2111 Rowlinson, A., & Anderson, G. E. 2019, *MNRAS*, 489,
2112 3316, doi: [10.1093/mnras/stz2295](https://doi.org/10.1093/mnras/stz2295)
- 2113 Rowlinson, A., O’Brien, P. T., Metzger, B. D., Tanvir,
2114 N. R., & Levan, A. J. 2013, *MNRAS*, 430, 1061,
2115 doi: [10.1093/mnras/sts683](https://doi.org/10.1093/mnras/sts683)
- 2116 Rowlinson, A., et al. 2010, *MNRAS*, 408, 383,
2117 doi: [10.1111/j.1365-2966.2010.17115.x](https://doi.org/10.1111/j.1365-2966.2010.17115.x)
- 2118 Rowlinson, A., Starling, R. L. C., Gourdj, K., et al. 2020,
2119 *arXiv e-prints*, arXiv:2008.12657.
2120 <https://arxiv.org/abs/2008.12657>
- 2121 Sagiv, A., & Waxman, E. 2002, *ApJ*, 574, 861,
2122 doi: [10.1086/340948](https://doi.org/10.1086/340948)
- 2123 Sarin, N., & Lasky, P. D. 2021, *General Relativity and*
2124 *Gravitation*, 53, 59, doi: [10.1007/s10714-021-02831-1](https://doi.org/10.1007/s10714-021-02831-1)
- 2125 Sathyaprakash, B. S., & Dhurandhar, S. V. 1991, *Phys.*
2126 *Rev.*, D44, 3819, doi: [10.1103/PhysRevD.44.3819](https://doi.org/10.1103/PhysRevD.44.3819)
- 2127 Shannon, R. M., Macquart, J.-P., Bannister, K. W., et al.
2128 2018, *Nature*, 1, doi: [10.1038/s41586-018-0588-y](https://doi.org/10.1038/s41586-018-0588-y)
- 2129 Shin, K., Masui, K. W., Bhardwaj, M., et al. 2022, *arXiv*
2130 *e-prints*, arXiv:2207.14316.
2131 <https://arxiv.org/abs/2207.14316>
- 2132 Spitler, L. G., Cordes, J. M., Hessels, J. W. T., et al. 2014,
2133 *ApJ*, 790, 101, doi: [10.1088/0004-637X/790/2/101](https://doi.org/10.1088/0004-637X/790/2/101)
- 2134 Sutton, P. J. 2013, *arXiv e-prints*, arXiv:1304.0210.
2135 <https://arxiv.org/abs/1304.0210>
- 2136 Sutton, P. J., Jones, G., Chatterji, S., et al. 2010, *New*
2137 *Journal of Physics*, 12, 053034,
2138 doi: [10.1088/1367-2630/12/5/053034](https://doi.org/10.1088/1367-2630/12/5/053034)
- 2139 Taracchini, A., Buonanno, A., Pan, Y., et al. 2014, *PhRvD*,
2140 89, 061502, doi: [10.1103/PhysRevD.89.061502](https://doi.org/10.1103/PhysRevD.89.061502)
- 2141 The LIGO Scientific Collaboration, the Virgo
2142 Collaboration, the KAGRA Collaboration, Abbott, R.,
2143 et al. 2021a, *arXiv e-prints*, arXiv:2111.03606.
2144 <https://arxiv.org/abs/2111.03606>
- 2145 —. 2021b, *arXiv e-prints*, arXiv:2111.03634.
2146 <https://arxiv.org/abs/2111.03634>
- 2147 Thornton, D., Stappers, B., Bailes, M., et al. 2013, *Science*,
2148 341, 53, doi: [10.1126/science.1236789](https://doi.org/10.1126/science.1236789)
- 2149 Totani, T. 2013, *Publ Astron Soc Jpn Nihon Tenmon*
2150 *Gakkai*, 65, doi: [10.1093/pasj/65.5.L12](https://doi.org/10.1093/pasj/65.5.L12)

- 2151 Troja, E., Cusumano, G., O'Brien, P. T., et al. 2007, *ApJ*,
2152 665, 599, doi: [10.1086/519450](https://doi.org/10.1086/519450)
- 2153 Urban, A. L. 2016, PhD thesis
- 2154 Usov, V. V., & Katz, J. I. 2000, *A&A*, 364, 655
- 2155 Wang, J.-S., Yang, Y.-P., Wu, X.-F., Dai, Z.-G., & Wang,
2156 F.-Y. 2016, *ApJL*, 822, L7,
2157 doi: [10.3847/2041-8205/822/1/L7](https://doi.org/10.3847/2041-8205/822/1/L7)
- 2158 Was, M., Sutton, P. J., Jones, G., & Leonor, I. 2012,
2159 *PhRvD*, 86, 022003, doi: [10.1103/PhysRevD.86.022003](https://doi.org/10.1103/PhysRevD.86.022003)
- 2160 Wen, D.-H., Li, B.-A., Chen, H.-Y., & Zhang, N.-B. 2019,
2161 *Physical Review C*, 99, doi: [10.1103/physrevc.99.045806](https://doi.org/10.1103/physrevc.99.045806)
- 2162 Williamson, A. R., Biwer, C., Fairhurst, S., et al. 2014,
2163 *Phys. Rev.*, D90, 122004,
2164 doi: [10.1103/PhysRevD.90.122004](https://doi.org/10.1103/PhysRevD.90.122004)
- 2165 Yamasaki, S., & Totani, T. 2020, *ApJ*, 888, 105,
2166 doi: [10.3847/1538-4357/ab58c4](https://doi.org/10.3847/1538-4357/ab58c4)
- 2167 Yamasaki, S., Totani, T., & Kiuchi, K. 2018, *PASJ*, 70, 39,
2168 doi: [10.1093/pasj/psy029](https://doi.org/10.1093/pasj/psy029)
- 2169 Yao, J. M., Manchester, R. N., & Wang, N. 2017, *ApJ*, 835,
2170 29, doi: [10.3847/1538-4357/835/1/29](https://doi.org/10.3847/1538-4357/835/1/29)
- 2171 Zhang, B. 2014, *ApJL*, 780, L21,
2172 doi: [10.1088/2041-8205/780/2/L21](https://doi.org/10.1088/2041-8205/780/2/L21)
- 2173 —. 2018, *ApJL*, 867, L21, doi: [10.3847/2041-8213/aae8e3](https://doi.org/10.3847/2041-8213/aae8e3)
- 2174 —. 2020a, *Nature*, 587, 45, doi: [10.1038/s41586-020-2828-1](https://doi.org/10.1038/s41586-020-2828-1)
- 2175 —. 2020b, *ApJL*, 890, L24, doi: [10.3847/2041-8213/ab7244](https://doi.org/10.3847/2041-8213/ab7244)
- 2176 Zink, B., Lasky, P. D., & Kokkotas, K. D. 2012, *PhRvD*,
2177 85, 024030, doi: [10.1103/PhysRevD.85.024030](https://doi.org/10.1103/PhysRevD.85.024030)